Theses and Dissertations

2014

Electrokinetics of Polar Liquids in Contact with Nonpolar Surfaces

Chih-Hsiu Lin
Lehigh University

Follow this and additional works at: http://preserve.lehigh.edu/etd

Part of the Chemical Engineering Commons

Electrokinetics of Polar Liquids

in Contact with Nonpolar Surfaces

by

Chih-Hsiu Lin

A Dissertation

Presented to the Graduate and Research Committee

of Lehigh University

in Candidacy for the Degree of

Doctor of Philosophy

in

Chemical Engineering

Lehigh University

January 2014

Certificate of Approval

Approved and recommended for acceptance as a dissertation in partial fulfillment of the requirements for the degree of Doctor of Philosophy.

_____
Date

                    _____
                    Professor Manoj K. Chaudhury
                    Dissertation Advisor

_____
Accepted Date   Committee Members:

                    _____
                    Professor Manoj K. Chaudhury, Committee Chair
                    Professor of Chemical Engineering

                    _____
                    Professor Andrew Klein, Committee Member
                    Professor of Chemical Engineering

                    _____
                    Professor Cesar A. Silebi, Committee Member
                    Professor of Chemical Engineering

                    _____
                    Professor Bryan W. Berger, Committee Member
                    Professor of Chemical Engineering

                    _____
                    Professor Gregory S. Ferguson, Committee Member
                    Professor of Chemistry

dedicated to my beloved parents

Tso-Chung Lin,

Shu-Ying Wu,

and

my brother, Jih-Chun Lin

Acknowledgements

This is such a journey for me at Lehigh. For the past few years in graduate school, I would not be able to reach this point without the help and support of people around me. I would like to take this opportunity to thank them.

Furthermore, I would like to thank the support of my family, especially my parents, Tso-Chung Lin and Shu-Ying Wu, and my brother, Jih-Chun Lin. Their support and encouragement are parts of my motivations to move on. I deeply appreciate their selfless love towards me.

Last but not least, I appreciate the efforts provided by Chris Keturakis, Jonathan Longley, and Steve Csernica in proofreading my dissertation. I would also like to thank the financial support from Office of Naval Research.

Table of Contents

Chapter 3. The Zeta Potential of Planar Hydrophobic Surfaces in Contact with Nonionic Surfactant Solutions

Chapter 6. Dissertation Summary

Appendices

Vita

List of Tables

List of Figures

Abstract

Surface science is widely applied in different engineering/scientific fields by exploiting the various physical and chemical properties of interfaces. Here, we explore the electrical properties at hydrophobe/liquid interfaces and the mechanical properties of hydrogels.

Most solid surfaces become charged when placed in contact with liquids. This interfacial charge is critical in practical applications such as colloidal suspensions and microfluidic devices. In order to study the charge at the hydrophobe/liquid interface, we developed a simple method to determine the zeta potential (an indication of surface charge strength) of planar hydrophobic surfaces by combining electroosmosis and capillarity. We showed that the measurement of the centerline velocity of the liquid inside the channel is enough to deduce the zeta potential of the surface. This method was further utilized to investigate the basic physics of the charge origin at the hydrophobe/liquid interface. Negative zeta potentials were observed on apparently passive nonpolar hydrocarbon and fluorocarbon surfaces when they are in contact with polar liquids (water, ethylene glycol, formamide, and dimethyl sulfoxide). The current models of charging via the adsorption of hydroxide ions on the interface or the dissociation of pre-existing moieties are not sufficient to illustrate the experimental observations. We hope that these results will inspire further experimental and theoretical studies in this important area of research that has potential practical implications.

On the other hand, mechanical properties of surfaces are also important from an adhesion perspective. A side project focuses on investigating the adhesion between thin hydrogel films and flat-end rigid studs. We designed a composite material that was composed of a polyvinyl alcohol (PVA) hydrogel coating covalently bonded to a thin polydimethylsiloxane (PDMS) film. This PVA coating passed a stability test and was characterized by high resolution x-ray photoelectron spectroscopy (XPS) and attenuated total reflectance-Fourier transform infrared spectroscopy (ATR-FTIR). This hydrogel layer was found to lower the removal shear stress of a silanized glass cube by ~60% (compared to a thin unmodified PDMS film). This reduction of the adhesive shear stress was presumably due to the lubrication of water kept in the swollen PVA gel.

Chapter 1

Introduction

Surface science is widely applied in different fields by exploiting various physical and chemical properties of interfaces.[1] A very important one is the surface electrical property. Almost all solid surfaces become charged when they come in contact with aqueous solutions.[2-8] These surface charges combined with the application of an electric field can induce electrokinetic phenomena, which can be utilized in applications such as micro-fluidics[3,8,9]. Moreover, mechanical properties of surfaces are also important because they determine the condition of a material in response to an applied load.[10] The adhesion of soft materials (e.g., rubber and hydrogels) is widely studied for a better understanding of contact mechanics.

1.1. CHARGE AT THE HYDROPHOBE/LIQUID INTERFACE

Charges at aqueous interfaces play important roles in many physical, chemical, and biological processes. In industrial cheese production, the curds, which are composed of the casein micelles generated during the curdling process, are affected by the calcium ions in the milk.[11] The electrolyte/metal interface is related to corrosion processes.[12,13] Interfacial charge also affects the stability of proteins[14] and colloidal suspensions[15] in

liquids. Microfluidic devices are good examples that utilize the electrokinetic phenomena induced by shearing the excess counter-ions at the solid/liquid interface.[3,8,9] All the systems involve the charge at hydrophobe/liquid interfaces.

It is still not clear why non-polar surfaces get charged while they are in contact with liquids. In the early 20th century, the air/water interface was considered neutral due to the fact that the surface tension of an electrolyte solution was higher than that of pure water. Onsager and Samaras[16] proposed a model with respect to the increase of the water surface tension that occurs with the addition of strong electrolytes. They stated that the electrostatic image force repelled the ions from the surface, so the outermost layer of aqueous electrolyte solution was devoid of ions. However, this model was over-simplified because, for example, the ion-solvent interaction and solvation entropic effects were not taken into consideration.[17,18] This model of electrolytes repelled from the interface prevailed for years, though Jones and Ray[19-23] reported a minimum of surface tension (i.e., net surface excess of ions) of electrolyte solutions at low concentration (~1 mM). Electrokinetic measurements showed results contradicting this model. In the late 19th century, observations had exhibited that air bubbles in water moved toward the positive electrode in an electric field, and later experiments confirmed the negative zeta potential at the air/water interface.[24,25] The origin of the charge at the hydrophobe/liquid interface still remains a controversy.

Before we go through the current theories of this interfacial charge, let us briefly review the background of the electrical double layer and the zeta potential.

1.1.1. Background of Electrical Double Layer, Zeta Potential and Electrokinetic

      Phenomena

When a charged surface is in contact with an aqueous phase, surface charges attract counter-ions near the surface, resulting in the formation of an electrical double layer (EDL). The earliest concept of EDL was proposed by Helmholtz, who considered the charge distribution in the aqueous solution near a mercury surface (Fig. 1.1). This simple model could be used to illustrate some features induced by the EDL. However, in real systems, co-ions (ions with the same sign as the charged surface) in the solution are not completely excluded from the region near the surface, and counter-ions are spread out forming a diffuse layer (Fig. 1.2). In the early 1900s, the model related to the diffuse layer was developed independently by Guoy and Chapman. The Guoy-Chapman model was able to offer quantitative predictions for low surface potential (~25 mV) with low ion concentration. Nevertheless, this model did not consider the finite size of the
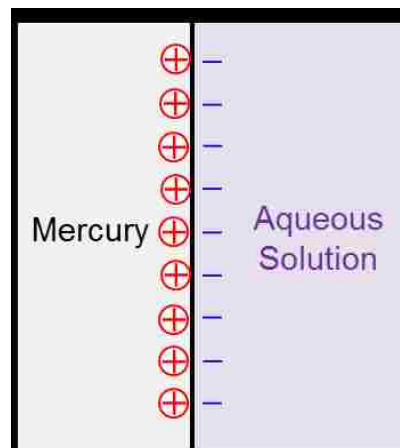
Figure 1.1. The Helmholtz model of the electrical double layer.[27]

ions, and it assumed the solution was ideal. Ions cannot reach the surface to a distance due to their finite size. Later, Stern suggested a model wherein the inner boundary of the diffuse layer was located near the charged surface about the radius of a hydrated counter-ion.[26-30]
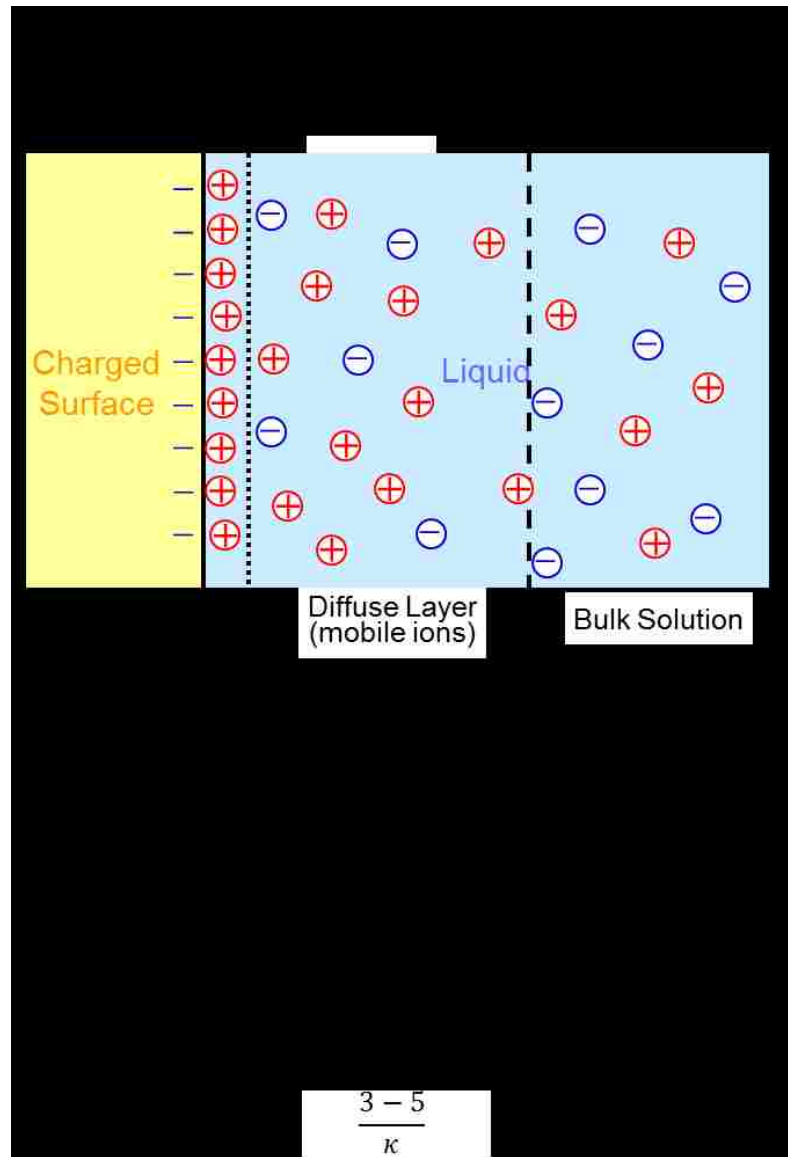
Figure 1.2. (Top) Schematics of the electrical double layer. (Bottom) Illustration of the electric potential distribution in a fluid near a charged surface. κ is the Debye-Hückel parameter.[26]

The liquid layer in an EDL can be subdivided into two regions according to the mobility of the counter-ions (Fig. 1.2). The layer containing the immobile counter-ions near the solid wall is the compact layer, and the region where the counter-ions are mobile is the diffuse layer. The electric potential distribution in an EDL in a dielectric medium can be described by the Poisson equation,

$$\nabla^2 \psi = -\frac{\rho}{\varepsilon_0},$$ (1.1)

where ψ is the electric potential, ρ is the charge density, ε and ε_0 are the dielectric constants in the medium and vacuum, respectively. The zeta potential is defined to be the electrical potential on the shear plane, which is the interface of the compact and diffuse layers in the EDL.[26,28,29] Generally, it is difficult to directly measure the electrical potential at the solid/liquid interface. Therefore, the zeta potential, which can be measured experimentally, is used as an indication and approximation of the surface potential.

Electrokinetic phenomena occur when the mobile counter-ions in an EDL migrate due to various causes, for example, a pressure gradient or electric field.[26,29] These phenomena can be utilized in many different fields, such as microfluidic devices[3,8,9], protein separation[31], and zeta potential measurement[30]. There are three basic electrokinetic phenomena: electroosmosis, electrophoresis, and streaming current/potential:

(1) Electroosmosis: This phenomenon happens while an electric filed is applied to the liquid within a microchannel. The counter-ions in the diffuse layer move as a

response to the electric field and drag the liquid.

(2) Electrophoresis: This phenomenon is best described by considering a particle suspended in a liquid phase. This particle will move when an electric field is applied to the liquid due to its surface charge. The particle may be solid, liquid or gas.

(3) Streaming current/potential: This phenomenon occurs when a pressure gradient is applied across a microchannel or capillary filled with liquid. As a response to the pressure gradient, the liquid is forced to move. The counter-ions in the diffuse layer migrate with the flow and generate a streaming current in the direction of the flow. The electrokinetic potential corresponding to this current is defined to be the streaming potential.

1.1.2. Theories of Charge at the Hydrophobe/Liquid Interface

As mentioned, it is interesting that a nonpolar surface gets charged while in contact with aqueous solutions. For example, oil droplets[5,6] and different polymers[2,32] bear different strengths of negative zeta potentials while they are in contact with aqueous solutions (Fig. 1.3). Surfaces modified with self-assembled monolayers terminated with hydrocarbon and fluorocarbon functionalities also give negative zeta potential with electrokinetic measurements.[33,34] It has been hypothesized[35-39] that the negative charges on hydrophobic surfaces are due to the adsorption of hydroxide ions (OH^-) in the solution. Marinova *et al.*[37] measured the negative zeta potentials of four

8
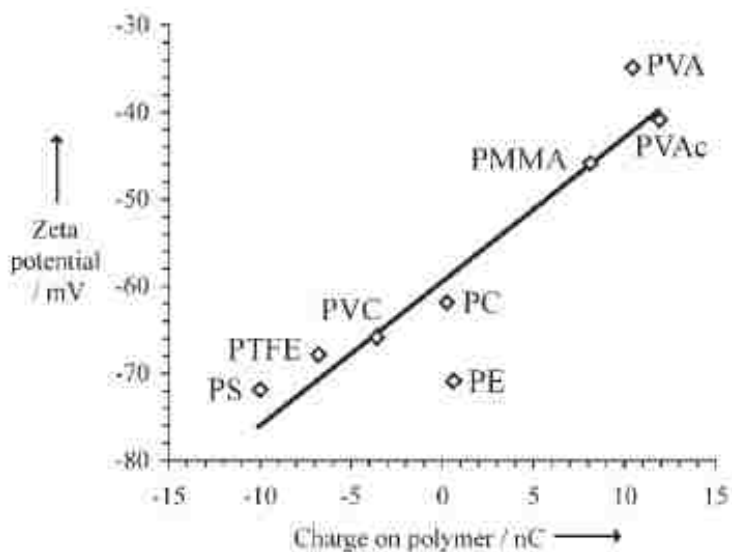
Figure 1.3. Correlation between the zeta potential and charge on eight polymers measured with contact electrification. PS: polystyrene; PTFE: polytetrafluoroethylene; PVC: poly(vinyl chloride); PE: polyethylene; PC: poly(bisphenol A carbonate); PMMA: poly(methyl methacrylate); PVA: poly(vinyl alcohol); PVAc: poly(vinyl acetate). (From reference [2], reprinted by permission.)

different types of oil droplets in contact with surfactant-free electrolyte solutions. They found that the zeta potential depended on the pH and ionic strength of the solution. They also deduced that the adsorption of the hydroxide ion was the cause of the negative charge on the oil droplet surface as well. Beattie and coworkers[38,39] have measured the zeta potential of oil drops in surfactant-free water and reported the surface charge density of oil droplets in water to be -5 ~ -7 $\mu C/cm^2$. They further proposed a model related to the suppression of dipole moment fluctuations of solvated ions near the hydrophobe implying that the OH⁻ ions are attracted to the water surface in contact with air or oil.[40] Using first-principles molecular dynamics (MD) simulations, Mundy *et al.*[41] predicted a slight tendency of OH⁻ ions towards the water surface without the influence

of counter-ions. Additionally, the electroosmosis of pure water in hydrophobic channels could be ascribed to the interfacial dipole orientation of water, but MD simulations have shown that this dipole orientation in a static electric field does not contribute to the zeta potential.[42] Utilizing the phase-sensitive sum-frequency vibrational spectroscopy (PS-SFVS), Tian and Shen showed that OH^- ions had higher adsorption energy and coverage than hydronium (H_3O^+) and chloride (Cl^-) ions on octadecyltrichlorosilane-modified quartz in contact with water.[43] Additionally, this negative interfacial charge is not only observed by electrokinetic measurements. Contact electrification, which is related to the charge transfer between two surfaces in contact, also shows negative charge on various hydrophobic surfaces[2] (Fig. 1.3).

On the other hand, some simulations and spectroscopic techniques show that H_3O^+ ions are the main species at the surface of water. The surface-sensitive vibrational sum-frequency scattering (SFS) experiments exhibited the same orientation of water molecules at the oil/water interface as the water on a negatively-charged surface. Nevertheless, there was no evidence of excess OH^- ions at the oil/water interface.[44] Synchrotron photoelectron spectroscopy (PES) measurements have shown no strong adsorption of OH^- ions at the water/vapor interface.[45] MD simulations and infrared (IR) spectroscopy showed a high affinity of H_3O^+ at the water surface.[46-49] As reviewed by Petersen and Saykally, resonant UV second-harmonic generation (SHG) experiments exhibited excess hydronium ions at the air/water interface.[50] However, these microscopic results contradict the observation of the macroscopic electrokinetic experiments which show the surface of water is negatively charged.

Recently, a new model has been proposed[51] wherein the negative charge at hydrophobe/water interface comes from the electron transfer between the H-bond acceptor and donor in a water dimer. The dangling OH peaks (i.e., unsaturated H-bond) were observed under the IR-visible sum-frequency generation (SFG) spectra at hydrophobe/water interfaces.[52] MD simulations also showed the imbalance of accepting and donating H-bonds at the oil/water interface.[44] This imbalance of H-bond could further lead to the negative zeta potential measured at the hydrophobe/water interface. [44,51,53,54] In addition, hydrated electrons have been detected at the air/water interface utilizing the nonlinear spectroscopic method of SHG.[55]

1.2. ADHESION OF SOFT MATERIALS

1.2.1. Adhesion of Soft Thin Confined Films

The adhesion of two surfaces is ascribed to the interfacial interactions with different types of forces involved.[56] Soft materials (e.g., rubber) offer good model systems to study adhesion since their surface and mechanical properties can be controlled by variables such as the chemical composition, molecular weight and cross-linking ratio.

Kendall[57] applied the energy balance concept proposed by Griffith[58] to analyze the fracture of elastic solids induced by adhesion tests. This concept inspired scientists to study the adhesion of thin soft materials. Ganghoffer and Gent[59] investigated the adhesion between a rubber layer and a flat cylindrical aluminum punch. Their results

showed that the Poisson's ratio was a strong parameter of the system. A small deviation from the complete incompressibility would reduce the rubber layer stiffness and detachment force. Yang and Li[60] proposed models of the adhesion between a flat-end cylindrical punch and a thin elastic film bonded on a rigid substrate. The pull-off force was affected by the interfacial boundary (frictionless or perfectly bonded) conditions. Shull and coworkers[61-65] investigated the adhesion of thin confined elastic films with respect to deformation and failure modes, geometric effects, and fingering instabilities. Lakrout *et al.*[66,67] examined the adhesion mechanisms between a flat rigid probe and thin elastic films. Chaudhury *et al.*[68,69] studied the adhesion between confined thin polydimethylsiloxane (PDMS) films and a flat-end rigid stud by applying normal and shear forces. These studies improved the understanding of the mechanism of removing a rigid punch from a soft thin elastic layer.

1.2.2. Application of Soft Material in Marine Biofouling

Two adhered objects will not be able to be separated with a reasonable force if they are both ideally rigid and there are no defects at the interface. However, if one object is deformable or coated with a layer of soft material, the other one can be removed with a finite force. One important application is to study the removal of hard foulants adhered to the ship surface.

Marine biofouling happens to all surfaces in contact with seawater due to the attachment of marine organisms. When a ship is in contact with the seawater, its surface

will be covered by a complex layer composed of bacteria, proteins and bioorganisms such as algae, zoospores and barnacles. (Fig. 1.4) The marine biofoulants change the morphology of the ship surface, causing a significant increase in the hydrodynamic drag and thus reducing the cruise efficiency. It is a time- and money-consuming process to remove these biofoulants. In order to prevent marine biofouling, anti-fouling coatings aim at reducing the settlement of bioorganisms via biocides or degrading the bonds between the bioorganism and surface using enzymes. Some materials are also used to inhibit the adsorption of organic particles (e.g., protein) as well.[70,71] Another type of material utilized to reduce/remove the biofoulant is the easy-release coating, which has low elastic modulus and surface energy. These properties ensure that marine organisms are bonded to it through weak interactions in an adhesive geometry which facilitates removal.[68,69,70-77] Therefore, the biofoulant will fall off due to the hydrodynamic force created by the ship movement.[70, 75] Here, we focus on studying the release mechanism of a pseudo-foulant from the surface of an easy-release coating.
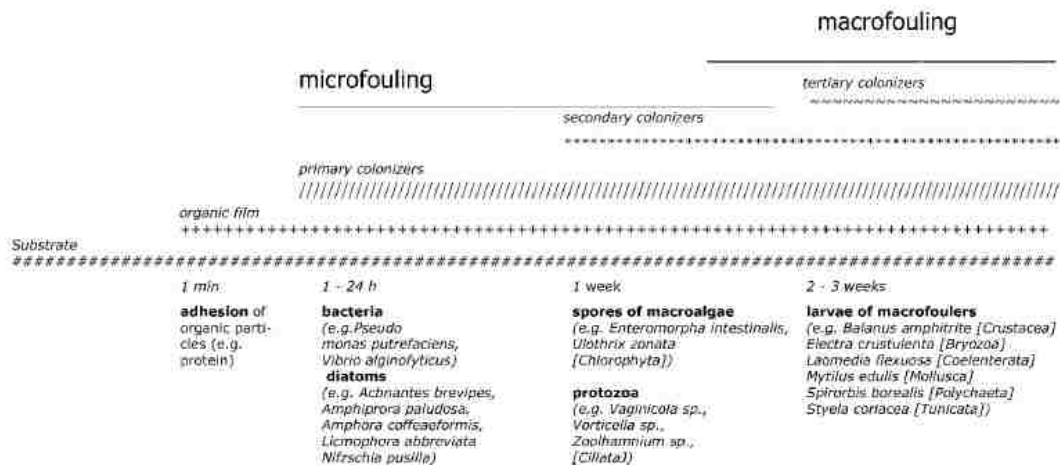
Figure.1.4. Temporal structure of the marine biofouling (from reference [70], reprinted by permission).

1.3. RESEARCH OBJECTIVES

   This research is aimed at investigating the charge at hydrophobe/liquid interface and the adhesion of hydrogels. The intermediate goals are as follows:

(1) Determine the zeta potential of a planar hydrophobic surface. A new technique is designed utilizing electro-capillarity.

(2) Examine the effect of OH^- ions on the zeta potential estimated with electrokinetic measurements, further offering an insight into the current theories about the origin of this interfacial charge. The aforementioned new technique is modified to measure the zeta potential of nonpolar surfaces in contact with polar organic solvents containing limited ions.

(3) Design a new polyvinyl alcohol (PVA)/polydimethylsiloxane (PDMS) composite material and study its underwater shear adhesion. The new material is characterized by using x-ray photoelectron spectroscopy (XPS), attenuated total reflectance-Fourier transform infrared spectroscopy (ATR-FTIR), ellipsometry, and a stability test.

1.4. THESIS LAYOUT

   The roadmap of this thesis is arranged into two main topics. First, the research aims to test the hypothesis that, measuring with electrokinetic techniques, the adsorption of OH^- ions on hydrophobic surfaces is the cause of surface charge in an aqueous environment. To address this issue, a new method is developed (Chapter 2) and

is used to estimate the zeta potential of different nonpolar surfaces with non-ionic surfactant solutions (Chapter 3) and various solvents (Chapter 4). The second goal is to study hydrogel adhesion. A new PVA/PDMS composite material is developed. PVA hydrogel is bonded covalently to a PDMS surface using a silane coupling agent. An underwater shear-induced experiment is utilized to investigate the release mechanism of a pseudo-barnacle (a silanized glass prism) sheared against PVA coated PDMS (Chapter 5). Chapter 6 contains the thesis conclusion and recommendations for future work.

REFERENCES

1. Adamson, A. W.; Gast, A. P. *Physical Chemistry of Surfaces*, 6th Ed. Wiley-Interscience: New York, NY, 1997, p 352-355.

2. McCarty, L. S.; Whitesides, G. M. *Angewandte Chemie International Edition* 2008, **47**, 2188-2207.

3. Tandon, V.; Bhagavatula, S. K.; Nelson, W. C.; Kirby, B. J. *Electrophoresis* 2008, **29**, 1092-1101.

4. Tandon, V.; Kirby, B. J. *Electrophoresis* 2008, **29**, 1102-1114.

5. Beattie, J. K. *Lab on a Chip* 2006, **6**, 1409-1411.

6. Marinova, K. G.; Alargova, R. G.; Denkov, N. D.; Velev, O. D.; Petsev, D. N.; Ivanov, I. B.; Borwankar, R. P. *Langmuir* 1996, **12**, 2045-2051.

7. Zimmermann, R.; Dukhin, S.; Werner, C. *Journal of Physical Chemistry B* 2001, **105**, 8544-8549.

8. Zimmermann, R.; Osaki, T.; Schweiss, R.; Werner, C. *Microfluidics and Nanofluidics* 2006, **2**, 367-379.

9. Huang, T. T.; Mosier, N. S.; Ladisch, M. R. *Journal of Separation Science* 2006, **29**, 1733-1742.

10. Roylance, D. *Mechanics of Materials.* John Wiley & Sons, Inc.: New York, NY, 1996.

11. Kapoor, R.; Metzger, L. E. *Comprehensive Reviews in Food Science and Food Safety* 2008, **7**, 194-214.

12. Kritzer, P. *The Journal of Supercritical Fluids* 2004, **29**, 1-29.

13. Tucceri, R. *Surface Science Reports* 2004, **56**, 85-157.

14. Cacace, M. G.; Landau, E. M.; Ramsden, J. J. *Quarterly Reviews of Biophysics* 1997, **30**, 241-277.

15. Tavaresa, F. W.; Bratkob, D.; Prausnitz, J. M. *Current Opinion in Colloid & Interface Science* 2004, **9**, 81-86.

16. Onsager, L.; Samaras, N. N. T. *The Journal of Chemical Physics* 1934, **2**, 528-536.

17. Lynden-Bell, R. M.; Rasaiah, J. C. *The Journal of Chemical Physics* 1997, **107**, 1981-1991.

18. Lynden-Bell, R. M.; Rasaiah, J. C.; Noworyta, J. P. *Pure and Applied Chemistry* 2001, **73**, 1721-1731.

19. Jones, G.; Ray, W. A. *Journal of the American Chemical Society* 1935, **57**, 957-958.

20. Jones, G.; Ray, W. A. *Journal of the American Chemical Society* 1937, **59**, 187-198.

21. Jones, G.; Ray, W. A. *Journal of the American Chemical Society* 1941, **63**, 288-294.

22. Jones, G.; Ray, W. A. *Journal of the American Chemical Society* 1941, **63**, 3262-3263.

23. Jones, G.; Ray, W. A. *Journal of the American Chemical Society* 1942, **64**, 2744-2745.

24. Beattie, J. K.; Djerdjev, A. N.; Warr, G. G. *Faraday Discussions* 2009, **141**, 31-39.

25. Graciaa, A.; Morel, G.; Saulner, P.; Lachaise, J.; Schechter, R.S. *Journal of Colloid and Interface Science* 1995, **172**, 131-136.

26. Li, D. Q. *Electrokinetics in Microfluidics*. Elsevier, Academic Press: San Diego, CA, 2004.

27. Hunter, R. J. *Foundations of Colloid Science Volume I*; Oxford University Press: New York, NY, **1987**.

28. Kirby, B. J. and Hasselbrink, E. F. *Electrophoresis* 2004, **25**, 187-202.

29. Masliyah, J. H.; Bhattacharjee, S. *Electrokinetic and Colloid Transport Phenomena*; John Wiley & Sons, Inc.: Hoboken, NJ, 2006.

30. Delgado, A.V.; González-Caballero, F.; Hunter, R.J.; Koopal, L.K.; Lyklema, J. *Journal of Colloid and Interface Science* 2007, **309**, 194-224.

31. Pioch, M.; Bunz, S.-C.; Neusüß, C. *Electrophoresis* 2012, **33**, 1517-1530.

32. Kirby, B. J.; Hasselbrink, E. F. *Electrophoresis* 2004, **25**, 203-213.

33. Hozumi, A.; Sugimura, H.; Yokogawa, Y.; Kameyama, T.; Takai, O. *Colloids and Surfaces A: Physicochemical and Engineering Aspects* 2001, **182**, 257-261.

34. Lin, C.-H.; Chaudhury, M. K. *Langmuir* 2008, **24**, 14276-14281.

35. Tandon, V.; Bhagavatula, S. K.; Nelson, W. C.; Kirby, B. J. *Electrophoresis* 2008, **29**, 1092-1101.

36. Dickinson, W. *Transactions of the Faraday Society* 1941, **37**, 140-148.

37. Marinova, K. G.; Alargova, R. G.; Denkov, N. D.; Velev, O. D.; Petsev, D. N.; Ivanov, I. B.; Borwankar, R. P. *Langmuir* 1996, **12**, 2045-2051.

38. Beattie, J. K.; Djerdjev, A. N.; Warr, G. G. *Faraday Discussions* 2009, **141**, 31-39.

39. Beattie, J. K.; Djerdjev, A. N. *Angewandte Chemie International Edition* 2004, **43**, 3568-3571.

40. Gray-Weale, A.; Beattie, J. K. *Physical Chemistry Chemical Physics* 2009, **11**, 10994-11005.

41. Mundy, C. J.; Kuo, I. F. W.; Tuckerman, M. E.; Lee, H S.; Tobias, D. J. *Chemical Physics Letters* 2009, **481**, 2-8.

42. Bonthuis, D. J.; Horinek, D.; Bocquet, L.; Netz, R. R. *Langmuir* 2010, **26**, 12614-12625.

43. Tian, C. S.; Shen, Y. R. *Proceedings of the National Academy of Sciences* 2009, **106**, 15148-15153.

44. Vácha, R.; Rick, S. W.; Jungwirth, P.; de Beer, A. G. F.; de Aguiar, H. B.; Samson, J.-S.; Roke, S. *Journal of the American Chemical Society* 2011, **133**, 10204-10210.

45. Winter, B.; Faubel, M.; Vácha, R.; Jungwirth, P. *Chemical Physics Letters* 2009, **474**, 241-247.

46. Vácha, R.; Buch, V.; Milet, A.; Devlin, P.; Jungwirth, P. *Physical Chemistry Chemical Physics* 2007, **9**, 4736-4747.

47. Buch, V.; Milet, A.; Vácha, R.; Jungwirth, P.; Devlin, J. P. *Proceedings of the National Academy of Sciences of the United States of America* 2007, **104**, 7342-7347.

48. Iuchi, S.; Chen, H. N.; Paesani, F.; Voth, G. A. *Journal of Physical Chemistry B* 2009, **113**, 4017-4030.

49. Takahashi, H.; Maruyama, K.; Karino, Y.; Morita, A.; Nakano, M.; Jungwirth, P.; Matubayasi, N. *Journal of Physical Chemistry B* 2011, **115**, 4745-4751.

50. Petersen, P. B.; Saykally, R. J. *Chemical Physics Letters* 2008, **458**, 255-261.

51. Ben-Amotz, D. *Journal of Physical Chemistry Letters* 2011, **2**, 1216-1222.

52. Miranda, P. B.; Shen, Y. R. *Journal of Physical Chemistry B* 1999, **103**, 3292-3307.

53. Khaliullin, R. Z.; Bell, A. T.; Head-Gordon, M. *Chemistry - A European Journal* 2009, **15**, 851-855.

54. Vácha, R.; Marsalek, O.; Willard, A. P.; Bonthuis, D. J.; Netz, R. R.; Jungwirth, P. *Journal of Physical Chemistry Letters* 2011, **3**, 107-111.

55. Sagar D. M.; Bain Colin D.; Verlet Jan R. R. *Journal of the American Chemical Society* 2010, **132**, 6917-6919.

56. Lee, L.-H., editor. *Fundamentals of Adhesion.* Plenum Press: New York, NY, 1991.

57. Kendall, K. *Journal of Physics D*: *Applied Physics* 1971, 4, 1186-1195.

58. Griffith, A. A. *Philosophical Transactions of the Royal Society A: Mathematical, Physical and Engineering Science* 1921, **221**, 163-198.

59. Ganghoffer, J.-F.; Gent, A. N. *The Journal of Adhesion* 1995, **48**, 75-84.

60. Yang, F.; Li, J. C. M. *Langmuir* 2001, **17**, 6524-6529.

61. Mowery, C. L.; Crosby, A. J.; Ahn, D.; Shull, K. R. *Langmuir* 1997, **13**, 6101-6107.

62. Shull, K. R.; Ahn, D.; Chen, W.-L.; Flanigan, C. M.; Crosby, A. J. *Macromolecular Chemistry and Physics* 1998, **199**, 489-511.

63. Shull, K. R.; Flanigan, C. M.; Crosby, A. J.; *Physical Review Letters* 2000, **84**, 3057-3060.

64. Crosby, A. J.; Shull, K. R.; Lakrout, H.; Creton, C. *Journal of Applied Physics* 2000, 88, 2956-2966.

65. Webber, R. E.; Shull, K. R.; Roos, A.; Creton, C. *Physical Review E* 2003, 68, 021805.

66. Lakrout, H.; Sergot, P.; Creton, C. *The Journal of Adhesion* 1999, **69**, 307-359.

67. Creton, C.; Lakrout, H. *Journal of Polymer Science: Part B: Polymer Physics* 2000, **38**, 965-979.

68. Chung, J. Y.; Chaudhury, M. K. *The Journal of Adhesion* 2005, **81**, 1119-1145.

69. Chaudhury, M. K. and Kim, K. H. *The European Physical Journal E* 2007, **23**, 175-183.

70. Yebra, D. M., Kiil, S., and Dam-Johansen, K. *Progress in Organic Coatings* 2004, **50**, 75-104.

71. Fingerman, M., Nagabhushanam, R., and Thompson, M.-F., editors. *Recent Advances in Marine Biotechnology, Volume 3: Biofilms, Bioadhesion, Corrosion, and Biofouling*. Science Publishers, Inc.: Enfield, NH, 1999.

72. Becka A.; Loeb G. *Biotechnology and Bioengineering* 1984, **26**, 1245-1251.

73. Swain, G. W.; Schultz, M. P. *Biofouling* 1996, **10**, 187-197.

74. Sun, Y. J.; Guo, S. L.; Walker, G. C.; Kavanagh, C. J.; Swain, G. W. *Biofouling* 2004, **20**, 279-289.

75. Brady, R. F. and Singer, I. L. *Biofouling* 2000, **15**, 73-81.

76. Singer, I. L.; Kohl, J. G.; Patterson, M. *Biofouling* 2000, **16**, 301-309.

77. Chaudhury, M. K.; Finlay, J. A.; Chung, J. Y.; Callow, M. E.; Callow, J. A. *Biofouling* 2005, **21**, 41-48.

Chapter 2

Using Electrocapillarity to Measure the Zeta Potential of a Planar Hydrophobic Surface [a]

ABSTRACT

A method is introduced for determining the zeta potential of planar surfaces by combining electroosmosis and capillarity. In this method, an electric field is applied across a channel, which is filled with aqueous solution seeded with fluorescent tracer particles. Some excess liquid is applied on both ends of the channel, which bulges out and modulates the capillary force across the channel by adjusting its curvature. While the velocity profile in the channel approaches steady state, a balance of the electroosmotic stress and Laplace pressure difference is achieved across the channel. However, as soon as the electric field is turned off, a Poiseuille flow develops in the channel due to the difference in the curvatures of the liquid bulges. We show that the measurement of the centerline velocity of the liquid inside the channel is enough to deduce the zeta potential of the surface. Utilizing this technique, the zeta potential of hydrophobic glass surface (silanized by *n*-hexadecyltrichlorosilane, HC-16) has been measured to be -52.2 ± 7.7 mV in distilled de-ionized water, which is in close agreement with the literature values.

2.1. INTRODUCTION

Almost all solid surfaces become charged when they come in contact with water. These charges attract counter-ions near the surface resulting in the formation of an electrical double layer (EDL). Zeta potential is defined as the electrical potential on the imaginary shear plane that is the interface of the compact layer and diffuse layer in the EDL.[1,2]

Zeta potentials of planar surfaces are usually measured using a rectangular microchannel in several ways as reviewed by Kirby and Hasselbrink[2] as well as Yan and Yang[3]. The traditional method measures the streaming potential or streaming current[2-7], which develops across the channel in response to a pressure driven flow. Another method proposed by Hozumi *et al.*[8] is to evaluate the entire velocity profile of the fluid across the height of the channel. Although this method estimates the zeta potential accurately, it is a somewhat tedious approach. Another problem with this method is that the zeta potential of the seed particles themselves that are used to measure the velocity profiles need to be known. Sze *et al.*[9] estimated the zeta potential from the slope of the current-time relation, which is measured in electroosmotic flow, in conjunction with the Smoluchowski equation. Recently, Yan *et al.*[3] developed a system for measuring the zeta potentials of the channel surfaces and tracer particles simultaneously by utilizing the microparticle image velocimetry. They analyzed the instantaneous particle velocity profile in both the open- and closed-ended rectangular microchannels by the least-square method. Nevertheless, two channels are required for this technique.

In this chapter, a simple method is introduced for the determination of the zeta

potential of a planar surface that is related to the electro-capillary drop switch idea of ref [10]. Electroosmosis involves the flow of excess counter-ions in the diffuse layer of the EDL due to the application of an electric field. The counter-ions drag the fluid to generate an electroosmotic flow. As an electric field is applied across the negatively surface-charged rectangular channel (Fig. 2.1), the fluid in the channel is driven to the negative electrode. Therefore, the volume of liquid on the positive-electrode side
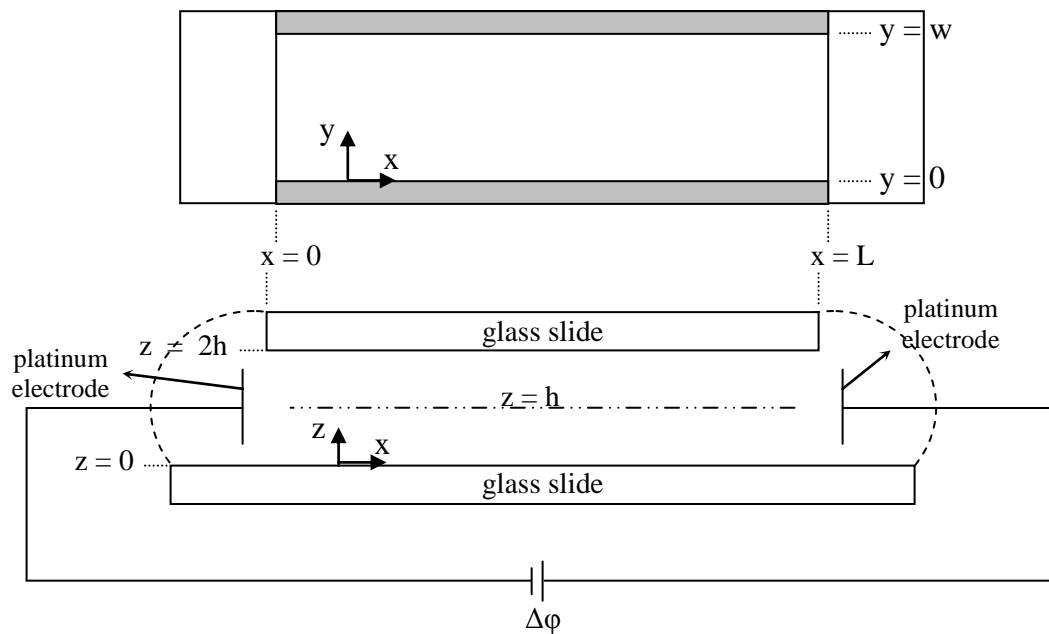
Figure 2.1. Schematic illustration of the microchannel prepared by glass slides. The upper part shows the top view (-z direction) of the channel. The grey rectangles are the Scotch® double-sided tape, which are used to attach the two slides at their edges, and w is the width of the channel. The lower part exhibits the front view (+y direction) of the channel. The dash lines indicate the fluid boundaries before an electric field applied. L and 2h represent, respectively, the length and height of this channel. z = h is the centerline of the channel. A potential difference Δφ in DC voltage is applied across the fluid in the channel via the platinum electrodes. The illustration is not to scale.

decreases, while that on the negative-electrode side increases. The changes of liquid volume lead to changes of the liquid boundary curvatures on both sides. This curvature difference gives rise to a Laplace pressure gradient that balances with the gradient of electrical and viscous stresses at a steady state. The amount of Laplace pressure difference is proportional to the zeta potential and the applied electric field strength. If the field is now turned off after the steady state is reached, Poiseuille flow of liquid occurs from the higher curvature towards the lower curvature region. By measuring the centerline velocity in the channel, under Poiseuille flow conditions, the Laplace pressure difference can be inferred and the zeta potential can be estimated.

In order to study the applicability of this method, we chose silanized glass as a model surface. Channels were formed by separating two such slides with two open ends. Zeta potential was measured by full velocity profile measurement as well as with the technique introduced here.

2.2. MEASUREMENT OF ZETA POTENTIAL

The single channel (Fig. 2.1) is filled with the test solution, which has been seeded with fluorescent tracer particles. After the electric field is applied, a steady state velocity profile develops within the channel. When the field is turned off, the centerline velocity is measured using the tracer particles. The analytical expressions used for this method are described below.

Let us consider the test channel shown in Fig. 2.1, the height of which is much

smaller than the length and width (*i.e.*, L/2h and w/2h >> 1). Thus, the edge effects (at y = 0 and w) should be negligible. The velocity profile is regarded as uniform along the x direction. As a result, this system can be reduced to a steady, fully-developed, and one-dimensional flow, where the standard balance of the viscous, electrical, and hydrostatic stresses[1,11,12] gives

$$\eta \frac{d^2 v}{dz^2} - \epsilon \epsilon_0 E\left(\frac{d^2 \psi}{dz^2}\right) - \frac{dp}{dx} = 0,$$ (2.1)

where η and v represent, respectively, the viscosity and velocity (in x direction) of the fluid in the channel. *E* is the applied electric field and *dp/dx* is the pressure gradient generated across the channel. ψ is the electrical potential at a given point in the channel. ε and ε_0 are the dielectric constants of the medium and the vacuum, respectively. It is assumed that the thickness of the EDL (λ) is very small compared with half of the channel height in this system (*i.e.* $\lambda \ll$ h). Hence, the electrical potential at the centerline of the channel (z = h) is not affected by the zeta potential of the channel wall at the shear plane (ζ_w). Using the well-known boundary conditions of electroosmotic flow, (no slip and no penetration at the walls, symmetrical velocity profile about the centerline, zero potential at the centerline of the channel, and finite potential at the wall), equation 2.1 can be integrated to yield the following well-known equation of electroosmosis[1,12]:

$$v = \frac{h^2}{2\eta} \frac{dp}{dx}\left(H^2 - 2H\right) - \frac{\epsilon \epsilon_0 E}{\eta}\left(\zeta_w - \psi\right) \text{ with } H = \frac{z}{h}.$$ (2.2)

Since the negatively charged tracer particle is used, equation 2.2 needs to be modified by its electrophoretic velocity (v_{ep})[3,13], that is,

$$v = \frac{h^2}{2\eta} \frac{dp}{dx} \left(H^2 - 2H\right) - \frac{\epsilon_0 E}{\eta} \left(\zeta_w - \psi\right) + \frac{2}{3} \frac{\epsilon_0 E}{\eta} f\zeta_p, \qquad (2.3)$$

where

$$v_{ep} = \frac{2}{3} \frac{\epsilon_0 E}{\eta} f\zeta_p.$$

ζ_p is the zeta potential of the tracer particle, and f is the Henry's function[1,3]. Two methods are used to estimate the ζ_w.

Standard Method: **Determination of zeta potential using the full velocity profile within the channel**

After applying an electric field across the channel, one waits until a steady electroosmotic flow is developed. ζ_w is evaluated by fitting the steady-state velocity profile across the height of the channel with equation 2.3. Since the experimental velocity profiles are measured far from the surface and the electrical double layer and since the surface potential drops off rapidly from the surface, $\psi(H) \approx 0$ in our case. The experimental velocity profile (v_{exp}) is as follows:

$$v_{exp} = A\left(H^2 - 2H\right) + B. \qquad (2.4)$$

A and B are defined as follows:

$$A = \frac{h^2}{2\eta} \frac{dp}{dx}, \quad B = -\frac{\epsilon_0 E}{\eta} \zeta_w + \frac{2}{3} \frac{\epsilon_0 E}{\eta} f\zeta_p. \qquad (2.5)$$

At steady state, the total mass flow rate is zero in the channel. Therefore, the electrophoretic velocity of the tracer particle is given by the non-zero component of the

27

velocity integration as follows:

$$v_{ep} = \frac{\int_0^2 v\,dH}{\int_0^2 dH} = -\frac{2}{3}A - \frac{\varepsilon_0 E}{\eta}\zeta_w + v_{ep}$$

$$\Rightarrow A = -\frac{3\varepsilon_0 \zeta_w}{2\eta}E. \tag{2.6}$$

The velocity profile of the tracer particles are measured and then fitted into equation 2.4 to yield the value of A.

Modified Method: **Determination of zeta potential by measuring the particle velocity at the centerline of the channel (H = 1) with the electric field turned off at steady state**

In this method, the electric field is turned off after the flow reaches a steady state. As soon as the field is off, the centerline velocity (v'_{max}) is measured. As the flow is now of the pure Poiseuille type, v'_{max} can be estimated as follows:

$$v'_{max} = -\frac{h^2}{2\eta}\frac{dp}{dx}. \tag{2.7}$$

The pressure gradient of equation 2.7, however, resulted from the balance of the electroosmotic stress, Thus, using eq. 2.5-2.7, one obtains

$$v'_{max} = \frac{3\varepsilon_0 \zeta_w}{2\eta}E. \tag{2.8}$$

Equation 2.8 implies that v'_{max} is a function of the applied field before it was turned off.

Equations 2.6 and 2.8 suggest that v'_{max} can also be calculated by the coefficient A (obtained in *Standard Method*) as follows:

$$v'_{max} = -A = \frac{3\varepsilon_0 \zeta_w}{2\eta} E.$$ (2.9)

According to equations 2.8 and 2.9, plots of v'_{max} against E are constructed for the two different methods. These plots should superimpose, and the value of ζ_w can be estimated from the slopes of these plots.

2.3. EXPERIMENTAL

2.3.1. Preparation and Analysis of Self-Assembled Monolayer (SAM) Surfaces

SAM surfaces were prepared by utilizing the procedure proposed by Chaudhury and Whitesides[14] with some modifications. Several Fisherbrand® glass slides ($75 \times 25 \times 1$ mm; Fisher Scientific) were cut into *ca.* 52 mm in length for channel preparation. All the slides were immersed in piranha solution (30 vol % hydrogen peroxide in 70 vol % sulfuric acid) for 30 minutes. The slides were thoroughly rinsed with distilled de-ionized water (DI water; Barnstead), followed by drying with ultra-pure nitrogen. These slides were then treated with oxygen plasma (model PDC-32G; Harrick Plasma) at 0.2 torr for 45 seconds. After the plasma treatment, the slides were transferred to a 15-cm Petri dish. A filter paper containing 400-μL *n*-hexadecyltrichlorosilane (HC-16; Gelest Inc.) was attached to the inner side of the Petri dish cover. This Petri dish, with the plasma-treated slides, was placed in a sealed glass container in vacuum for 2 h.

Subsequently, these slides were gently rinsed with DI water and dried with ultra-pure nitrogen. For fluorocarbon SAM surfaces, instead of using a filter paper, the *1H,1H,2H,2H*-perfluorodecyltrichlorosilane (FC-10; Lancaster Synthesis) was mixed with 3 g of mineral oil (Sigma-Aldrich) in a small Petri dish (dia. 3 cm) and placed at the center of the large Petri dish (dia. 15 cm) with the clean glass slides for silanization.[15]

The stability of the SAM layer was evaluated with the immersion of NaOH solution at pH 10. The hydrophobicity of these surface-modified slides was evaluated by the advancing (θ_a) and receding (θ_r) contact angles of water measured with the sessile drop method.

2.3.2. Experimental Setup

The test channel was prepared with two glass slides with the same surface functionalities. For the length of the two slides, one was 52 mm and the other was 75 mm. Since the walls of the channel were hydrophobic because of HC-16 of FC-10 functionality, they were not suitable for containing aqueous solutions. In order to solve this problem, a glass cutter was used to slightly scratch on the two shorter edges (i.e., at x = 0 and L in Fig. 2.1) of the 52-mm slide at the silanized side. Both ends of the channel thus became hydrophilic so that aqueous solutions could be easily held in the channel. This slide, which was attached with Scotch® double-sided tapes[16] along the longer edges, was affixed to the other 75-mm silanized one to form the channel.

This microchannel was filled with DI water[17] seeded with fluorescent particles (FluoSpheres® carboxylate-modified microspheres, 0.5 µm, yellow-green fluorescent; Invitrogen Co.) by applying gentle suction from one end of the channel. Monitored by a multimeter, a power supply (Cat. No. 3-1008; Buchler Instruments) was used to control the output DC voltage applied across the channel (Fig. 2.2). The channel was adjusted to lie horizontally on the stage of the microscope (model Diaphot; Nikon). The incident light source was provided from a Nikon 100-W mercury lamp with a HB-10101AF power supply. Incident light, which was transferred to fluorescent emission via the fluorescence filter (Nikon DM510), passed through the objective (40× magnification) and reached to the sample. Simultaneously, the image of the fluorescent particles was observed and recorded on the computer via a Sony XC-75 CCD camera.
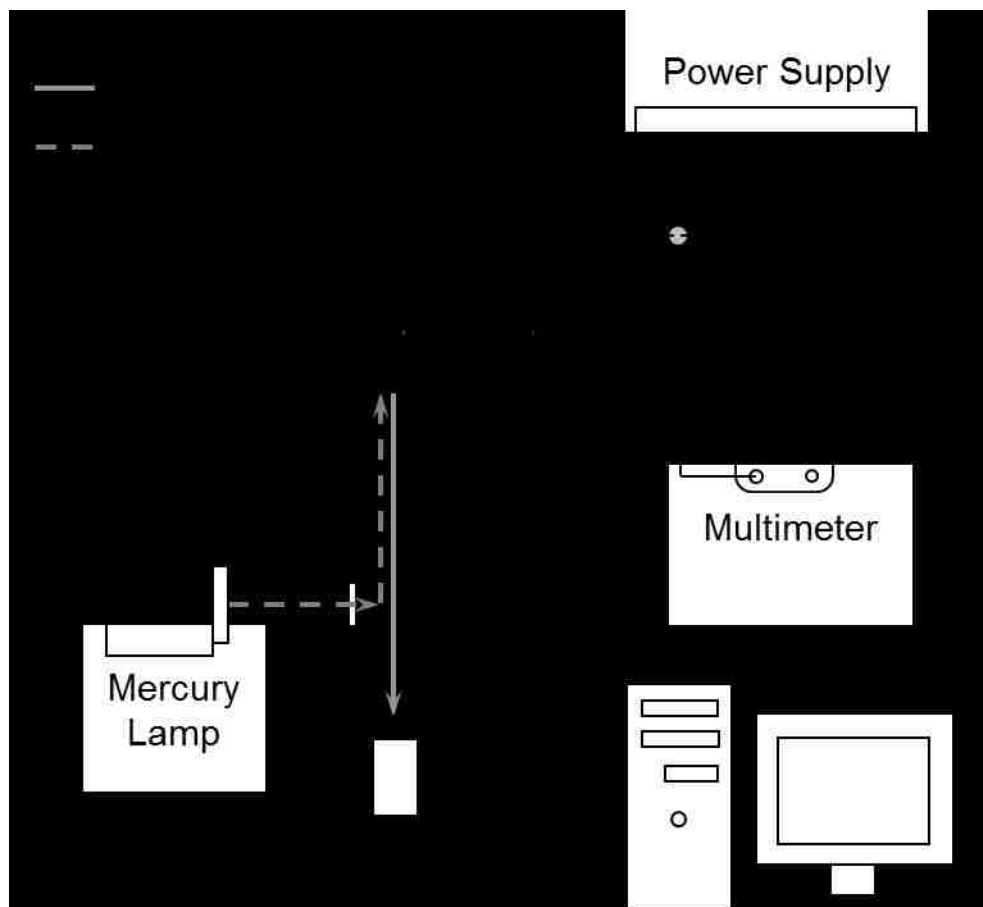
Figure 2.2. Schematic illustration of the experimental setup. The incident light from the mercury lamp is re-directed by the fluorescence filter. The transferred fluorescent light reaches the test channel after passing through the microscope objective. The voltage difference of the channel is controlled by the power supply and measured with a multimeter. The fluorescent light emitted from the seeded particles is observed through the CCD camera. A computer connected with the CCD camera records the images of the fluorescent particles.

2.3.3. Measurement of Velocity Profile in the Channel

Before the application of electric fields across the system, the particles exhibit Brownian motion without any net drift thus ensuring that the fluid in the channel is in a static state. After the field was applied, the objective of the microscope was adjusted to focus on different layers in the channel at different applied voltages. The velocity profiles at x ~ L/2 and y ~ w/2 (i.e., at half the channel length and width, respectively, in Fig. 2.1) were measured as they approached a steady state (approximately 5-15 min). The uppermost and bottommost focused planes were determined first to allow the estimation of the height (2h) and centerline (z = h) of the channel. First, the images of the particles on different layers were recorded (for *Standard Method*). Then, the objective was focused on the centerline of the channel for the subsequent image recording immediately after turning off the power supply (for *Modified Method*). These recorded images were analyzed using ImageJ software coupled with SpotTracker plug-in[18]. Several focused fluorescent particles in the image sequences were selected for estimating the particle velocities, which were used to calculate the zeta potential (ζ_w^{HC-16}) of the HC-16 surface.

2.4. RESULTS AND DISCUSSION

2.4.1. Analysis of SAM Surfaces

As expected, the SAM-coated glass slides became hydrophobic as evidenced from the contact angle of water on these surfaces (Table 2.1). The advancing and receding

contact angle on these surfaces were very similar to the literature values[19-21].

Table 2.1. Water contact angles of test glass surfaces.

Material	Advancing (θ_a)	Receding (θ_r)
Piranha-treated glass slide	$< 5°$	$< 5°$
Glass slide with HC-16 SAM surface	$110°\ \pm 2$	$96°\ \pm 2$
Glass slide with FC-10 SAM surface	$117°\ \pm 2$	$93°\ \pm 1$

According to the literature[21], a SAM prepared from tetradecyltrichlorosilane should be stable in 0.1 N HCl for more than 40 h at room temperature. However, loss of 50% of monolayer was found in the immersion of 0.1 N NaOH (i.e., pH 13) after 80 min. Although the pH we used for the experiment was smaller than 13, it was essential to examine the stability of the silanized surfaces in contact with NaOH at pH 10. The water contact angles (Fig. 2.3) showed that the SAMs prepared by both HC-16 and FC-10 were still stable with the treatment of NaOH at pH 10 within 2 days. This result gave us confidence that the silanized surfaces were stable in the solution condition that we used for zeta potential measurement. Nevertheless, monolayer began to degrade dramatically after about 300 min for HC-16 surface and 60 min for FC-10 substrate in the immersion of NaOH at pH 11 (data not shown).
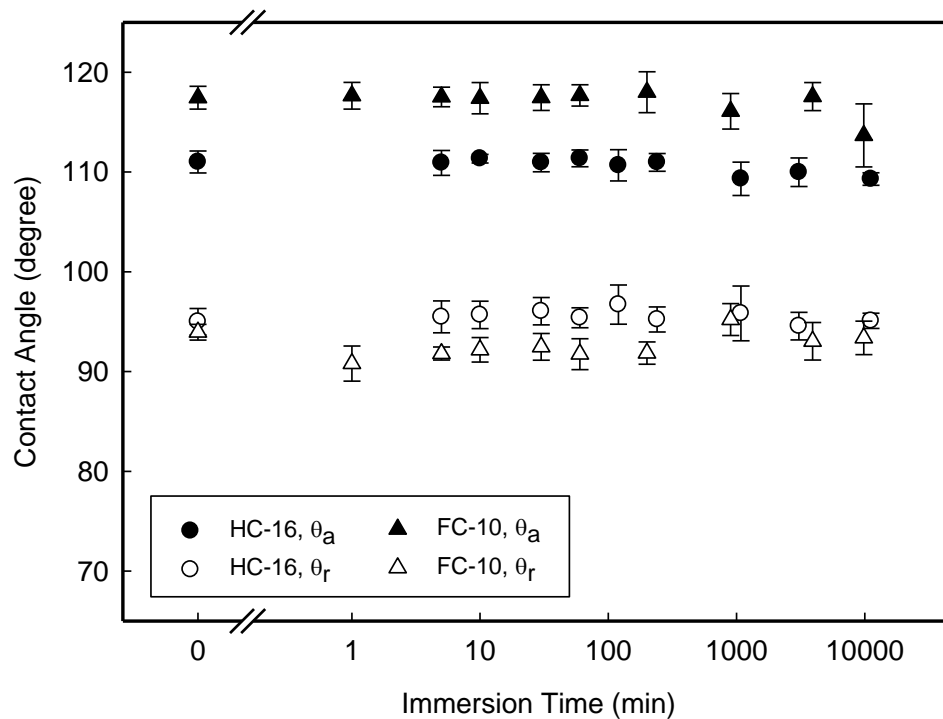
Figure 2.3. The water contact angles of HC-16 (circles) and FC-10 (triangles) surfaces, which were immersed in NaOH solution at pH 10. The advancing (θ_a, closed symbols) and receding (θ_r, open symbols) contact angles were measured with the sessile drop method.

2.4.2. ζ_w Measurement of the Channel

The length (L), height (2h), and width (w) of the test channel (Fig. 2.1) are about 52 mm, 0.1 mm, and 20 mm, respectively, which satisfies the assumption that L/2h and w/2h >> 1, so that the edge effects in the channel are negligible.

In the first method, the entire velocity profile of the tracer particles was measured and fitted to equation 2.4. The coefficients (A and B) of equation 2.4 are estimated by quadratic regression of the data shown in Fig. 2.4. Using the coefficient A, the left-hand side of equation 2.9 is calculated at the corresponding electric field strength (Fig. 2.5,

open squares). The plot of this parameter against $-E$ yields the value of HC-16 surface zeta potential (ζ_w^{HC-16}) as -50.1 mV utilizing the standard values of the viscosity ($\eta = 8.94 \times 10^{-4}$ N-s/m^2) and dielectric constant ($\varepsilon = 78.5$) of water. Combing this result with two more repeated measurements, the ζ_w^{HC-16} was estimated to be -48.3 ± 1.5 mV.
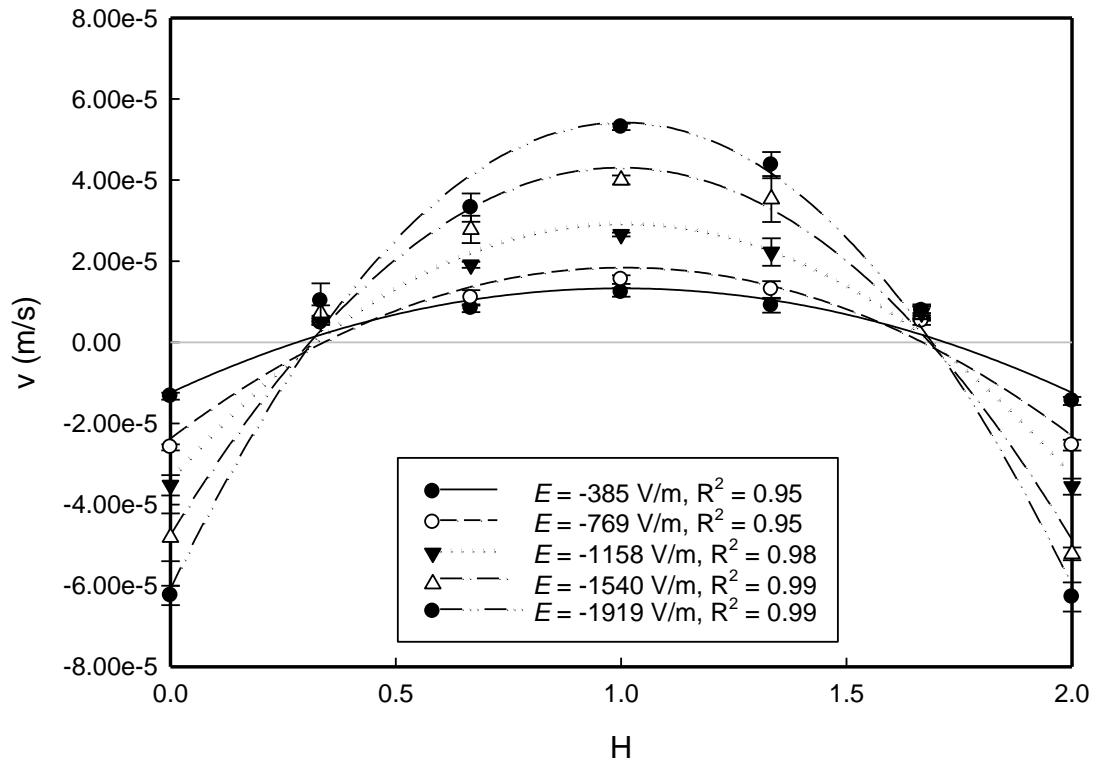
Figure 2.4. The particle velocity profiles across the height of the channel under different electric field strength (E) in distilled de-ionized water. Each datum reported here is the average of five measurements. The electric field in a rectangular channel is estimated as $E = \Delta\varphi/L$. The pH of the DI water was measured to be 6.5 at 25 °C. The dimensionless x coordinate is H = z/h (Fig. 2.1). Each quadratic regression is fitted into eq. 2.4 by particle velocities (v) sampled in seven different layers in the channel with the electric field on.

$\zeta_w^{\text{HC-16}}$ was next calculated with the proposed method (eq. 2.8), where the maximum centerline velocity of the tracer particle was measured after turning off the field (Fig. 2.5, closed circles). $\zeta_w^{\text{HC-16}}$ is found to be -53.9 mV from the slope of equation 2.8 and -51.1 ± 2.8 mV based on three measurements. The values of the zeta potential obtained by both methods agree within ±~5% similar thus giving us confidence about the validity of the method proposed here.
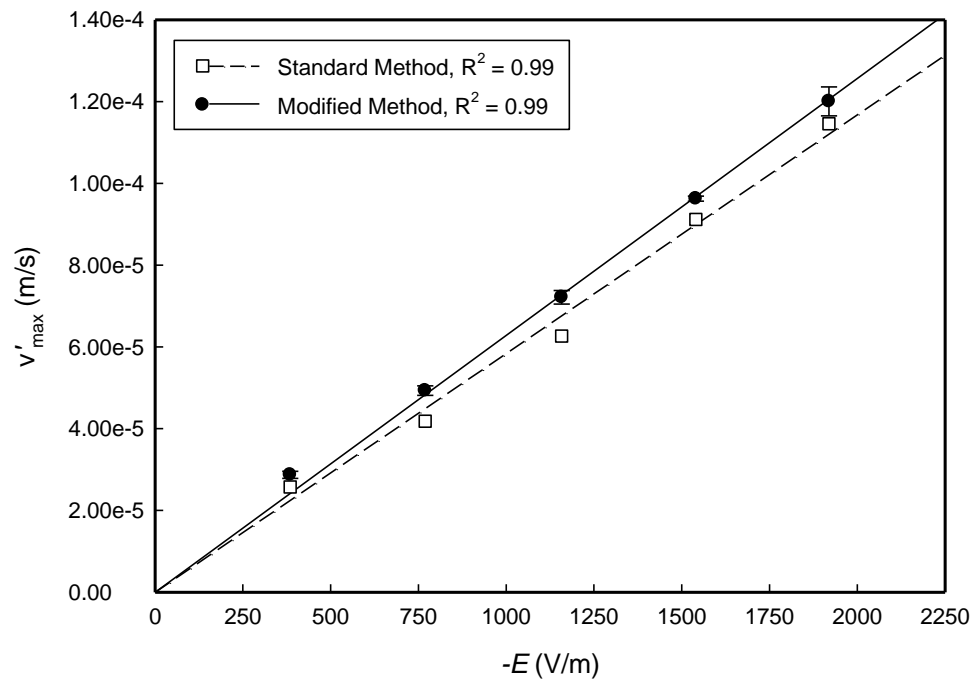
Figure 2.5. The relation between average particle velocities (v'_{max}) and applied electric field strength (E). The slopes of the standard linear regressions are 5.84×10^{-8} for *Standard Method* and 6.28×10^{-8} for *Modified Method*. The inner surfaces of the channel were silanized with HC-16. For the open-square ($\square$), the values of v'_{max} are calculated with parameter A determined by curve fitting of the data shown in Fig. 2.4 with eq. 2.4. This reveals the relation between v'_{max} and E while the electric fields are on (eq. 2.9). For the closed-circles ($\bullet$), the velocity profile of the particle in the channel was allowed to reach a steady state with the testing electric field. Then, v'_{max}, the particle velocity at the centerline (z = h in Fig. 2.1) was measured immediately after the electric field was turned off (eq. 2.8).

Using the *Modified Method*, repeated measurement of the zeta potential shows the value of $\zeta_w^{\text{HC-16}}$ to be -52.2 ± 7.7 mV in DI water (pH ~6.7). The negative zeta potential of a hydrophobic surface in water is consistent with numerous reports[3,6,8,9,22-33] in the literature. The zeta potential that we measure is more negative than that (~ -30 mV at pH 7) of a comparable –CH_3-modified surface as reported by Hozumi[8] and Shyue[26]. This could be attributed to the use of DI water in our studies, in contrast to the 1-mM potassium chloride aqueous solutions used by the other groups. It is well-known that for electrolyte solutions, ions suppress the EDL thereby causing the magnitude of zeta potential to decrease.[3,5,9,23] Since there are no electrolyte ions in the system, except those arising from the dissociation of water, the zeta potential is more negative in our case.

We further examined the zeta potentials of HC-16 and FC-10 surfaces as a function of pH (Fig. 2.6). The FC-10 surface exhibits more negative zeta potential (~30-45 mV) than that of the HC-16 one at values of pH ranging from 4.0 to 10.0. The zeta potential values of these two surfaces become more and more negative with the pH and reach constants (-66.1 mV for HC-16 and -106.0 mV for FC-10) above pH 7.0. A more detailed discussion about the difference of the zeta potential between HC-16 and FC-10 surfaces is provided in Chapter 4.4.2.
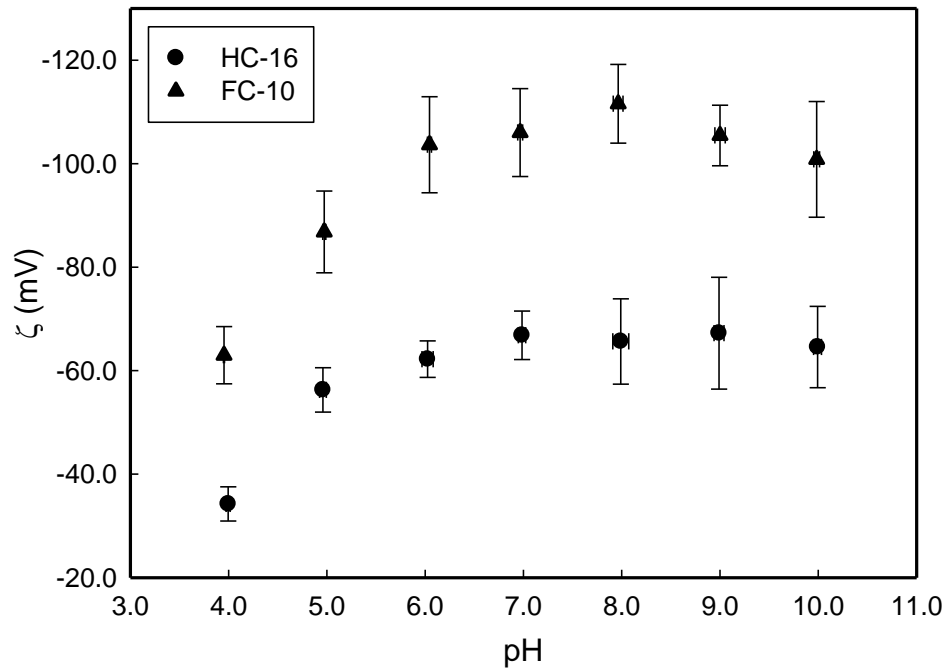
Figure 2.6. Zeta potentials (ζ) of HC-16 (circles) / FC-10 (triangles) surfaces as a function of pH. The pH of DI water was adjusted by adding either HCl or NaOH.

2.5. SUMMARY

We successfully implemented a simple method of measuring zeta potential by taking advantage of the electro-capillary effect. This modified method yields values of zeta potential that are consistent with the standard method. The advantage of this method is that only the velocity of the seeded particle at the centerline of the channel is needed without the consideration of its zeta potential.

REFERENCES

1. Li, D. Q. *Electrokinetics in Microfluidics*; Elsevier Academic Press: San Diego, CA, 2004.

2. Kirby, B. J.; Hasselbrink, E. F. *Electrophoresis* 2004, **25**, 187-202.

3. Yan, D. G.; Yang, C.; Nguyen, N. T.; Huang, X. Y. *Electrophoresis* 2006, **27**, 620-627.

4. Werner, C.; Körber, H.; Zimmermann, R.; Dukhin, S.; Jacobasch, H. J. *Journal of Colloid and Interface Science* 1998, **208**, 329-346.

5. Gu, Y. G.; Li, D. Q. *Journal of Colloid and Interface Science* 2000, **226**, 328-339.

6. Zimmermann, R.; Dukhin, S.; Werner, C. *Journal of Physical Chemistry B* 2001, **105**, 8544-8549.

7. Delgado, A. V.; González-Caballero, E.; Hunter, R. J.; Koopal, L. K.; Lyklema, J. *Pure and Applied Chemistry* 2005, **77**, 1753-1805.

8. Hozumi, A.; Sugimura, H.; Yokogawa, Y.; Kameyama, T.; Takai, O. *Colloids and Surfaces A: Physicochemical and Engineering Aspects* 2001, **182**, 257-261.

9. Sze, A.; Erickson, D.; Ren, L. Q.; Li, D. Q. *Journal of Colloid and Interface Science* 2003, **261**, 402-410.

10. Vogel, M. J.; Ehrhard, P.; Steen, P. H. *Proceedings of the National Academy of Sciences* 2005, **102**, 11974-11979.

11. Deen, W. M. *Analysis of Transport Phenomena*; Oxford University Press: New York, NY, 1998, p 252-254.

12. Masliyah, J. H.; Bhattacharjee, S. *Electrokinetic and Colloid Transport Phenomena*;

Wiley-Interscience: Hoboken, NJ, 2006, p 221-243.

13. Marziali, A.; Pel, J.; Bizzotto, D.; Whitehead, L. A. *Electrophoresis* 2005, **26**, 82-90.

14. Chaudhury, M. K.; Whitesides, G. M. *Langmuir* 1991, **7**, 1013-1025.

15. It has been observed the FC-10 would react with moisture and form white precipitate quickly while exposed to the air. As a result, instead of using a filter paper, mineral oil was utilized as a carrier medium.

16. The use of the double sticky tape to seal the channel may of some concern as it may provide potential contamination. We, however, feel that this effect is negligible in our experiments because of the thin thickness (~ 100 micron) of the tape exposed towards water. We also found that the value of the ζ_w^{HC-16} obtained after repeated washing and filling the channel with degassed DI water yielded same zeta potential values, which gave us some confidence that the role of potential impurities is negligible.

17. There are evidences that the small air bubbles present in water can adhere to a surface and modify its properties. In order to eliminate the possible effects of dissolved gases and bubbles, it is recommended that water can be purified by first boiling and then cooling under nitrogen (e.g., reference 28). We performed a controlled experiment in which DI water was first boiled then cooled in a nitrogen environment at room temperature. ζ_w^{HC-16} measured (-50.0 mV) with this method is found to be close to that (-52.2 mV) we measured with DI water. We thus feel that the dissolved gas or potential air bubbles in DI water had minimum influence in

our experiments.

18. Sage, D.; Neumann, F. R.; Hediger, F.; Gasser, S. M.; Unser, M. *IEEE Transactions on Image Processing* 2005, **14**, 1372-1383.

19. Chung, J. Y.; Kim, K. H.; Chaudhury, M. K.; Sarkar, J.; Sharma A. *European Physical Journal E* 2006, **20**, 47-53.

20. Ulman A. *An Introduction to Ultrathin Organic Films: From Langmuir-Blodgett to Self-Assembly*; Academic Press, Inc.: San Diego, CA, **1991**.

21. Wasserman, S. R.; Tao, Y. T.; Whitesides, G. M. *Langmuir* 1989, **5**, 1074-1087.

22. Yoon, R. H.; Yordan, J. L. *Journal of Colloid and Interface Science* 1986, **113**, 430-438.

23. Marinova, K. G.; Alargova, R. G.; Denkov, N. D.; Velev, O. D.; Petsev, D. N.; Ivanov, I. B.; Borwankar, R. P. *Langmuir* 1996, **12**, 2045-2051.

24. Karraker, K. A.; Radke, C. J. *Advances in Colloid and Interface Science* 2002, **96**, 231-264.

25. Churaev N. V.; Ralston J.; Sergeeva I. P.; Sobolev V. D. *Advances in Colloid and Interface Science* 2002, **96**, 265-278.

26. Shyue, J. J.; De Guire, M. R. *Langmuir* 2004, **20**, 8693-8698.

27. Kirby, B. J.; Hasselbrink, E. F. *Electrophoresis* 2004, **25**, 203-213.

28. Beattie, J. K.; Djerdjev, A. M. *Angewandte Chemie International Edition* 2004, **43**, 3568-3571.

29. Beattie, J. K. *Lab on a Chip* 2006, **6**, 1409-1411.

30. Najafi, A. S.; Drelich J.; Yeung A,; Xu, Z. H.; Masliyah J. *Journal of Colloid and*

Interface Science 2007, **308**, 344-350.

31. Boyson, T. K.; Pashley, R. M. *Journal of Colloid and Interface Science* 2007, **316**, 59-65.

32. McCarty, L. S.; Whitesides, G. M. *Angewandte Chemie International Edition* 2008, **47**, 2188-2207.

33. Tandon, V.; Bhagavatula, S. K.; Nelson, W. C.; Kirby, B. J. *Electrophoresis* 2008, **29**, 1092-1101.

Chapter 3

The Zeta Potential of Planar Hydrophobic Surfaces in Contact with Nonionic Surfactant Solutions [b]

ABSTRACT

The new technique introduced in Chapter 2 has been used to estimate the zeta potential of hydrophobic glass surfaces (silanized by either *n*-hexadecyltrichlorosilane, or *1H,1H,2H,2H*-perfluorodecyltrichlorosilane) in contact with the aqueous solutions of polyoxyethylene (23) lauryl ether (Brij 35). The zeta potentials here remain constant for a while and then they continue to become less negative as the concentration of the surfactant increases above the critical micelle concentration (CMC). This effect, where changes take place beyond CMC, but not below it, leads to a complementary Gibbs plot, where all the changes occur below CMC but not above it. This change in the zeta potential could be caused by either the adsorption of hydroxide ions in the solution or the H-bond concentration variation near the poly(ethylene oxide) chain in Brij 35.

3.1. INTRODUCTION

Hydrophobic surfaces have been widely utilized to design microchannels.[1-4] Since most surfaces become charged while they are in contact with aqueous solutions, these charges may affect the application of the channels. The zeta potential (an indication of the strength of the surface charge) of a hydrophobic surface is dependent on the solution properties, for example, pH, electrolyte concentration, and surfactant additives. As reviewed by Kirby and Hasselbrink[5], the zeta potential of various polymer surfaces becomes more and more negative with the increase of pH. It is also well-known[1,5-8] that the addition of electrolytes decreases the magnitude of zeta potential since ions could affect the electrical double layer at the solid/liquid interface. Introducing non-ionic surfactants[5,8-13] into the solution can alter the zeta potential as well.

The adsorption of nonionic surfactants containing poly(ethylene oxide) (PEO) on different surfaces has been widely studied.[13-23] For hydrophobic surfaces, the surfactant is considered[13-25] to be adsorbed on the substrate with the hydrophobic end, whereas the hydrophilic moiety turns towards to the solution. Tiberg and Grant *et al.*[20-22] proposed that the polyoxyethylene alcohols are capable of forming monolayers on two hydrocarbon substrates, diethyloctylchlorosilane silanized silica and hexadecanethiol coated gold. Szymczyk and Jańczuk[23] also investigated the monolayer formed by two polyoxyethylene alkylphenols at different mix ratios on a poly(tetrafluoroethylene) surface. Furthermore, with the PEO surfactant populated on the surface, it has been reported[5,8-13] that a hydrophobic substrate still exhibits negative zeta potential.

In this chapter, we studied the zeta potential of a hydrocarbon surface as a function

of the concentration of polyoxyethylene (23) lauryl ether at a given pH (~6.7). Utilizing a surface modified with such a nonionic surfactant, we aimed at investigating the possible cause of the negative zeta potential of hydrophobic surfaces in contact with aqueous solutions.

3.2. EXPERIMENTAL

3.2.1. Preparation of Self-Assembled Monolayer (SAM) Surfaces and Measurement of Zeta Potentials

The detailed procedures of SAM preparation and zeta potential measurement are given in Chapter 2.3.1. The glass slide surface was silanized with either *n*-hexadecyltrichlorosilane (HC-16; Gelest Inc.) or *1H,1H,2H,2H-*perfluorodecyltrichlorosilane (FC-10; Lancaster Synthesis).

The solution of polyoxyethylene (23) lauryl ether (Brij 35, $CH_3(CH_2)_{11}(OCH_2CH_2)_{23}OH$; Sigma) was prepared with fresh DI water. These solutions seeded with fluorescent tracers (FluoSpheres® carboxylate-modified microspheres, 0.5 µm, yellow-green fluorescent; Invitrogen Co.) were utilized to fill the channel. In each experiment, the channel was rinsed with DI water then filled with the lowest concentration of Brij 35. After the measurement was completed with one specific concentration of the surfactant, the channel was then filled with a surfactant of higher concentration and the process was repeated until the highest concentration of the surfactant was used.

3.2.2. Measurement of the Properties of the Surfactant

The pH of the Brij 35 solution was adjusted to ~6.7 by addition of 20-mM NaOH solution. Brij 35 contained some oxidizing impurities as reported in the literature[26]. The solution viscosities were measured with a rheometer (model AR 1000-N; TA Instruments). The surface tension of Brij 35 aqueous solution at different concentration was measured by the du Noüy ring method (Fisher model 215 autotensiomat surface tension analyzer; Fisher Scientific). The Brij 35 solution was also utilized as a test liquid for the contact angle measurement on the HC-16 and FC-10 surfaces with the sessile drop method. The advancing (θ_a) and receding (θ_r) angles of the liquid drops were estimated after 10 and 60 seconds of the solution droplet in contact with the surface, respectively.

3.3. RESULTS AND DISCUSSION

3.3.1. Verification of New Technique of Zeta Potential Measurement in the Presence of
    a Nonionic Surfactant

The zeta potential of the HC-16 surface ($\zeta_w^{HC\text{-}16}$) was estimated by both the *Standard* and *Modified Method* as mentioned in Chapter 2.2. The viscosities of the Brij 35 solutions were measured, and the effect of viscosity change was rather insignificant to the zeta potential. We again note the consistency of the $\zeta_w^{HC\text{-}16}$ values estimated by both the methods with different Brij 35 solutions (Table 3.1). A closed-cell elctroosmosis was also performed to measure $\zeta_w^{HC\text{-}16}$ (Fig. 3.1; see Chapter 4.2 for

detailed experimental procedures), and the zeta potential values are in fairly good agreement with the new technique. These results provide further confidence to the method of measuring zeta potential proposed in Chapter 2.

Table 3.1. Experimental results of $\zeta_w^{HC\text{-}16}$ calculation in both the methods, with the utilization of different concentrations of Brij 35 aqueous solutions.

Brij 35 concentration ($\times 10^{-6}$ M)	Below CMC				Above CMC		
	0	0	10.0	50.1	100.5	252.1	751.3
Standard Method $\zeta_w^{HC\text{-}16}$ (mV)	-48.3	-50.2	-69.8	-77.6	-64.5	-59.3	-56.5
Modified Method $\zeta_w^{HC\text{-}16}$ (mV)	-51.1	-52.2	-78.3	-83.0	-71.6	-62.8	-56.5
pH of Brij 35 solution	6.5	6.7	6.7	6.6	6.6	6.5	6.1
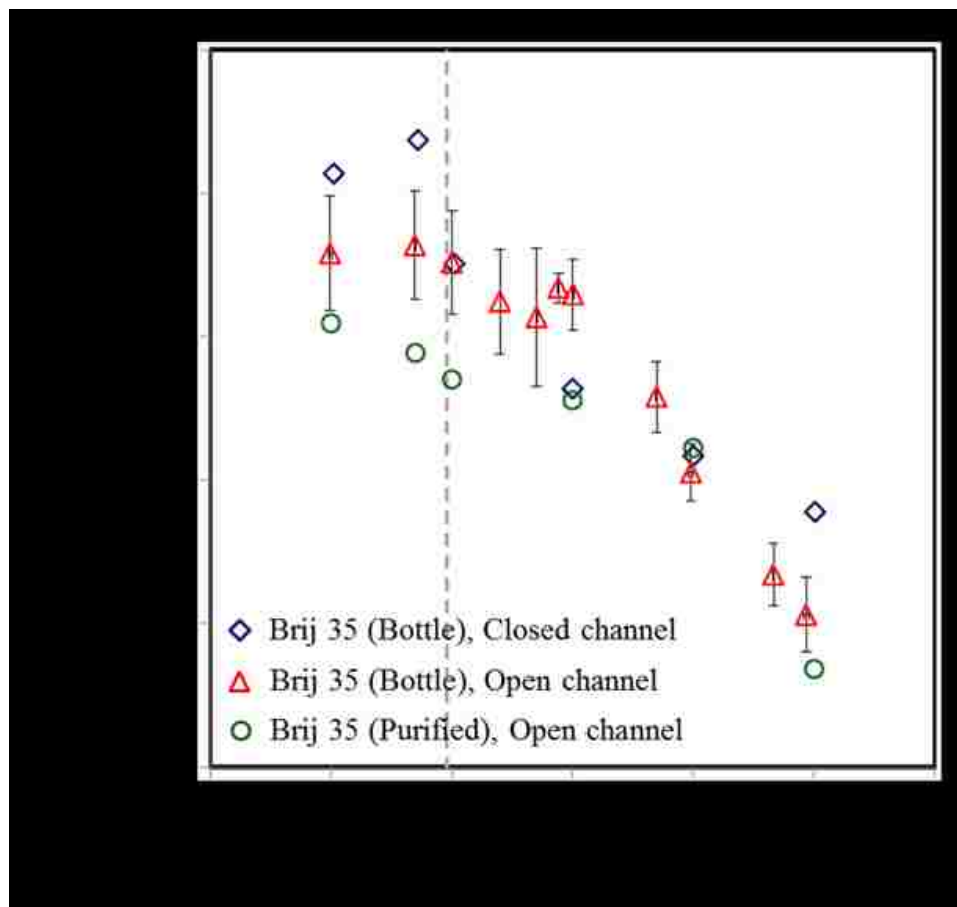
Figure 3.1. Zeta potential (ζ_w) of the HC-16 surface as a function of the Brij 35 concentration. The pH of the Brij 35 solutions prepared with Brij 35 straight from the bottle is adjusted to ~ 6.7 by adding 20-mM NaOH solution. The ζ_w was measured by using closed-cell electroosmosis (diamonds; see Chapter 4.2 for procedures) or electro-capillarity (triangles; see Chapter 2.2 and 2.3 for procedures). The vertical dash line is the critical micelle concentration (91 μM) of Brij 35. The circles represent the results of ζ_w tested with purified Brij 35 using the electro-capillarity method.

3.3.2. Zeta Potentials of Hydrocarbon and Fluorocarbon Surfaces in Contact with Non-ionic Surfactant Solutions

We now use this new method to measure $\zeta_w^{HC\text{-}16}$ and $\zeta_w^{FC\text{-}10}$ (zeta potential of HC-16 and FC-10 surfaces, respectively) using different Brij 35 solutions. We studied the effect of a nonionic surfactant, Brij 35, which has both hydrocarbon and oligo(ethylene oxide) (OEO) moieties. Under water, the hydrocarbon chains can be adsorbed onto the silanized surface to form a monolayer, whereas the OEO groups come in contact with water.[27] As the concentration of the surfactant is increased, it would form micelles at and above the critical micelle concentration (CMC).

Fig. 3.2 summarizes the data of $\zeta_w^{HC\text{-}16}$ and $\zeta_w^{FC\text{-}10}$ measured with different concentrations of Brij 35 solutions. The value of $\zeta_w^{HC\text{-}16}$, at first, becomes more negative (-72.7 mV) than that (-52.2 mV) of pure water, while $\zeta_w^{FC\text{-}10}$ is less negative (-87.3 mV) than that (-96.6 mV) of pure water below the CMC. The trends continue as long as the concentration of Brij 35 in DI water is lower than its CMC (91 μM)[28]. The strengths of both $\zeta_w^{HC\text{-}16}$ and $\zeta_w^{FC\text{-}10}$ decrease systematically above the CMC.
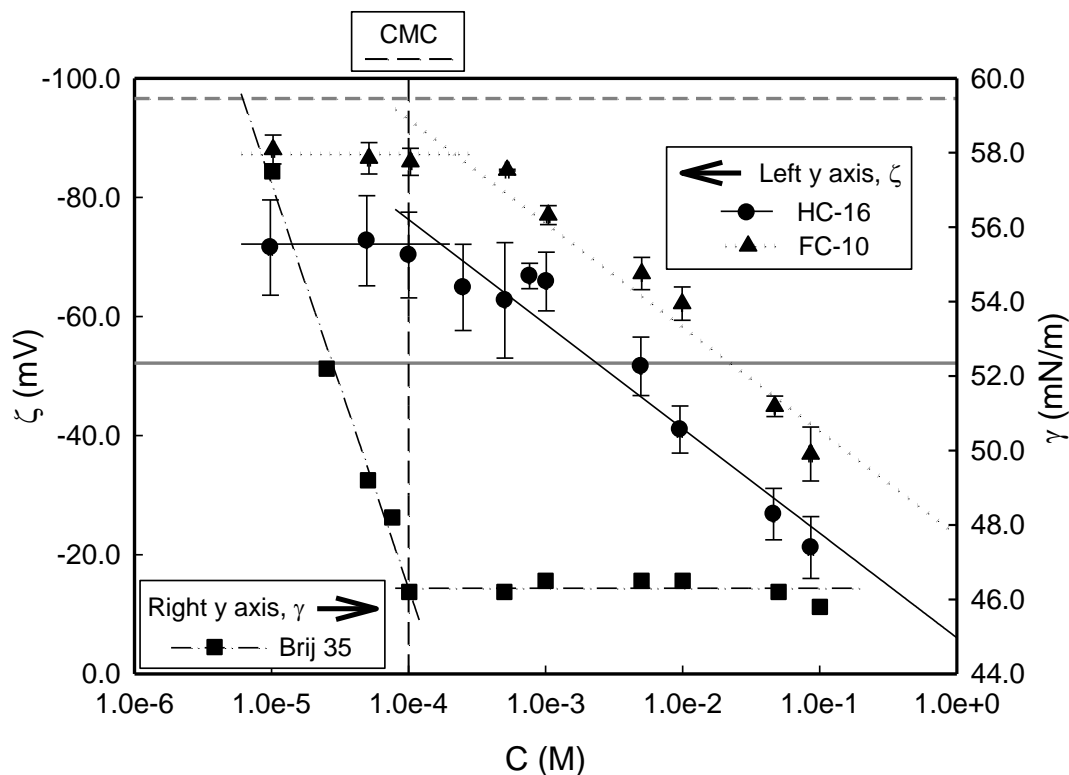
Figure 3.2. The relation between the zeta potential (ζ; left axis) of the HC-16 (circles) / FC-10 (triangles) surface and the concentration (C) of Brij 35 aqueous solution at a given pH (~6.7). The vertical dash line indicates the CMC of Brij 35. Above the CMC, the solid line (ζ = 17.6 log C - 6.1, R^2 = 0.93) and dotted line (ζ = 17.5 log C - 23.3, R^2 = 0.94) are semi-logarithmic regressions of the results tested for HC-16 and FC-10 surfaces, respectively. Additionally, utilizing DI water, the grey solid line exhibits zeta potential (-52.2 mV) of HC-16 substrate, and the grey dash line shows the result (-96.6 mV) of FC-10 surface. The squares indicate the surface tension (γ; right axis) of the Brij 35 solution at pH ~6.7.

The pH of water (~ 6.7) was not affected until the concentration of the surfactant reached about 0.1 mM. The pH of the Brij 35 aqueous solutions decreased gradually above 0.1 mM eventually approaching to approximately 3.8 at concentration of 100 mM (Table 3.2). The pH of the solution was adjusted close to 6.7 by addition of small amount of sodium hydroxide (NaOH). The amount of sodium hydroxide needed to raise the pH was, however, rather low. For example, in the case of the solution with the lowest pH (i.e., 100-mM Brij 35), about 1.7 mL of 15-mM NaOH was added in order to raise the pH of this 10-mL surfactant solution from 3.8 to 6.8. However, we did not observe significant differences of the surface zeta potential between the pH-adjusted and the native solutions. In both cases, the magnitude of zeta potential decreased with the increase of surfactant concentration finally reaching a value of about -21.2 mV at a

Table 3.2. The conductivity of Brij 35 solutions prepared with/without purification.

Brij 35 concentration (M)	Conductivity (µS/cm)		
	Straight from Bottle		After Purification
	Before adding NaOH	pH adjusted to ~ 6.7	All pH ~6.7
10^{-5}	0.54 ± 0.01 (pH = 6.8)	0.54 ± 0.01	0.22 ± 0.01
5×10^{-5}	0.77 ± 0.01 (pH = 6.7)	0.77 ± 0.01	0.22 ± 0.01
10^{-4}	0.95 ± 0.01 (pH = 6.4)	1.29 ± 0.01	0.23 ± 0.01
10^{-3}	7.43 ± 0.01 (pH = 5.4)	3.38 ± 0.01	0.23 ± 0.01
10^{-2}	40.90 ± 0.10 (pH = 4.3)	28.63 ± 0.06	0.58 ± 0.03
10^{-1}	118.53 ± 0.31 (pH = 3.8)	171.97 ± 0.61	6.2 ± 0.1

surfactant concentration of 86 mM for the HC-16 surface (see Fig. 3.3). The addition of electrolytes into the solution could affect the surface zeta potential by charge regulation in the electrical double layer. [6-8,12,29-31] However, the effect seems to be negligible as we did not observe significant differences of the zeta potentials in the two cases.
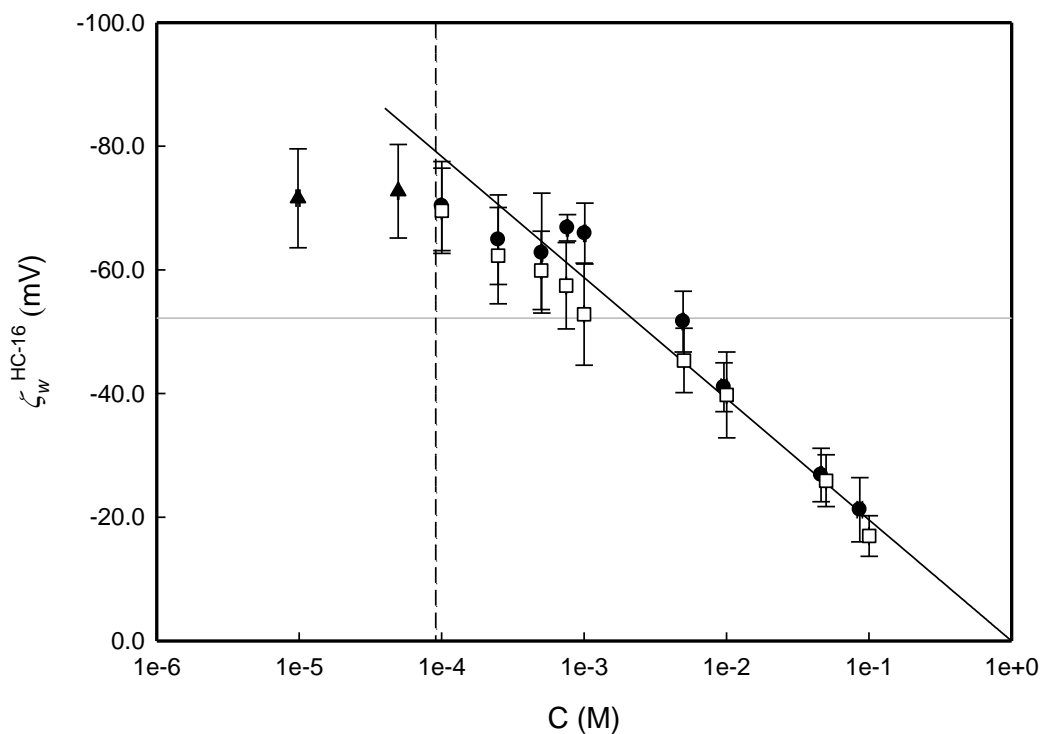
Figure 3.3. The zeta potential of HC-16 surface (ζ_w^{HC-16}) versus different concentrations of Brij 35 aqueous solutions (C). The dash line points the CMC of Brij 35 (91 μM). The grey line points the ζ_w^{HC-16} tested with DI water (-52.2 mV). The closed triangles (▲) are the results tested below the CMC of Brij 35, while the closed circles (●) are the ones determined above the CMC of Brij 35 with the condition that the solution pH was adjusted to about 6.7 by using the NaOH solution. The solid line gives the semi-logarithmic regression result of closed circles and shows $\zeta_w^{HC-16} = 19.6\log C$ with $R^2 = 0.92$. The open squares (□) represent the data obtained above the CMC of Brij 35 with the natural pH.

We further inspected the effect of the impurity in the solution by purifying the surfactant using dialysis. A 0.1 M Brij 35 solution was first placed in a dialysis bag (MWCO 3500 Daltons, 3 Specttra/Por® dialysis membrane; Spectrum Laboratories, Inc.) in a DI water bath for five days. The water bath was exchanged with fresh DI water twice a day. The purified Brij 35 was then diluted to the desired concentration, and the conductivity was measured (conductivity meter model 23226-523; VWR International, LLC) to check the quality of the surfactant solution (Table 3.2). The pH of all the Brij 35 solution after purification was ~6.7 without adding any NaOH. The reduced conductivity also revealed the removal of the acidic impurities from the solutions. The ζ_w^{HC-16} values tested with purified Brij 35 solutions were comparable with the unpurified solutions (Fig. 3.1), and the trend was similar as well.

There are several hypotheses[4,6-9,29,33-39] that the negative value of the hydrophobic surface zeta potential could be due to the adsorption of hydroxide ions at the interface. Some reports in the literature[4,6,9,38,39] also illustrate that a surface populated with nonionic surfactant containing poly(ethylene oxide) groups also exhibits a negative zeta potential. It has been suggested[8,9,12,40] that the adsorption of hydroxide ions is responsible for this phenomenon as well. In our system, there should be a finite quantity of hydroxide ions in the solution at a given pH (~6.7). If the available surface area for adsorption increases, then the number density of the hydroxide ions on a surface should decrease and so should the magnitude of zeta potential (Fig. 3.4). As the number of micelles increases with the surfactant concentration in our system, the available surface area of hydroxide ions also increases. With a finite source of hydroxide ions, the ζ_w of

54
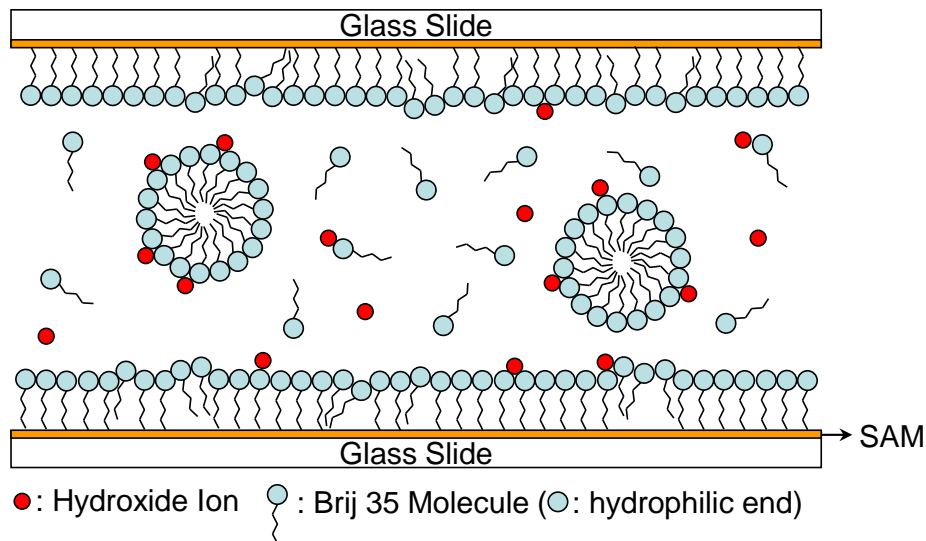
Figure 3.4. Schematic illustration of the channel filled with the Brij 35 aqueous solutions above the CMC. This figure shows a possible distribution of hydroxide ions and surfactant molecules in the channel.

the SAM surface become less negative as the number of micelles increases above the CMC. At this juncture, we should mention the experiment of Beattie and Djerdjev[33], who observed the effect of the increase in the surface area of oil in water emulsions on solution pH by repeated passing of the emulsion through a homogenizer. As the oil drops broke down to smaller and smaller sizes with the concomitant increase of the surface area of the emulsion, the pH of the emulsion decreased. In this case, the adsorption of the hydroxide ions at the oil/water interface decreased the hydroxide ions so much from the solution that some additional sodium hydroxide was needed to maintain a constant pH of the solution. The adsorption of the hydroxide ions at the oil/water interface also increased the stability of the emulsion.

As discussed in Chapter 1.1.2, on the other hand, more and more spectroscopic evidence has shown that it is the hydronium ion to be the excess species at the air/water interface. Therefore, we could not rule out other possible causes to the negative zeta potential of the SAM surface. Recently, a new theory suggested[41] that the partial charge transfer of the hydrogen bond between the water dimer could contribute to the negative zeta potential at hydrophobe/water interface. Studies also showed that when the concentration of poly(ethylene oxide) (PEO) in water increases, the concentration of the hydrogen bonds on PEO chains decrease.[42,43] These hydrogen bonds include the bond between water molecules and the bond between water hydrogen and ether oxygen. If the zeta potentials of the SAM surfaces are contributed by the charge transfer caused by the imbalance of the hydrogen bond, one can consider that the presence of Brij 35 could also decrease the strength of the zeta potential with the increase of the concentration due to less hydrogen bonds forming near the surface. More studies are required to clarify the origin of the charges at the interface between the hydrophobic surface and the liquid.

Additionally, the FC-10 surface exhibits more negative values (~10-20 mV) of the zeta potential than those of a HC-16 surface measured with Brij 35 solutions. This difference could be due to that these two surfaces carry different Brij 35 molecule adsorption patterns at the solid/liquid interface.

3.3.3. Adsorption of Brij 35 on Hydrocarbon and Fluorocarbon Surfaces

The Brij 35 molecules, either adsorbed on the surface or suspended in the solution, could influence the zeta potential of the surface. As a result, we would like to understand the role of Brij 35 on both solid/liquid interfaces. These HC-16 and FC-10 surfaces were studied by measuring the advancing (θ_a) and receding (θ_r) contact angles with the Brij 35 solution at different concentration. The data of contact angles combined with the surface tension (γ) of the solution are utilized to calculate the surface excess (Γ_{sl}) of Brij 35 on the solid/liquid interface. The combination of Young's equation[44] and Gibbs adsorption equation[45] gives

$$\gamma_l^* \cos \theta^* = \gamma_s - \gamma_{sl}^* = \gamma_s - \left(\gamma_{sw} - \int \Gamma_{sl} d\mu_{\text{Brij35}}\right) = \gamma_w \cos \theta_w + \int \Gamma_{sl} d\mu_{\text{Brij35}} \qquad (3.1)$$

where μ_{Brij35} is the chemical potential of Brij 35 in the solution, and θ is the equilibrium contact angle estimated by the method proposed by Tadmor[46]. The asterisk indicates the value measured with the Brij 35 solution. The subscript letters of s, l, and w represent solid surface, liquid phase, and DI water, respectively. Equation 3.1 can be rearranged, by differentiating both sides, to be

$$\Gamma_{sl} = \frac{d\left(\gamma_l^* \cos \theta^* - \gamma_w \cos \theta_w\right)}{d\mu_{\text{Brij35}}} = \frac{1}{2.303RT} \frac{d\left(\gamma_l^* \cos \theta^* - \gamma_w \cos \theta_w\right)}{d(\log C)} \quad , \qquad (3.2)$$

where R is the gas constant (8.31 J/mol K), T is the room temperature (~296 K in our experiments), and C is the Brij 35 concentration (with the unit mol/L). Therefore, the areas per Brij 35 molecule at the HC-16 (a_{sl}^{HC}) and FC-10 (a_{sl}^{FC}) surfaces can be calculated by the surface excesses of HC-16 (Γ_{sl}^{HC}) and FC-10 (Γ_{sl}^{FC}) substrates, respectively. With the application of eq. 3.2 and semi-logarithmic regressive slopes

(below the CMC) in Fig. 3.5, a_{sl}^{HC} and a_{sl}^{FC} are evaluated to be, respectively, about 76

and 110 Å^2. The difference between a_{sl}^{HC} and a_{sl}^{FC} indicates the different packing

density of Brij 35 on hydrocarbon and fluorocarbon surfaces. The smaller value of a_{sl}^{HC}

than a_{sl}^{FC} implies a denser arrangement of Brij 35 molecules on a hydrocarbon surface

than that of a fluorocarbon substrate.
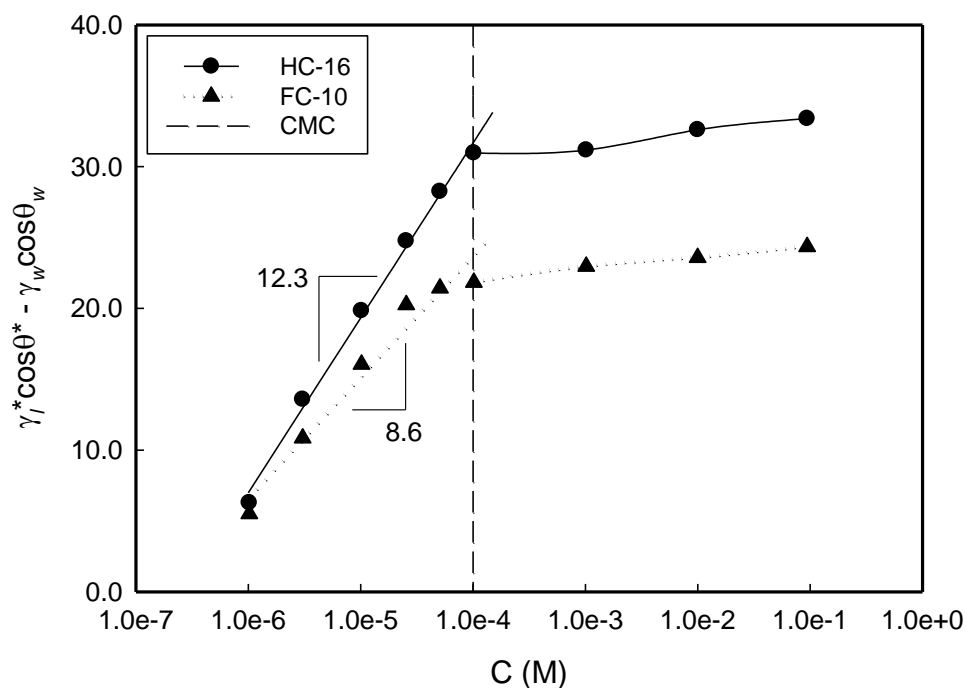
Figure 3.5. The relation of the liquid surface energy difference ($\gamma_l^* \cos\theta^* - \gamma_w \cos\theta_w$) at the three-phase contact line between Brij 35 solution and DI water as a function of Brij 35 concentration (C). (Equation 3.2) The circles are the data of HC-16 and triangles are the ones of FC-10. The dash line indicates the critical micelle concentration (CMC) of Brij 35. Below the CMC, the solid line and dotted line are the semi-logarithmic regressive results for HC-16 and FC-10, respectively.

The result of different packing density of Brij 35 on these two hydrophobic surfaces is in accordance with the viewpoint that hydrocarbon chain is more favorable to the hydrocarbon surface than the fluorocarbon one. The different affinity[24,47-51] between hydrocarbon/hydrocarbon and hydrocarbon/fluorocarbon moiety interactions suggests[24,48] that the adsorption of the hydrocarbon chain is more favorable on the hydrocarbon surface than on the fluorocarbon one. Hence, the Brij 35 hydrophobic end, which is composed of a hydrocarbon chain (with 12 carbon atoms on a linear backbone), could bear higher affinity to the $-CH_3$ terminated surface than to the $-CF_3$ one. The affinity difference causes a denser Brij 35 molecule packing, which is also supported by the results of a_{sl}^{HC} and a_{sl}^{FC}, on the HC-16 surface than on the FC-10 surface. The different adsorption pattern of Brij 35 causes different zeta potentials on hydrocarbon and fluorocarbon surfaces.

3.3.4. Zeta Potential of PVA-Coated PDMS in Contact with Brij 35 Solutions

The new technique was also utilized to study the zeta potential of 10% cross-linked polyvinyl alcohol (PVA, 98-99% hydrolyzed, M.W. 88000-97000) with Brij 35 solutions at different concentrations. (A detailed sample preparation process is given in Chapter 5.2.2) A control experiment was first performed to estimate the zeta potential (-51.1 ± 3.2 mV) of the coating substrate, polydimethylsiloxane (PDMS, Sylgard 184; Dow Corning). The PVA surface also bears negative zeta potential while it contacts with aqueous solutions. (Fig. 3.6) According to the literature[52,53], the negative charge of the

PVA surface could presumably come from the residual acetate groups ($-OCOCH_3$) in the polymer. It was hypothesized that the acetate group would be ionized due to the acidic C–H bond in α position related to acetate functionality as follows

.
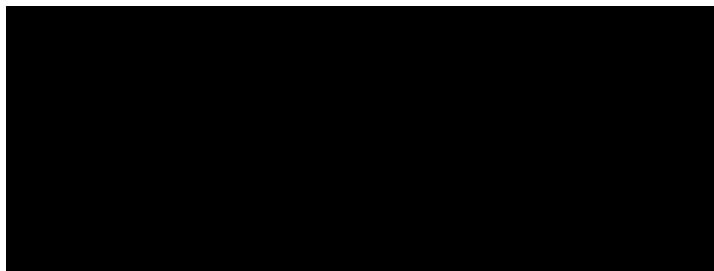
These residual acetate groups are unavoidable in the PVA synthesis process.[54]
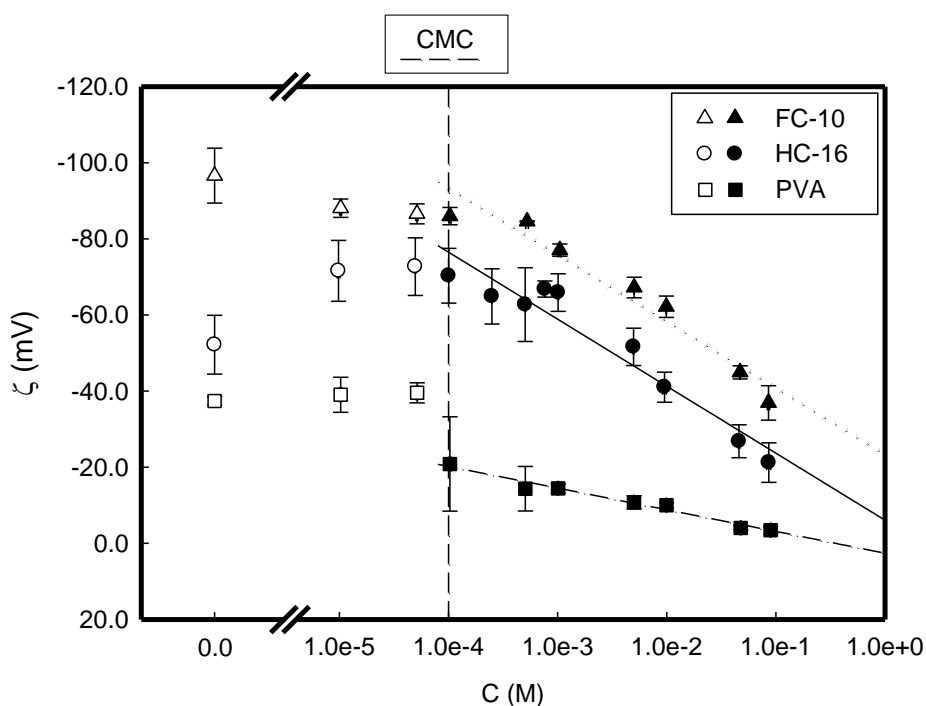
Figure 3.6. The zeta potential (ζ) of three different surfaces, FC-10 (triangles), HC-16 (circles), and 10% cross-linked PVA (squares), as a function of Brij 35 concentration (C). The open symbols are the results below the CMC of Brij 35, while the closed symbols are the ones above the CMC. The dotted, solid, and dash-dot lines are the semi-logarithmic regression of the data points of FC-10, HC-16, and PVA above the CMC, respectively.

Similar to hydrocarbon and fluorocarbon surfaces, the zeta potential of PVA remains constant below the CMC, and decreases with the concentration of Brij 35 above the CMC. Brij 35 molecules can be adsorbed to the PVA surface via the hydrophobic interaction between the hydrophobic end of the surfactant and the alkyl groups on the PVA backbone, or via the H-bonding between the oligo(ethylene oxide) groups (OEO) of the surfactant and the hydroxyl (–OH) as well as the residual –OCOCH$_3$ groups in PVA. In addition, it has been reported[55] that the adsorption of OEO nonionic surfactants on PVA surface is mainly contributed by the hydrophobic interaction between hydrophobic groups (–CH$_2$) on PVA backbone and hydrocarbon tail of the surfactant. The surfactants reach the adsorption equilibrium on PVA above the CMC. Therefore, the adsorption of the surfactant could screen the residual –OCOCH$_3$ groups, thus leading to the decrease of the magnitude of zeta potential above the CMC.

3.4. SUMMARY

Using the new technique proposed in Chapter 2, the zeta potential changes of the HC-16 and FC-10 surfaces with different concentrations of Brij 35 were examined. As long as the concentration of the surfactant is below its CMC, the zeta potential of the SAM-coated glass remains constant to about -72.7 mV for the hydrocarbon surface and -87.3 mV for the fluorocarbon substrate. The strengths of the hydrophobic surface zeta potentials decrease with the Brij 35 concentration above the CMC. It still remains unclear the cause of the zeta potential at the hydrophobe/liquid interface. As a result, it

is necessary to investigate the effect of hydroxide ions to the negative zeta potential indicated by the electrokinetic measurements, which is discussed in Chapter 4.

REFERENCES

1. Zimmermann, R.; Osaki, T.; Schweiss, R.; Werner, C. *Microfluidics and Nanofluidics* 2006, **2**, 367-379.

2. Roach, L. S.; Song, H.; Ismagilov, R. F. *Analytical Chemistry* 2005, **77**, 785-796.

3. Huang, T. T.; Mosier, N. S.; Ladisch, M. R. *Journal of Separation Science* 2006, **29**, 1733-1742.

4. Tandon, V.; Bhagavatula, S. K.; Nelson, W. C.; Kirby, B. J. *Electrophoresis* 2008, **29**, 1092-1101.

5. Kirby, B. J.; Hasselbrink, E. F. *Electrophoresis* 2004, **25**, 203-213.

6. Marinova, K. G.; Alargova, R. G.; Denkov, N. D.; Velev, O. D.; Petsev, D. N.; Ivanov, I. B.; Borwankar, R. P. *Langmuir* 1996, **12**, 2045-2051.

7. Zimmermann, R.; Dukhin, S.; Werner, C. *Journal of Physical Chemistry B* 2001, **105**, 8544-8549.

8. Karraker, K. A.; Radke, C. J. *Advances in Colloid and Interface Science* 2002, **96**, 231-264.

9. Yoon, R. H.; Yordan, J. L. *Journal of Colloid and Interface Science* 1986, **113**, 430-438.

10. Somasundaran, P.; Snell, E. D.; Fu, E.; Xu, Q. *Colloids and Surfaces* 1992, **63**,

49-54.

11. Saulnier, P.; Lachaise, J.; Morel, G.; Graciaa A. *Journal of Colloid and Interface Science* 1996, **182**, 395-399.

12. Chan, Y. H. M.; Schweiss, R.; Werner, C.; Grunze, M. *Langmuir* 2003, **19**, 7380-7385.

13. Lin, C.-H.; Chaudhury, M. K. *Langmuir* 2008, **24**, 14276-14281.

14. Bernett, M. K.; Zisman, W. A. *Journal of Physical Chemistry* 1959, **63**, 1241-1246.

15. Clunie, J. S.; Ingram, B. T. Adsorption of Nonionic Surfactants. In: *Adsorption from Solution at the Solid/Liquid Interface*; Parfitt, G. D. and Rochester, C. H., Ed.; Academic Press, Inc.: Orlando, FL, 1983, p105-152.

16. von Rybinski, W.; Schwuger, M. J. Adsorption and Wetting. In: *Surfactant Science Series, Vol. 23: Nonionic Surfactants: Physical Chemistry*; Schick, M. J., Ed.; Marcel Dekker, Inc.: New York, 1987; p 45-107.

17. Tiberg, F.; Brinck, J.; Grant, L. *Current Opinion in Colloid and Interface Science* 2000, **4**, 411-419.

18. Kumar, N.; Varanasi, K.; Tilton, R. D.; Garoff, S. *Langmuir* 2003, **19**, 5366-5373.

19. Zhmud, B.; Tiberg, F. *Advances in Colloid and Interface Science* 2005, **113**, 21-42.

20. Tiberg, F. *Journal of the Chemical Society*, *Faraday Transactions* 1996, **92**, 531-538.

21. Grant, L. M.; Tiberg, F.; Ducker, W. A. *Journal of Physical Chemistry B* 1998, **102**, 4288-4294.

22. Grant, L. M.; Ederth, T.; Tiberg, F. *Langmuir* 2000, **16**, 2285-2291.

23. Szymczyk, K.; Jańczuk, B. *Langmuir* 2008, **24**, 7755-7760.

24. Fletcher, P. D. I. Fluorinated and Semi-fluorinated Surfactants. In: *Specialist Surfactants*; Robb, I. D., Ed.; Blackie Academic & Professional (an Imprint of Chapman & Hall), London, UK, 1997; p104-142.

25. Myers, D. *Surfactant Science and Technology*, 2nd Ed. VCH Publishers, Inc.: New York, USA, 1992; p 267-311.

26. Ashani, Y.; Catravas, G. N. *Analytical Biochemistry* 1980, **109**, 55-62.

27. Haidara, H.; Chaudhury, M. K.; Owen, M. J. *Journal of Physical Chemistry* 1995, **99**, 8681-8683.

28. Becher, P. Micelle Formation in Aqueous and Nonaqueous Solutions. In: Schick, M. J., editor. *Surfactant Science Series, Vol. 1: Nonionic Surfactants*; Marcel Dekker, Inc.: New York, NY, 1966, p 480.

29. Yan, D. G.; Yang, C.; Nguyen, N. T.; Huang, X. Y. *Electrophoresis* 2006, **27**, 620-627.

30. Werner, C.; Körber, H.; Zimmermann, R.; Dukhin, S.; Jacobasch, H. J. *Journal of Colloid and Interface Science* 1998, **208**, 329-346.

31. Gu, Y. G.; Li, D. Q. *Journal of Colloid and Interface Science* 2000, **226**, 328-339.

32. Sze, A.; Erickson, D.; Ren, L. Q.; Li, D. Q. *Journal of Colloid and Interface Science* 2003, **261**, 402-410.

33. Beattie, J. K.; Djerdjev, A. M. *Angewandte Chemie International Edition* 2004, **43**, 3568-3571.

34. Beattie, J. K. *Lab on a Chip* 2006, **6**, 1409-1411.

35. Najafi, A. S.; Drelich J.; Yeung A,; Xu, Z. H.; Masliyah J. *Journal of Colloid and Interface Science* 2007, **308**, 344-350.

36. Boyson, T. K.; Pashley, R. M. *Journal of Colloid and Interface Science* 2007, **316**, 59-65.

37. McCarty, L. S.; Whitesides, G. M. *Angewandte Chemie International Edition* 2008, **47**, 2188-2207.

38. Zangi, R.; Engberts, J. B. F. N. *Journal of the American Chemical Society* 2005, **127**, 2272-2276.

39. Kuldin, K. N.; Car, R. *Journal of the American Chemical Society* 2008, **130**, 3915-3919.

40. Kreuzer, H. J.; Wang, R. L. C.; Grunze, M. *Journal of the American Chemical Society* 2003, **125**, 8384-8389.

41. Ben-Amotz, D. *Journal of Physical Chemistry Letters* 2011, **2**, 1216-1222.

42. Smith, G. D.; Bedrov, D.; Borodin O. *Physical Review Letters* 2000, **85**, 5583-5586.

43. Dormidontova, E. E. *Macromolecules* 2002, **35**, 987-1001.

44. Adamson, A. W.; Gast, A. P. *Physical Chemistry of Surfaces, 6ᵗʰ Ed.* Wiley-Interscience: New York, USA, 1997; p 352-355.

45. Rosen, M. J. *Surfactants and Interfacial Phenomena, 3ʳᵈ Ed.* Wiley-Interscience: Hoboken, USA, 2004; p 60-97.

46. Tadmor, R. *Langmuir* 2004, **20**, 7659-7664.

47. Fowkes, F. M. *Industrial and Engineering Chemistry* 1964, **56**, 40-52.

48. Mukerjee, P.; Sharma, R.; Pyter, R. A.; Gumkowski, M. J. Adsorption of Surfactants and Solubilization in Adsorbed Layers. In: *Surfactant Adsorption and Surface Solubilization*; Sharma, R., Ed.; American Chemical Society: Washington, D.C., USA, 1995, p 22-35.

49. Takiue, T.; Matsuo, T.; Ikeda, N.; Motomura, K.; Aratono, M. *Journal of Physical Chemistry B* 1998, **102**, 5840-5844.

50. Villeneuve, M.; Nomura, T.; Matsuki, H.; Kaneshina, S.; Aratono, M. *Journal of Colloid and Interface Science* 2001, **234**, 127-136.

51. Krafft, M. P.; Riess, J. G. *Chemical Reviews* 2009, **109**, 1714-1792.

52. Wiśniewska, M. *Colloid* and *Polymer Science* 2011, **289**, 341-344.

53. Wiśniewska, M. *Journal of the American Ceramic Society* 2007, **90**, 3608-3614.

54. Pritchard, J. G. *Polymer Monographs Vol.4: Poly(vinyl alcohol) – Basic Properties and Uses*. Gordon and Breach, Science Publishers Ltd.: London, UK, 1970.

55. El-Feky, A. A., Shalaby, M. N., and El-Shamy, A. A. *The Journal of Dispersion Scince and Technology* 2009, **30**, 445-450.

Chapter 4

Electrokinetics of Polar Liquids in Contact with Nonpolar Surfaces [c]

ABSTRACT

Zeta potentials of several polar protic (water, ethylene glycol, formamide) as well as polar aprotic (dimethyl sulfoxide) liquids were measured in contact with three nonpolar surfaces using closed-cell electroosmosis. The test surfaces were adsorbed monolayers of alkyl siloxanes, fluoroalkyl siloxanes and polydimethylsiloxanes (PDMS) grafted onto glass slides. All of these liquids exhibited substantial electrokinetics in contact with the nonpolar surfaces with these observations: the electrokinetic effect on the fluorocarbon-coated surface was the strongest; and on a PDMS grafted surface, the effect was the weakest. Even though these hygroscopic liquids contain small amounts of water, the current models of charging based on the adsorption of hydroxide ions at the interface or the dissociation of pre-existing functionalities (e.g., silanol groups) appear to be insufficient to account for the various facets of the experimental observations. The results illustrate how ubiquitous the phenomenon of electrokinetics is with polar liquids contacting such apparently passive nonpolar surfaces.

4.1. INTRODUCTION

It is inferred from electrokinetic measurements that the interfaces of various hydrophobic nonpolar solids in contact with pure water become negatively charged. This result is surprising considering the absence of dissociable groups on such solids that could give rise to charging. While it has been stipulated in the literature[1-5] that the adsorption of hydroxide ions is responsible for negative charge at the interface of water and non-polar materials, spectroscopic as well as the theoretical studies[6-12] have largely failed to provide strong evidence for such a model. Although certain MD simulations[13] argued for only a slight accumulation of hydroxide ions at the interface, the preponderance of the evidence from various simulations and spectroscopic studies[9-12], on the other hand, suggest that hydronium ions – not hydroxide ions – accumulate in excess at the interface. Recently, a new effort has been made to explain the charging at the interface of water in contact with hydrophobic surfaces based on donor-acceptor interactions.[14] In this model, partial charge transfer inherent in hydrogen bonds between water molecules gives rise to a zeta potential at the interface, where the isotropic symmetry of the bulk is broken and charge separation is imbalanced. Such an explanation of charging at the water/nonpolar interface implies that other types of H-bonding liquids, e.g., ethylene glycol and formamide, should exhibit non-negligible electrokinetic effects as well.

Nearly two decades ago, Yaminsky and Johnston[15] reported that a hydrophobized glass slide acquires negative charge when it is withdrawn from water. In fact, they found that this effect is not restricted to water alone; charging of variable magnitudes is

also observed with formamide, mercury and certain solutions of water and ethanol, but not with such pure dielectric liquids as alkanes. The authors speculated that the surfaces acquire charge when a non-wetting liquid breaks its adhesive bonds during the retraction of the solids in a manner akin to triboelectricity.[16] However, for such a charge separation to occur, there has to be a difference in the chemical potential of the electrons on the two surfaces with an energy barrier preventing instantaneous charge neutralization during the interfacial separation process. These results then lead to the question: is it possible that the negative zeta potential of water in contact with hydrophobic surfaces is related to a contact-charging phenomenon? The Yaminsky-Johnston experiments should be clearly demarcated from the standard electrokinetic measurements in that the former involves retraction of a solid from a pre-wetted liquid, whereas the latter is performed when the solid remains wetted by a liquid. In order to bridge these two types of experiment, electrokinetic measurements are needed with various polar liquids against non-polar surfaces while they maintain interfacial contact. In this paper, we pursue such a study by measuring the zeta potentials of hydrophobically modified glass slides in contact with polar liquids (ethylene glycol, formamide, and dimethyl sulfoxide) and compare the results with the same surfaces in contact with water. Amongst these liquids, both ethylene glycol and formamide can autoionize only sparingly, whereas dimethyl sulfoxide is a non-ionizable aprotic liquid.[17] All of these liquids are however hygroscopic and contain trace amounts of water. Detailed analysis of the electrokinetic data of these liquids, even in the presence of small amounts of water, and how they depend on the chemical nature of

hydrophobization suggests that an explanation beyond that of the adsorption of hydroxide ions may be warranted in order to explain the observed charging phenomena.

4.2. EXPERIMENTAL

4.2.1. Materials

The liquids used for the experiments were deionized water (DI water; Barnstead), ethylene glycol (EG, spectrophotometric grade, 99+%; Alfa Aesar), formamide (FA, spectrophotometric grade, 99+%; Alfa Aesar), and dimethyl sulfoxide (DMSO, HPLC grade, 99.9+%, packaged under argon in re-sealable ChemSeal™ bottles; Alfa Aesar). In one set of experiments, the as-received EG and FA were heated to 120 ºC for 2 h under a bubble purge of nitrogen to dry the solvents as much as possible. DMSO was used either straight from the bottle or after vacuum distillation. Both EG and DMSO were distilled under partial vacuum (at ~10 Torr), the latter over calcium hydride (≥97.0%; Sigma-Aldrich). Formamide was used either as received or after equilibrating 100 mL of it with 10 g of mixed-bed resin (cat. No. M8032; Sigma-Aldrich) under a bubble purge of nitrogen for 1 h in order to remove the excess ions. This treatment, however, introduces some amount of water to the solvent. In some experiments, we also added deliberately small amounts of water to the test liquids. Two different fluorescent particles were used in the particle image velocimetry (PIV): FluoSpheres carboxylate-modified microspheres (0.5 μm, yellow-green fluorescent; Invitrogen Co.), and FMY yellow UV fluorescent microspheres (1μm-5μm; Cospheric), from which the

smallest particles were extracted. *n*-Hexadecyltrichlorosilane (HC-16, 95%; Gelest Inc.), *1H,1H,2H,2H*-perfluorodecyltrichlorosilane (FC-10, 96%; Alfa Aesar) and trimethylsiloxy-terminated polydimethylsiloxane (DMS-T22, M.W. 9430; Gelest Inc.) were used as received. The fluid connecter (cat. No. 72-1437) and Tygon® laboratory tubing (R-3603, I.D. 1/16 in., O.D. 1/8 in.) were purchased from Harvard Apparatus, Inc.

The amount of water in EG was determined by attenuated total reflectance-Fourier transform infrared spectroscopy (ATR-FTIR, Nicolet iS10; Thermo Scientific), using its peak in the 1600-1720 cm^{-1} region and calibrated standards prepared by adding known amounts of water in EG. The amounts of water in FA and DMSO were determined using nuclear magnetic resonance spectroscopy (NMR, DRX 500; Bruker BioSpin) by dissolving them in DMSO-d6 (D, 99.9%; Cambridge Isotope Laboratories, Inc.) for FA and chloroform-d (D, 99.8%; Cambridge Isotope Laboratories, Inc.) for DMSO, respectively. Once the in-house spectroscopic measurements were calibrated against the coulometric Karl Fischer titrations (Intertek Pharmaceutical Services, Whitehouse, NJ), the internal measurements were performed for routine analysis of water in the solvents. The pH and the conductivity of the test liquids were measured using a pH meter (model 215 with Gel-filled pH electrode #300737.1; Denver Instrument) and a conductivity meter (model 23226-523; VWR International, LLC), respectively.

For particle velocimetry, all the liquids were seeded with dilute fluorescent particles. For EG and FA, the FluoSpheres particles were freeze-dried followed by re-dispersion in the test liquids via sonication. For DMSO, the FMY particles were first

washed through a syringe filter (Acrodisc® 25 mm premium syringe filter with 0.45 µm GHP membrane; Pall Life Sciences) with DMSO. The particles were then flushed back to the syringe (5-mL disposable syringe, model 26214; Exel International) with additional DMSO, and then filtered through Whatman GF/C filter paper a few times to remove the large (>1.2 µm) particles. The filtrate with concentrated particles was added to the test liquid of DMSO before the electrokinetic measurements. The surface tensions of all the liquids were measured by the du Noüy ring method (Fisher model 215 autotensiomat surface tension analyzer; Fisher Scientific). To check if any contaminants leached out of the tracer particles, the surface tensions of the liquids were measured before and after they were seeded with the particles. Since the surface tension values did not change, we were assured that there was no detectable contamination.

4.2.2. Preparation of Test Channels

The assembly of the test channel is shown in Fig. 4.1. The glass slide ($75 \times 25 \times 1$ mm, cat. No. 12-550-A3; Fisher Scientific) that formed the upper part of the channel was cut to dimensions of $50 \times 25 \times 1$ mm, whereas that forming the bottom of the channel had the as-received dimensions. After both the glass slides were cleaned with piranha solution and dried with a nitrogen purge, the ends of both slides were covered with transparent Scotch® tape as shown in Fig. 4.1a. The slides were treated with an oxygen plasma (model PDC-32G; Harrick Plasma) and then some of those were allowed to react with the vapor of either HC-16 or FC-10 as reported in the
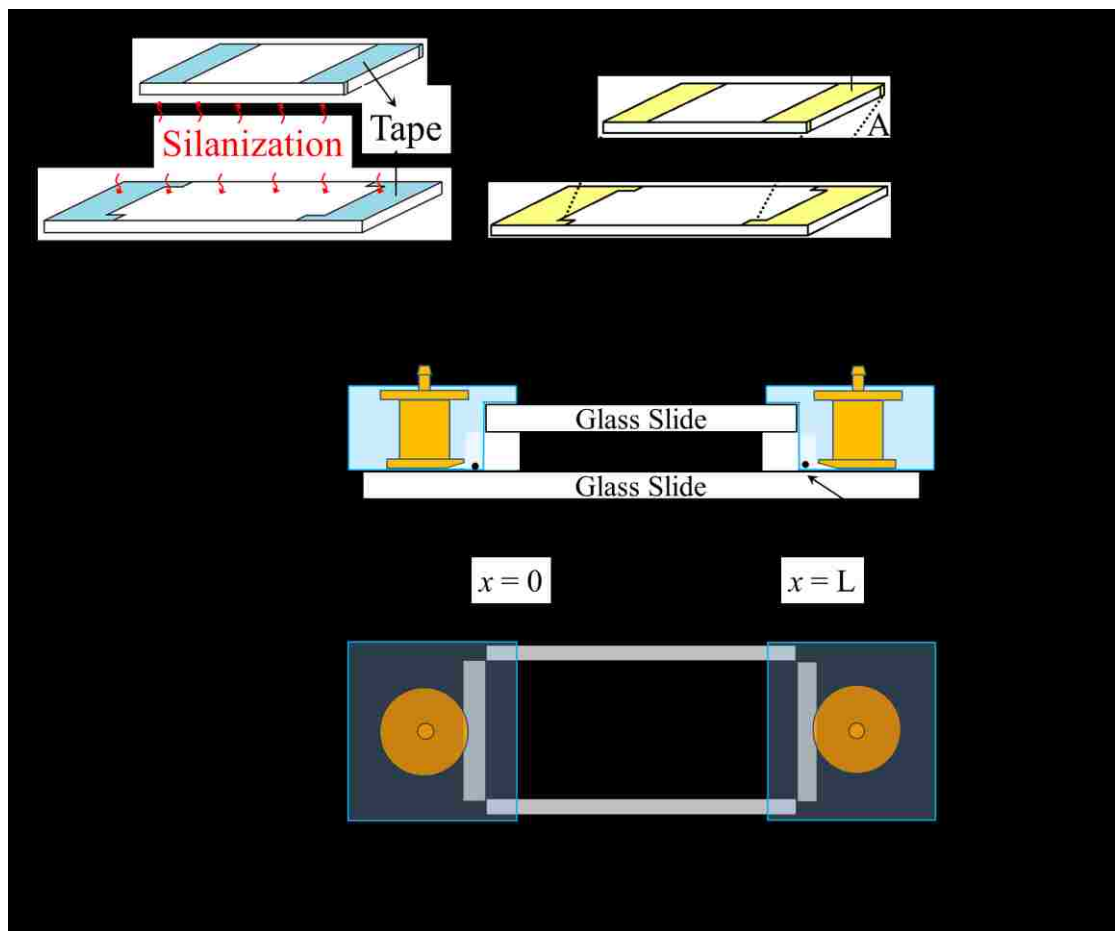
Figure 4.1. Schematic diagrams summarizing the preparation of the testing channel. (a) The two end regions of the glass slides were covered by transparent tape (blue area) to protect the glass surface from silanization. (b) After silanization, the tapes were removed, and the channel was assembled with double-sided tape (gray rectangles in (d)). The yellow areas represent glass surfaces. (c) Side view of the channel. The two ends of the channel were closed with PDMS blocks imbedded with fluid connecters. The platinum electrode was pushed through the PDMS block and placed near the end of the channel. The testing cell was filled with test liquid and placed on the platform of an epifluorescence microscope. (d) Top view of the channel. A voltage ($\Delta\varphi$) was applied across the channel via a power supply. L is the length of the channel.

literature.[18,19] The tape that was utilized to protect the end of the glass slides from silanization was removed following the completion of the silanization. Although accurate measurements of thicknesses of the grafted silane layers could not be carried out on glass because the substrate was not extremely smooth, and because the refractive index of the substrate closely matched that of the silane, the thicknesses of equivalent silanized layers on silicon wafers could be characterized using variable angle spectroscopic ellipsometry (model V-VASE® with WVASE32 software; J.A. Woollam Co., Inc.). These measurements gave to a thickness of 2.5 nm for HC-16 and 1.6 nm for FC-10 on an equivalent polished silicon wafer.[20,21]

Some of the glass slides were modified with a thin layer (5 nm) of PDMS (DMS-T22) using a method reported recently in the literature[22]. After the slide was cleaned by piranha solution and then oxygen plasma, it was fully wetted by DMS-T22 and covered with another glass slide placed above it. The sample was kept in an oven at 80 ºC for 24 h, followed by cooling to room temperature. The sample was then gently rinsed with distilled chloroform (ACS grade; EMD) and dried with a stream of nitrogen. Although we have not measured the thickness of the grafted layer of PDMS on glass, similar treatment on a silicon wafer produced the ellipsometric thickness of the adsorbed film of 5 nm.

All of the surfaces were characterized by the contact angles of the test liquids (DI water, ethylene glycol, formamide and dimethyl sulfoxide), atomic force microscopy (AFM, Nanodimension V; Vecco), and x-ray photoelectron spectroscopy (XPS). The contact angles were measured by using the drop inflation and deflation methods. Angles

measured on both sides of each drop were averaged from three measurements performed at different spots of each sample. High-resolution XPS scans in the C_{1s} and Si_{2p} regions were carried out at a 15º take-off angle with a SCIENTA ESCA-300 instrument using monochromatic Al K_α x-rays generated from a rotating anode operated at 4.5 kW and a pass energy of 150 eV.

The test channel was prepared by assembling two similar glass slides with double-sided Scotch® tape as shown in Fig. 4.1b. A PDMS block embedded with a fluid connecter was prepared using Sylgard 184 (Dow Corning) following the methodology described in the literature.[23] Before assembling the channel, the bottom sides of the PDMS blocks were treated with oxygen plasma at 0.2 Torr for 45 s to enhance adhesion. Clamps were used to affix the plasma-treated PDMS blocks onto the two ends of the channel for 24 h to ensure intimate contact between the PDMS and the surface (Fig. 4.1c and 4.1d).

One obvious concern with the prepared channel was the possibility that impurities might leach from the PDMS and the tape used in the assembly process and contaminate the test liquids. In order to ascertain that this was not the case, test liquids were passed through one of the ports of the assembled channel via a Tygon® tube, and then collected through the other port. Once enough liquid was collected, its surface tension was measured and compared with pure liquids. No measurable differences in surface tension ensured that the contamination of the test liquids by putative impurities was not an issue of concern.

4.2.3. Measurement of Velocity Profiles of Liquids

The test liquid seeded with fluorescent particles was injected into the channel through a Tygon® tube and the fluid connecter utilizing a 5-mL disposable syringe. After the test cell was fully filled with the liquid with no visible air bubbles, its fluid connecters were sealed with solid PDMS plugs. As shown in Fig. 4.1d, platinum electrodes (Premion®, 0.25 mm dia.; Alfa Aesar) were pushed through the PDMS blocks and placed near both the ends of the channel. The test-ready channel was then placed horizontally on the platform of a microscope (model Diaphot; Nikon). When a specific voltage was applied via a power supply (cat. no. 3-1008 from Buchler Instruments or model GPS-1850D from Good Will Instrument Co., Ltd) across the channel through the platinum electrodes, the fluorescent particles began to move, which were observed with the epifluorescence setup (model DM510; Nikon) of the microscope by focusing at different depths of the channel. For each test, electric fields at five different strengths were applied, and the images of particles were recorded on the computer via a CCD camera (model XC-75; Sony).[18]

4.3. THEORY: DETERMINATION OF ZETA POTENTIAL

We begin with the standard equation of electrokinetics[18,24] that balances the viscous, electrical, and normal stresses:

$$\eta \frac{d^2 \mathrm{v}(z)}{dz^2} = \varepsilon \varepsilon_0 E \frac{d^2 \psi(z)}{dz^2} + \frac{dp}{dx} \quad, \tag{4.1}$$

where $\mathrm{v}(z)$ is the velocity of the fluid moving along the length (x direction) of the

channel, $\psi(z)$ is the electrical potential that is uniform in the x direction but varies along the depth of the channel, η and ε are the viscosity and dielectric constant of the test liquid, ε_0 is the dielectric constant in vacuum, and dp/dx and E are the pressure gradient and the electric field, which are uniform along the depth (z direction) but vary across the length of the channel, respectively. These equations are traditionally solved with the following boundary conditions:

$$z = 0 \text{ or } 2h, \; v = v_s, \; \psi = \zeta_w$$

$$z = h, \; dv/dz = 0, \; d\psi/dz = 0 \tag{4.2}$$

where 2h is the depth of the channel, and ζ_w is the zeta potential at each of the channel walls that is in contact with the liquid. The liquid can potentially slip against the wall with a slip velocity v_s. The general solution of eq. 4.1 with the help of the boundary conditions given in eq. 4.2 is as follows:

$$v(H) = \frac{h^2}{2\eta}\frac{dp}{dx}\left(H^2 - 2H\right) - \frac{\varepsilon\varepsilon_0 E}{\eta}\left(\zeta_w - \psi(H)\right) + v_s, \quad H = \frac{z}{h} \; . \tag{4.3}$$

As fluorescent particles are utilized as tracers in the system and each particle has its own electrophoretic velocity (v_p), the velocity profile of the liquid as measured (v_{exp}) with the tracer particles is the superposition of v and v_p, i.e., $v_{exp} = v + v_p$. The electrophoretic velocity of the particle is same as the depth average value of v, i.e.,

$$v_{exp}(H) = \frac{h^2}{2\eta}\frac{dp}{dx}\left(H^2 - 2H\right) - \frac{\varepsilon\varepsilon_0 E}{\eta}\left(\zeta_w - \psi(H)\right) + v_s + \frac{1}{2}\int_0^2 v_{exp}(H)dH \; . \tag{4.4}$$

Following the standard protocol, the slip velocity (v_s) of the test liquids against the walls of the flow channel can be expressed[25] as

$$v_s = b\frac{dv}{dz}\Big|_{z=0} = b\left(\frac{\varepsilon\varepsilon_0 E}{\eta}\frac{d\psi}{dz}\Big|_{z=0} - \frac{h}{\eta}\frac{dp}{dx}\right). \tag{4.5}$$

Here, b is the slip length, and $\frac{dv}{dz}\Big|_{z=0}$ is the velocity gradient at the wall. By integrating eq. 4.1, the electrical potential gradient $\left(\frac{d\psi}{dz}\Big|_{z=0}\right)$ at the wall can be obtained (eq. 4.8) from the solution of the Poisson-Boltzmann equation (eq. 4.6, for a symmetric electrolyte):

$$\frac{d^2\psi(z)}{dz^2} = \frac{2qen_\infty}{\varepsilon_0}\sinh\left(\frac{qe\,\psi(z)}{k_BT}\right) = \frac{\kappa^2}{A}\sinh(A\,\psi(z)) \tag{4.6}$$

with

$$A = \frac{qe}{k_BT} \quad\text{and}\quad \kappa = \left(\frac{2n_\infty q^2 e^2}{\varepsilon_0 k_BT}\right)^{1/2}, \tag{4.7}$$

where q is the charge of the ion, e is the elementary charge, n_∞ is the number of the ions per unit volume, k_B is the Boltzmann constant, T is room temperature (296 K), and κ is the Debye-Hückel parameter.

$$\frac{d\psi}{dz}\Big|_{z=0} = \frac{\kappa}{A}\sqrt{2[\cosh(A\zeta_w)-1]}. \tag{4.8}$$

Now, combining eqs. 4.4, 4.5 and 4.8, we have the velocity profile in the channel as follows:

$$v_{exp}(H) = \frac{dp}{dx}\left[\frac{-2bh + h^2(H^2-2H)}{2\eta}\right] + \frac{\varepsilon\varepsilon_0 E}{\eta}\frac{b\kappa}{A}\sqrt{2[\cosh(A\zeta_w)-1]} - \frac{\varepsilon\varepsilon_0 E}{\eta}(\zeta_w - \psi(H)) + \frac{1}{2}\int_0^2 v_{exp}(H)dH, \tag{4.9}$$

where, the surface potential[26,27] has the following form:

$$\psi(\mathrm{H}) = \frac{4}{A}\left\{\tanh^{-1}\left[\tanh\left(\frac{A}{4}\zeta_w\right)\exp(-\kappa h\mathrm{H})\right] + \tanh^{-1}\left[\tanh\left(\frac{A}{4}\zeta_w\right)\exp(-\kappa h(2-\mathrm{H}))\right]\right\} \quad (4.10)$$

The velocity profile of a particle at a depth H can be obtained experimentally and fitted with eq. 4.9 to obtain the zeta potential (ζ_w), provided that the slip length (b) and the pressure gradient (dp/dx) are known.

Various studies in the literature suggest that the value of b is in the range of 20 nm or less.[25,28] Thus, one approach would be to take reasonable values of b from the literature and fit the velocity profiles to determine under what conditions a best fit is obtained. In order to increase the reliability of such a fit, we measured velocity profiles of the tracer particles at five different values of the applied field E (Fig. 4.2). In all cases, we found that the centerline velocity of the tracer particles is linearly proportional to the electric field, suggesting that the pressure gradient dp/dx has to be proportional to E. This observation is in agreement with our previous publication[18], in which we devised a way to measure the centerline velocity of the tracer particles in both the presence and the absence of an electric field. In the latter case, the flow still occurred, as the electro-osmotically generated pressure gradient was stored via capillarity. It is thus reasonable to set the pressure gradient in the channel to be a linear function of the electric field:

$$\frac{dp}{dx} = D\varepsilon_0 E \quad (4.11)$$

where D is a constant. Now, dividing the velocity v_{exp} by the electric field and dielectric constant, and multiplying it by the viscosity, we obtain an expression for the mobility[29] ($\tilde{V}_{\mathrm{exp}}(\mathrm{H})$) of the fluid as:

$$\tilde{V}_{exp}(H) = -\frac{\eta v_{exp}}{\varepsilon \varepsilon_0 E} = \frac{D}{2}\left[2bh - h^2\left(H^2 - 2H\right)\right] - \frac{b\kappa}{A}\sqrt{2\left[\cosh\left(A\zeta_w\right) - 1\right]} + \left(\zeta_w - \psi(H)\right) + \left\langle\tilde{V}_{exp}\right\rangle,$$

$$(4.12)$$

where $\left\langle\tilde{V}_{exp}\right\rangle$ is the depth average value of $\tilde{V}_{exp}$, which is related to the electrophoretic mobility (μ_e) of the tracer particle:

$$\mu_e = -\frac{v_p}{E} = \frac{\varepsilon_0}{\eta}\left\langle\tilde{V}_{exp}\right\rangle \qquad (4.13)$$
.
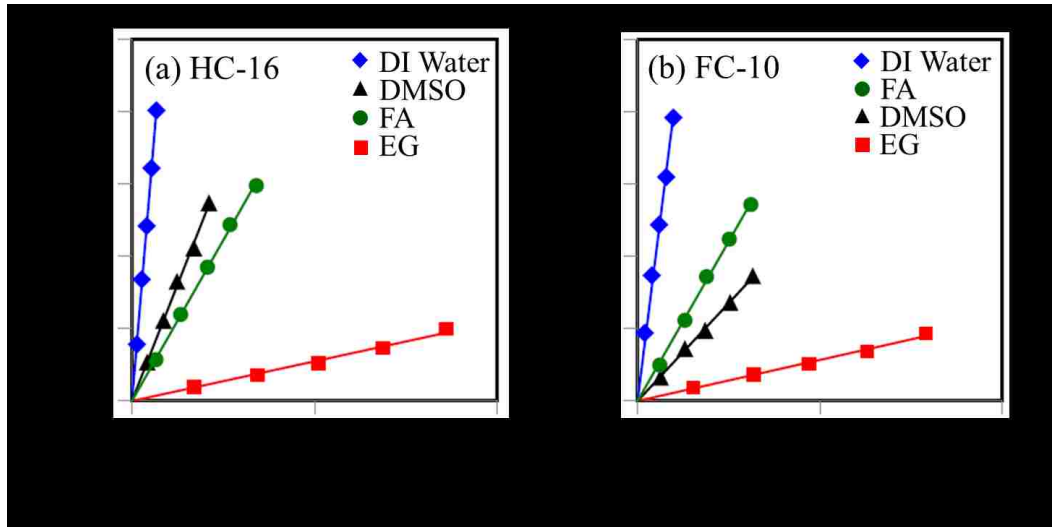
Figure 4.2. Centerline (H=1) velocity of the tracer particles in the channel as a function of electric field strength (-*E*). These (a) HC-16 and (b) FC-10 silane-treated surfaces were tested with four different liquids: DI water, dimethyl sulfoxide (DMSO), formamide (FA), and ethylene glycol (EG).

4.4. RESULTS AND DISCUSSION

4.4.1. Characterization of Silanized Surfaces

The test surfaces were characterized by atomic force microscopy, wettability, and the x-ray photoelectron spectroscopy (XPS). The corresponding results are summarized in Table 4.1, Table 4.2 and Figure 4.3, respectively. The values of the root mean square (RMS) roughness collected by AFM over an area of 2 μm × 2 μm indicate that the surfaces of the glass slides are relatively smooth, but that they are rough enough to (potentially) prevent slippage of the liquids at the wall.[28]

Table 4.1. The root mean square (RMS) roughness of the silanized glass surfaces over an area of 2 μm × 2 μm.

	Glass slide (pre-treated with piranha solution)	HC-16 modified	FC-10 modified
RMS roughness (nm)	0.60 ± 0.15	0.60 ± 0.10	1.04 ± 0.35

Table 4.2. The contact angles of the test surfaces with different liquids. θ_a: advancing contact angle; θ_r: receding contact angle; $\theta_h = \theta_a - \theta_r$.

Liquid	Molar Volume (cm³/mol)	HC-16 modified			FC-10 modified			grafted PDMS		
		θ_a (°)	θ_r (°)	θ_h (°)	θ_a (°)	θ_r (°)	θ_h (°)	θ_a (°)	θ_r (°)	θ_h (°)
DI Water	18.0	110 ± 1	96 ± 1	14	117 ± 2	93 ± 1	24	103 ± 2	98 ± 1	5
EG	55.7	84 ± 1	76 ± 1	8	99 ± 1	69 ± 1	30	87 ± 1	83 ± 1	4
DMSO	70.9	71 ± 1	61 ± 1	10	84 ± 1	70 ± 1	14	78 ± 1	74 ± 1	4
FA	39.7	93 ± 1	83 ± 1	10	107 ± 1	82 ± 1	25	95 ± 1	91 ± 1	4
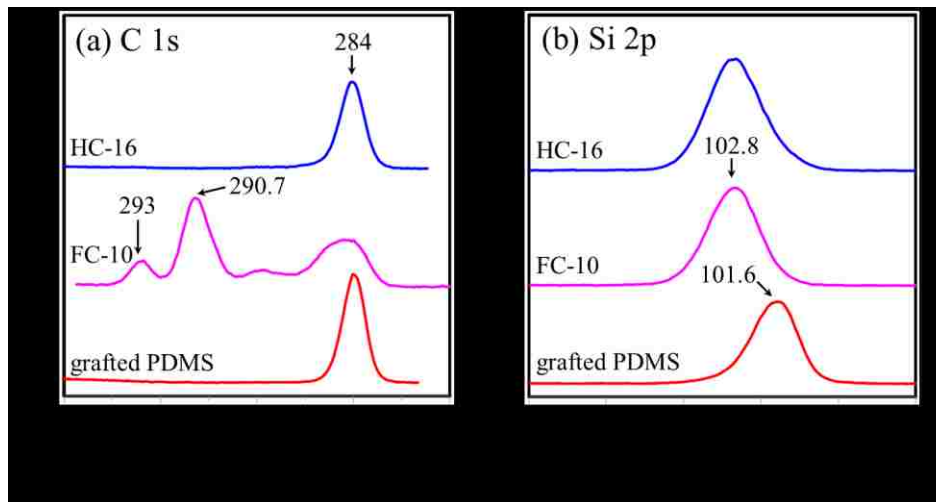
Figure 4.3. X-ray photoelectron spectra (XPS) in the (a) C 1s and (b) Si 2p regions of glass surfaces modified with hydrocarbon silane (blue), fluorocarbon silane (pink) and grafted PDMS (red).

The contact angles of the liquids on these surfaces are comparable to the previously reported values[18,20,21,30], with the observation that the hystereses of the liquids on the fluorocarbon surface are significantly higher than those on the hydrocarbon surface. These monolayers are very stable in water at neutral pH, as evidenced by the fact that the surface properties of the treated slides remain unaffected even after immersion in pure water for a week. There is a view in the literature[31] that the hysteresis of a test liquid on a surface would systematically decrease with its molar volume. In the current study, however, such a correlation is not observed. For example, ethylene glycol, with a molar volume three times as large as that of water, in fact, exhibits only a slightly higher hysteresis than water, whereas DMSO with an even a larger molar volume than water has a lower hysteresis.

Inspection of the C_{1s} region of the XPS spectra (Fig. 4.3) reveals that photoemissions from the carbon atoms of the HC-16 and the PDMS surfaces appear only at low binding energy, whereas that from the fluorocarbon surface gives rise to peaks at significantly higher binding energies reflecting the withdrawal of electrons from carbon atoms by the fluorine atoms. Weak photoemission at about 287.4 eV and slight broadening of the peak around 284 eV may indicate incomplete fluorination of the as-received silane. The prominent functionalities are, however, $-CF_3$ (~ 293 eV) and $-CF_2$ (~ 291 eV). Contact angle of water on this surface is insensitive to pH (2 to 12), which is consistent with the absence of ionizable groups such as carboxylic acid. Even though these XPS spectra were collected at a 15° take-off angle, the thin alkyl or fluoroalkyl siloxane monolayers could not fully attenuate the Si_{2p} photoelectrons (103

83

eV) ejected from the SiO_2 of the supporting glass.

4.4.2. Zeta Potentials of Silanized Glass Slides in Various Liquids

Fig. 4.4 summarizes the depth-dependent mobilities $[\tilde{V}_{exp}(H) - \langle \tilde{V}_{exp} \rangle]$ of four representative liquids (DI water, ethylene glycol, DMSO and formamide) in contact with the fluorocarbon and hydrocarbon silane-modified glass slides, which are corrected for the mobility of the tracer particles inside the channel (the uncorrected velocity profiles can be found in Appendix A). These measurements were carried out at five different electric-field strengths (Fig. 4.2) for each liquid on each surface. It is gratifying that all five sets of data nicely cluster around a single parabolic velocity profile in each case.

At the outset of the zeta potential analysis, we recognized that there are at least two unknown parameters: the slip length (b) and the Debye length (κ^{-1}). If these two parameters are known, the velocity profile can be fitted to equation 4.12 in order to extract the value of the zeta potential in a straightforward way. Before such a fit could be attempted, however, we also needed to address the possible uncertainty in the position of the particles (h') very close to the wall, which we expect to be somewhat larger than the radius of a single fluorescent particle. In our first attempt, we estimated the Debye lengths from the concentrations of the hydronium and hydroxide ions of the water present in these liquids (assuming a neutral pH) and those arising from the autoionization of the test liquid itself. The Debye lengths (κ^{-1}) were thus calculated to be
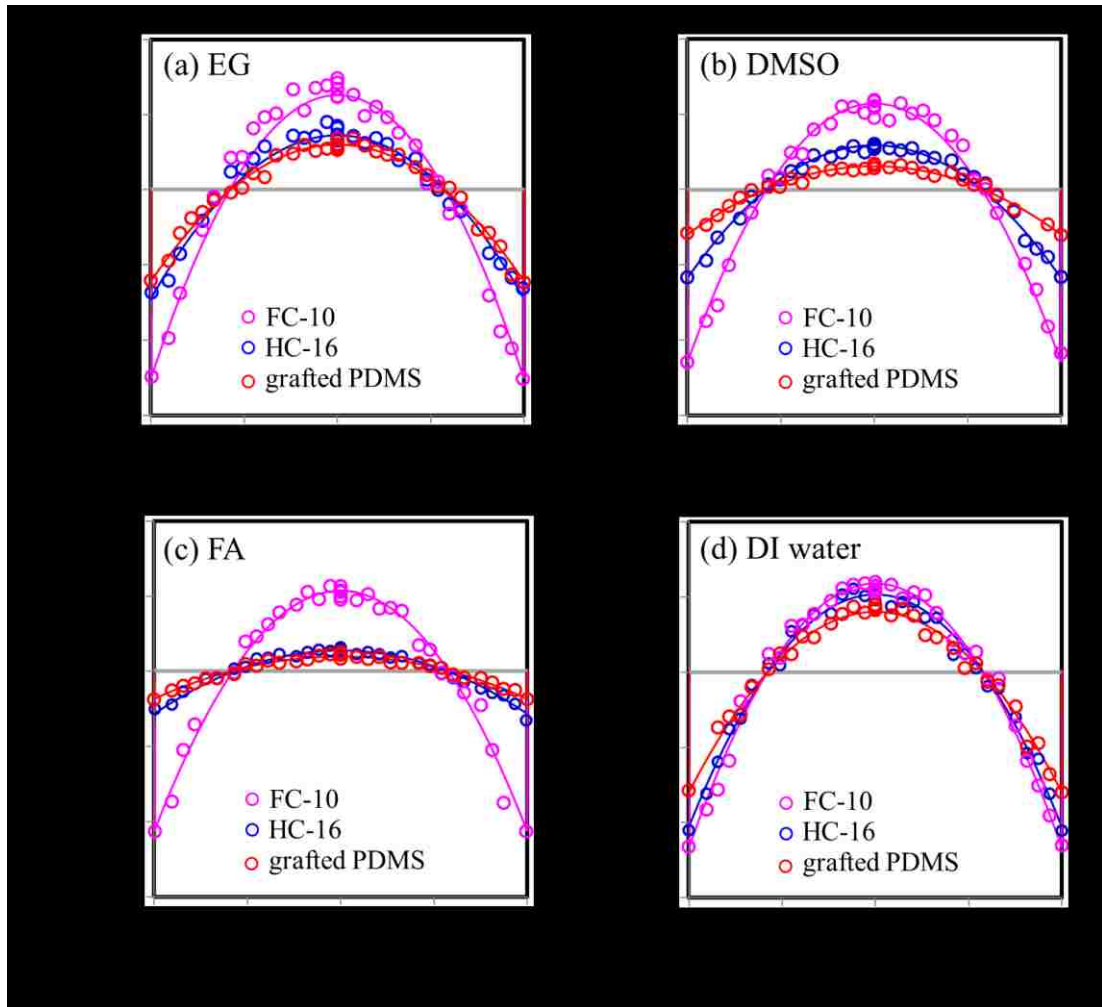
Figure 4.4. The mobility ($\tilde{v}_{exp}$) of the particles across the height (H) of a channel hydrophobized with fluorocarbon silane (pink), hydrocarbon silane (blue) and grafted PDMS (red). The experiment was carried out with (a) ethylene glycol (EG), (b) dimethyl sulfoxide (DMSO), (c) formamide (FA) and (d) DI water as test liquids. The curves are obtained from eq. 4.12 with the subtraction of $\langle \tilde{v}_{exp} \rangle$, as described in the text.

2 μm for ethylene glycol (autoionization constant = 10^{-16}), 6 μm for formamide (autoionization constant = 10^{-17}), 23 μm for DMSO, and 1 μm for pure water, respectively.[17] With these estimated Debye lengths, and with the help of a rather large electro-osmotic data set for each liquid, a multi-variable optimization was performed by adjusting the values of b, h', D and ζ_w to find the best fit between the experimental data and equation 4.12. The correlation coefficients (R^2) of the best fits, however, had values less than 0.9 for all cases (e.g. 0.88 for water, 0.82 for EG, 0.59 for FA and 0.76 for DMSO on the hydrocarbon surface, and 0.90 for water, 0.85 for EG, 0.65 for FA and 0.84 for DMSO on the fluorocarbon surface, respectively). The actual concentrations of the hydronium ions in the non-aqueous liquids are, however, much smaller than the above estimates based on their pH (all greater than 9) measured with a standard pH meter. While these values are somewhat unreliable (the actual pH is even higher) owing to the fact that protons diffusing out of the electrode influence the measurement, they still produce rather large Debye length for all the liquids (10 μm for EG, 20 μm for FA and 500 μm for DMSO). These suggest that the autoionization of the residual water or the carrier liquids do not yield the correct values of the Debye length in any of the cases, including pure water. Next, we performed a multi-variable optimized fitting of the experimental data by allowing the Debye length to be a variable as well. Such an analysis revealed that the slip length has to be vanishingly small, the Debye length has to be << 1 μm, and h' has to be less than 5 times the radius of the tracer particle (i.e., the particle is indeed very close to the walls of the channel) in order to obtain R^2 > 0.98. However, the lack of the precise knowledge of these parameters still makes it difficult
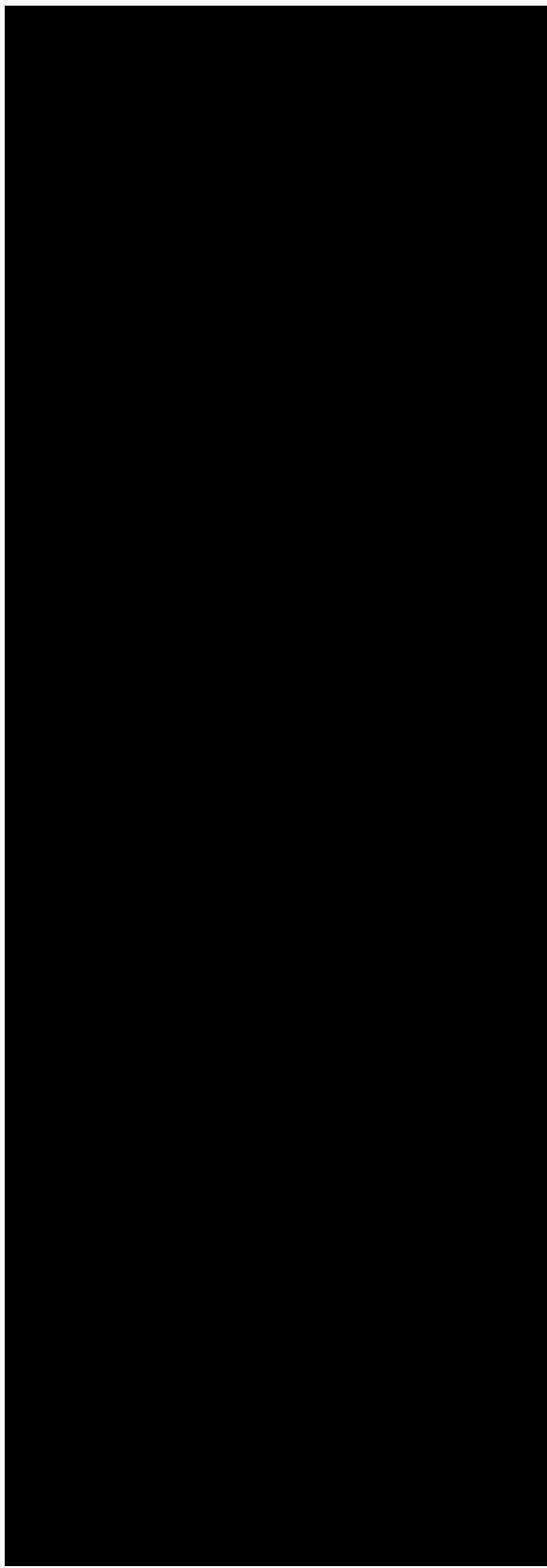
to estimate the absolute values of the zeta potential. For a sufficiently thick channel, i.e.,
h >> b, and for a very short Debye length, the velocity profile of the tracer particle
above an electrical screening layer can be written in the following form:

$$\tilde{V}_{exp}(H) = -\frac{\eta V_{exp}}{\varepsilon \varepsilon_0 E} = -\frac{D}{2}\left[h^2\left(H^2 - 2H\right)\right] + \zeta'_w + \left\langle \tilde{V}_{exp} \right\rangle \qquad (4.14)$$

where, $\zeta'_w = \zeta_w - (b\kappa k_B T / qe)\sqrt{2\left[\cosh(A\zeta_w) - 1\right]}$ is the apparent zeta potential of the surface,
the value of which would be same as the true zeta potential ζ_w if the fluid does not slip at
the wall. Since the roughness (≥ 0.6 nm) of both the hydrocarbon and fluorocarbon
substrates are larger than the threshold roughness[28] of wall slippage, it is possible that
the slip lengths (b) are vanishingly small in our experiments so that $\zeta'_w \sim \zeta_w$. We
re-emphasize that the integrated values of $\tilde{V}_{exp}(H)$ for each liquid yielding the values
of the mobility of the particle (μ_e) are essentially the same on both the hydrocarbon and
fluorocarbon surfaces, thus signifying that slippage of the liquids, if any, is not different
on the two types of surface. Even when the values of μ_e differed slightly in different
measurements, the estimated ζ'_w values were found to be rather robust. Within the above
scenario, the apparent zeta potential ζ'_w of each liquid contacting either surface can be
obtained by a straightforward fit of the experimental velocity data to equation 4.14 or
can be taken from the intercept of the ordinates of Fig. 4.4 for each surface.

Table 4.3 summarizes the apparent zeta potentials estimated for each liquid against
the hydrocarbon and the fluorocarbon surfaces. Significant zeta potential is indeed
observed with each of the test liquids in contact with both of the hydrophobic surfaces,
with the striking fact that its value on the fluorocarbon surface is substantially larger

Table 4.3. Zeta potential (ζ'_w) of glass surfaces modified with hydrocarbon silane (HC-16), fluorocarbon silane (FC-10) and grafted PDMS measured with different liquids.

than that on the hydrocarbon one. From the very outset, we note that there is no correlation between the zeta potentials and the dipole moments of these liquids, which contrasts a model[32] suggesting that orientation of water dipoles at the interface contributes to the zeta potential.

We discussed above that the autoionization of the residual water or the carrier liquids do not yield the correct values of the Debye length needed to explain the electro-kinetic effects observed with any of the polar liquids. Additional measurements carried out with the HC-16 and FC-10 surfaces show that the zeta potentials of ethylene glycol, formamide or DMSO are, in fact, rather insensitive to the amount of residual water (Figure 4.5). For example, the zeta potential observed with ethylene glycol against a HC-16 surface remains around -90 mV even when the concentration of water
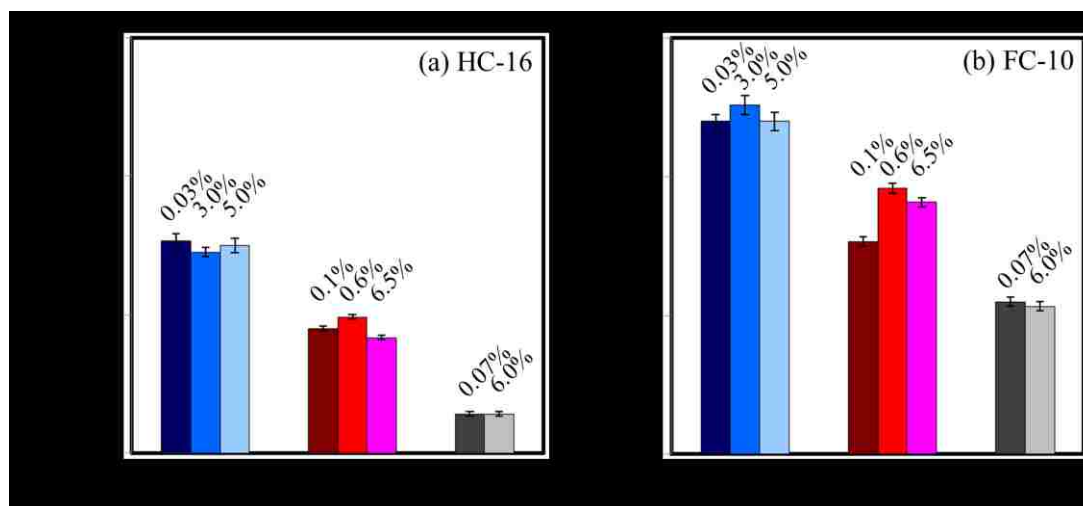
Figure 4.5. Bar graphs showing the zeta potentials of (a) HC-16 and (b) FC-10 silane modified glass tested against the ethylene glycol (EG), dimethyl sulfoxide (DMSO) and formamide (FA). The weight percent of water of each probe liquid is shown above the bars.

in the solvent increases from 0.03 % to 5 % (w/w). Formamide and DMSO also show similar trends. The conductivity (151 μS/cm) of the as-received formamide used to test the zeta potential was rather high. However, when the liquid was treated with a mixed-bed resin, its conductivity decreased to 25 μS/cm, while its water content increased from 0.07% to 6% and pH decreased from 9.5 to 5.1. Remarkably, both the treated and the untreated formamide displayed very similar zeta potentials against HC-16 surface as shown in Figure 4.5. We expected the hydroxide ion concentration to increase with the dielectric constant of each probe liquid, and using the law of mass action, zeta potential to increase with the concentration of water as well. We thus find, so far, no clear evidence to support a model in which the ionization of the residual water or that of the carrier liquid plays a major role in the observed electro-kinetic phenomena.

As is usually the case with the surface chemistry experiments, it is tempting to attribute such types of anomalous results to impurities on the test surfaces that would deprotonate and give rise to surface charging. Since XPS did not provide evidence for the presence of such dissociable functional groups as carboxylic acid, one possibility is that the silanol groups of the support or from the silane used to modify the surfaces could be the source of such ionization. While such a picture would also be consistent with our findings (Fig. 2.6) and some observations reported in the literature[37,38] that the zeta potentials of the silanized silica surfaces increase with pH, it does not resolve some of the other issues satisfactorily. For example, let us take the case of formamide, which was used both as-received and after its treatment with a mixed-bed resin. Owing to the

fact that the conductivity and the dielectric constant of the as-received formamide are both higher than those of water, this solvent provides a better environment for the putative silanol groups (isoelectric point ~ 2) to deprotonate than water. Thus one might expect formamide to display a higher surface charge density than water and thus a higher zeta potential, which is not the case. Furthermore, the zeta potentials of ethylene glycol, whose dielectric constant is considerably smaller than those of water and formamide, are quite comparable to that of water on the HC surface. For ethylene glycol on the FC surface, the zeta potential is actually slightly higher than water and nearly three times as large as that for formamide. Thus, the dissociation of a pre-existing group such as silanol to yield the negative charge does not appear to account entirely the trends of the zeta potentials observed with all the liquids against the various surfaces.

4.4.3. Comparison with the Grafted PDMS Film

Perhaps, a somewhat clearer picture emerges when we examine what happens when these polar liquids contact PDMS-coated glass slides for which the Si_{2p} photoelectrons arising from glass are fully attenuated. The signals of the Si_{2p} photoelectrons ejected from the 5-nm-thick grafted film correspond to the more electron-rich silicon atoms of PDMS, relative to those of silica. Furthermore, there is no evidence of any oxidized carbon species on such surfaces. The contact angles of the probe liquids also exhibit much lower hysteresis on this surface, thus indicating that these surfaces are rather homogeneous and devoid of pinning sites of the types that give

rise to contact angle hysteresis (Table 4.2).

Significant zeta potentials are observed with this surface as well (Fig. 4.4 and Table 4.3). Even though the magnitudes of the potentials on the PDMS-grafted surface are considerably smaller than the FC-10-coated glass slide, the values are only slightly smaller than the HC-16-coated glass slide, thus suggesting the effects observed with the HC-16 surface may indeed be mainly due to the hydrocarbon groups with a small effect arising from the underlying silica. The fluorocarbon monolayer, which can exhibit considerable disorder with a high area fraction of grain boundaries, can expose both silica as well as the acidic α-methylene group to H-bonding and thus donor-acceptor interactions may prevail with the probe liquids. What appears clear from these studies is that it is not imperative that a dissociative functional group exist on a surface in order to give rise to charging in contact with polar liquids.

4.4.4. Comparison with the 40-µm-thick PDMS Films

There is, nevertheless, another aspect of this system as revealed by the electrokinetics of these liquids on the 40-µm-thick polydimethylsiloxane (PDMS) coated glass substrates. XPS studies (Fig. 4.6) confirm that the silicon on the ideal network PDMS surface is in a lower oxidation state than that in the monolayers on glass. A PDMS-grafted (5 nm) glass slide, with no observable highly oxidized Si_{2p} groups in its XPS spectrum, on the other hand, exhibits a zeta potential of about -80 mV against deionized water that is comparable to that of the HC monolayer on silica. This surface

also exhibited the lowest contact angle hysteresis (5º) with water. The zeta potentials of commercial PDMS (Sylgard 184; Dow Corning) are also measured, and they are comparable with the zeta potentials estimated with grafted and ideal network PDMS surfaces (Fig. 4.7 and Table 4.4). Sylgard 184 contains siliceous fillers and shows a tail on the XPS spectra in the Si_{2p} region at 102.5 eV (a higher oxidation state) (Fig. 4.6). Taken together, all these results suggest that although there exist certain non-trivial effects of the underlying substrate (i.e., glass) on the zeta potential of the grafted organic layers, a pure hydrophobic surface can also exhibit non-negligible zeta potentials in contact with polar protic and aprotic liquids. The electrophoretic mobilities of the tracer particles on the PDMS elastomers (Table 4.4), are very similar to what has been observed with the HC and FC monolayers on glass (Table 4.3).
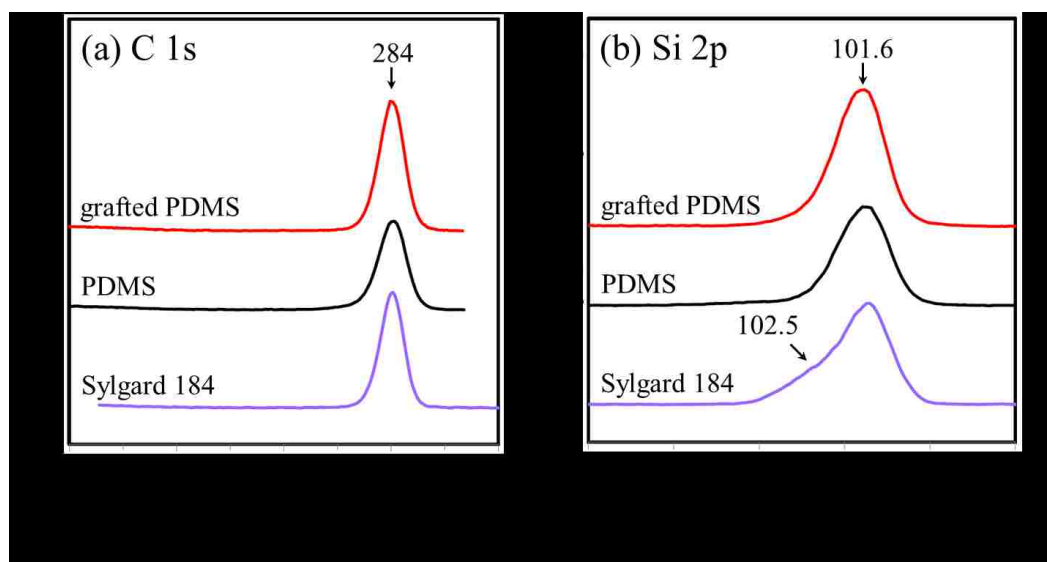
Figure 4.6. X-ray photoelectron spectra (XPS) in the (a) C 1s and (b) Si 2p regions of glass surfaces modified with grafted PDMS (red), ideal network PDMS (black), and Sylgard 184 (purple).
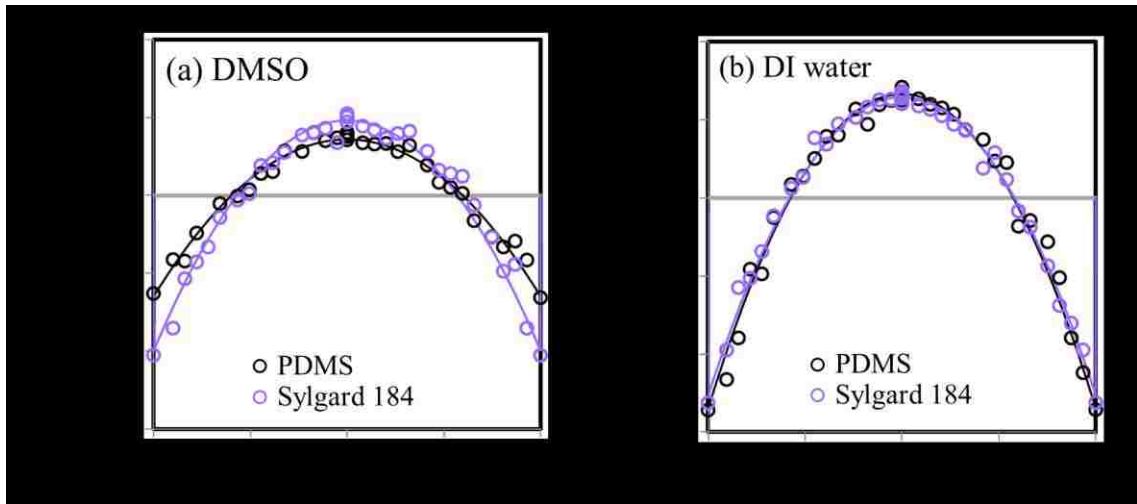
Figure 4.7. The mobility ($\tilde{v}_{exp}$) of the particles across the height (H) of a channel coated with 40-µm-thick ideal network PDMS (black) and Sylgard 184 (purple) films. The experiment was carried out with (a) dimethyl sulfoxide (DMSO) and (b) DI water as test liquids. The curves are obtained from eq. 4.12 with the subtraction of $\langle \tilde{v}_{exp} \rangle$, as described in the text.

Table 4.4. Zeta potential of PDMS elastomer coated glass measured with dimethyl sulfoxide (DMSO) and DI water.

Liquid	$\mu_e \times 10^{-9}$ (m^2/V s)			ζ'_w (mV)		
	Grafted PDMS	PDMS	Sylgard 184	Grafted PDMS	PDMS	Sylgard 184
DMSO	7.0	3.8	3.5	-30 ± 1	-13 ± 1	-20 ± 1
Water	50.9	40.1	44.1	-80 ± 2	-81 ± 2	-76 ± 1

4.5. SUMMARY AND CONCLUSIONS

This research adds to the repertoire of observations[5,18,37-39] of electro-kinesis of water in contact with numerous hydrophobic surfaces. There is a common consensus in the literature that certain amount of charging does occur with any hydrophobic surface in contact with water. Finite zeta potentials have also been reported for hydrophobic self-assembled monolayers on gold[40-42], though there are large variations in the reported data depending upon the conditions used. For example, whereas Knoll *et al.*[40,41] reported a zeta potential in the range of -100 mV for aqueous electrolyte solutions in contact with flat surfaces of alkanethiol-modified gold, Yang and Abbott[42] reported a zeta potential of only 2 mV for alkanethiol-modified colloidal particles in water. Based on such a small value of zeta potential, Yang and Abbott[42] attributed their results to impurities. While our observations do not lead to a conclusive picture of the origin of electro-kinesis at the interfaces of various polar liquids in contact with hydrodrophobic surfaces, they do illustrate how ubiquitous the phenomenon is even with some of the passive surfaces studied here. The strengths of the zeta potentials are so significant in these systems that it obligates us to be cautious in the quantitative interpretation of the zeta potentials measured even in more obvious situations involving ionizable functional groups.

We do not claim that our silanized glass surfaces present pure hydrophobic groups to the probe liquids. The finite wetting hysteresis observed with such surfaces suggests that there are defects. While the absolute values of the advancing and receding contact angles of water on our HC-16 treated glass surface are quite comparable to some of the

carefully prepared monolayers[20] on silicon, there are reports[43,44] in the literature that monolayers of even lower hysteresis can be prepared depending upon the preparation condition, reactivity and the smoothness of the substrate. However, it might be virtually impossible to produce a sufficiently defect-free monolayer coated surface of large enough surface area to conduct these measurements. Furthermore, the structures of such alkylsiloxane-coated substrates are known[45] to have a thin intercalated water layer. In spite of these complexities, the zeta potentials of various probe liquids in contact with the HC-16 treated glass surface are found to be rather close to those of a PDMS-grafted (5 nm) glass surface that is much more passive by wettability and XPS. The higher hysteresis of the fluorocarbon monolayer coated glass, however, suggests that it may not be all that passive in comparison to the other surfaces. Here, disorder and non-ideal surface coverage could indeed expose the underneath silica and the α-methylene group to the probe liquid. High zeta potentials of various probe liquids, including, aprotic DMSO, observed on surfaces suggest that electro-osmosis can be a very sensitive tool to study surface heterogeneity and defects.

Amongst all the surfaces studied here, the PDMS coating turned out to be most passive in terms of wettability, XPS and zeta potential. By extrapolating the results obtained with the HC and FC surfaces in terms of their insensitivity to the amount of the water present in the probe liquids, and that there is no evidence of any pre-existing functionality that would de-protonate, we feel that a non-conventional explanation would be needed to explain the charging of a passive surface as PDMS in contact with polar liquids.

We feel that the recent suggestions[6,14] of charging of hydrophobic surfaces in contact with water based on the transfer of charge inherent in hydrogen bonding deserve careful consideration. It has been well-known since the days of Mulliken[46] that hydrogen bonds between water molecules involve a transfer of electronic charge. According to this model[14], although the charge transfer is symmetrical in the bulk, the balance between the donating and accepting H-bonds is broken near a hydrophobic surface that leads to a net negative charge. Although certain details still need to be worked out[14] (e.g. the nature of the charged species that drag the liquid near the wall need to be established), this explanation of the charging at water/hydrophobic interfaces is promising and implies that other types of H-bonding liquids like ethylene glycol and formamide could show similar effects. However, in order to explain the differences with various surfaces, and especially the result obtained with the aprotic liquid (DMSO), additional factors need to be considered. The results with the aprotic DMSO on the FC surface is particularly striking, as this liquid exhibits a zeta potential as high as water or ethylene glycol, whereas its zeta potential against the HC and the PDMS surfaces are substantially lower than those two liquids. This result could be a manifestation of substantial donor-acceptor interaction between basic DMSO with the underneath silica and/or the acidic α-methylene of the fluorocarbon. In addition, as the fluorine atom is considerably more electronegative than carbon, a carbon-fluorine bond is considerably more polar than a carbon-hydrogen bond[47], which may further disrupt the charge transfer between the molecules of the hydrogen-bonding liquids. There is also the possibility that various probe liquids may themselves participate in donor-acceptor

interactions with the fluorocarbon surface. Indeed, a fluorocarbon surface (e.g. Teflon) is more negative than a hydrocarbon surface (e.g. polyethylene) in the triboelectric series[16,48] as well. Recently, some interesting developments have taken place in the field of contact charging[49-52], where both ion and electron transfer have been considered. These views may be refined and blended with the picture proposed by Vácha *et al.*[6] to improve our understanding of the zeta potentials observed with various protic and aprotic liquids against hydrophobic surfaces. The model also needs to be developed further in order to understand the results of Yaminsky and Johnston[15], who observed charging of a hydrophobized glass slide when it is retracted from water, formamide, and other liquids. When such a substrate is retracted from a liquid, it might emerge as a neutral species if the charge equilibrates quickly. However, in the presence of an energy barrier, such a substrate may emerge with a net charge, which will eventually equilibrate with atmosphere. Thus, it may also be necessary to invoke an activated intermediate state in the charge-transfer interaction.

Separation of contact charges coupled with an activated intermediate state suggests the possibility that the contact and separation of a liquid and a solid involve irrecoverable work, which could be another hitherto unsuspected cause of contact-angle hysteresis in some situations. It is plausible that the large hysteresis observed with all of these liquids on the fluorocarbon surface may be partially related to such hysteretic contact-separation processes. Further systematic work is warranted to resolve these issues. The observations of this work suggest the need to extend experimental and theoretical studies of electrokinetic phenomena beyond water and oil, to include a much

larger spectrum of liquid-substrate combinations. The series of novel surfaces reported in reference [47], in which the headgroup properties of self-assembled monolayers can be varied systematically, may be valuable for such types of studies.

REFERENCES

1. Dickinson, W. *Transactions of the Faraday Society* 1941, **37**, 140-148.

2. Marinova, K. G.; Alargova, R. G.; Denkov, N. D.; Velev, O. D.; Petsev, D. N.; Ivanov, I. B.; Borwankar, R. P. *Langmuir* 1996, **12**, 2045-2051.

3. Beattie, J. K.; Djerdjev, A. M. *Angewandte Chemie International Edition* 2004, **43**, 3568-3571.

4. Beattie, J. K.; Djerdjev, A. M.; Warr, G. G. *Faraday Discussions* 2009, **141**, 31-39.

5. Tandon, V.; Bhagavatula, S. K.; Nelson, W. C.; Kirby, B. J. *Electrophoresis* 2008, **29**, 1092-1101.

6. Vácha, R.; Rick, S. W.; Jungwirth, P.; de Beer, A. G. F.; de Aguiar, H. B.; Samson, J.-S.; Roke, S. *Journal of the American Chemical Society* 2011, **133**, 10204-10210.

7. Winter, B.; Faubel, M.; Vácha, R.; Jungwirth, P. *Chemical Physics Letters* 2009, **474**, 241-247.

8. Petersen, P. B.; Saykally, R. J. *Chemical Physics Letters* 2008, **458**, 255-261.

9. Vácha, R.; Buch, V.; Milet, A.; Devlin, J. P.; Jungwirth, P. *Physical Chemistry Chemical Physics* 2007, **9**, 4736-4747.

10. Buch, V.; Milet, A.; Vácha, R.; Jungwirth, P.; Devlin, J. P. *Proceedings of the National Academy of Sciences U.S.A.* 2007, **104**, 7342-7347.

11. Iuchi, S.; Chen, H. N.; Paesani, F.; Voth, G. A. *Journal of Physical Chemistry B* 2009, **113**, 4017-4030.

12. Takahashi, H.; Maruyama, K.; Karino, Y.; Morita, A.; Nakano, M.; Jungwirth, P.; Matubayasi, N. *Journal of Physical Chemistry B* 2011, **115**, 4745-4751.

13. Mundy, C.-J.; Kuo, I. F. W.; Tuckerman, M. E.; Lee, H.-S.; Tobias, D. J. *Chemical Physics Letters* 2009, **481**, 2-8.

14. Ben-Amotz, D. *Journal of Physical Chemistry Letters* 2011, *2*, 1216-1222.

15. Yaminsky, V. V.; Johnston, M. B. *Langmuir* 1995, **11**, 4153-4158.

16. Harper, W. R. *Contact and Frictional Electrification*; Laplacian Press: Morgan Hill, CA, 1998.

17. Izutsu, K. *Electrochemistry in Nonaqueous Solutions*; Wiley-VCH: Weinheim, Germany, 2002.

18. Lin, C.-H.; Chaudhury, M. K. *Langmuir* 2008, **24**, 14276-14281.

19. Chaudhury, M. K.; Whitesides, G. M. *Langmuir* 1991, **7**, 1013-1025.

20. Wasserman, S. R.; Tao, Y.-T.; Whitesides, G. M. *Langmuir* 1989, **5**, 1074-1087.

21. Ulman A. *An Introduction to Ultrathin Organic Films: From Langmuir-Blodgett to Self-Assembly*; Academic Press, Inc.: San Diego, CA, 1991.

22. Krumpfer, J. W.; McCarthy, T. J. *Faraday Discussions* 2010, **146**, 103-111.

23. Gao, C.; Xu, B.; Gilchrist, J. F. *Physical Review E* 2009, **79**, 036311.

24. Masliyah, J. H.; Bhattacharjee, S. *Electrokinetic and Colloid Transport Phenomena*; John Wiley & Sons, Inc.: Hoboken, NJ, 2006, p 221-361.

25. Rothstein, J. P. Slip on Superhydrophobic Surfaces. *Annual Review of Fluid Mechanics* 2010, **42**, 89-109.

26. Hunter, R. J. *Zeta Potential in Colloid Science: Principles and Applications*; Academic Press, Inc.: London, U.K., 1986, p 363-369.

27. Das, S.; Chakraborty, S. *Langmuir* 2010, **26**, 11589-11596.

28. Zhu, Y. X.; Granick, S. *Physical Review Letters* 2002, **88**, 106102.

29. Electrokinetic mobility is defined as the ratio of velocity to electric field. Since the mobility here is multiplied by the viscosity and divided by the dielectric constant of the liquid, $\tilde{V}_{exp}(H)$ is strictly speaking a depth dependent electrokinetic potential.

30. Mettu, S.; Chaudhury, M. K. *Langmuir* 2010, **26**, 8131-8140.

31. Timmons, C. O.; Zisman, W. A. *Journal of Colloid and Interface Science* 1966, **22**, 165-171.

32. Wilson, M. A.; Pohorille, A.; Pratt L. R. *Journal of Chemical Physics* 1989, **90**, 5211-5213.

33. *Ethylene Glycol Product Guide*; MEGlobal: Midland, MI.

34. Kaatze, U.; Pottel, R.; Schäfer M. *Journal of Physical Chemistry* 1989, **93**, 5623-5627.

35. Hernández-Luis, F.; Galleguillos-Castro, H.; Esteso, M. A. *Fluid Phase Equilibria* 2005, **227**, 245-253.

36. Riddick, J. A.; Bunger, W. B.; Sakano, T. K. *Organic Solvents: Physical Properties and Methods of Purification*, 4th ed.; John Wiley & Sons, Inc.: New York, 1986.

37. Hozumi, A.; Sugimura, H.; Yokogawa, Y.; Kameyama, T.; Takai, O. *Colloids and Surfaces A: Physicochemical and Engineering Aspects* 2001, **182**, 257-261.

38. Shyue, J.-J.; De Guire, M. R.; Nakanishi, T.; Masuda, Y.; Koumoto, K.; Sukenik C. N. *Langmuir* 2004, **20**, 8693-8698.

39. Kirby, B. J.; Hasselbrink, E. F. *Electrophoresis* 2004, **25**, 203-213.

40. Schweiss, R.; Welzel, P. B.; Werner, C.; Knoll, W. *Langmuir* 2001**, 17***, 4304-4311.

41. Schweiss, R.; Welzel, P. B.; Werner, C.; Knoll, W. *Colloids and Surfaces A: Physicochemical and Engineering Aspects* 2001, **195**, 97-102.

42. Yang, Z. Q.; Abbott, N. L. *Langmuir* 2010, **26**, 13797-13804.

43. Maoz, R.; Sagiv, J. *Journal of Colloid and Interface Science* 1984, **100**, 465-496.

44. Kessel, C. R.; Granick, S. *Langmuir*, 1991, **7**, 532-538.

45. Angst, D. L.; Simmons, G. W. *Langmuir*, 1991, **7**, 2236-2242.

46. Mulliken, R. S.; Person, W. B. *Annual Review of Physical Chemistry* 1962, **13**, 107-126.

47. Graupe, M.; Takenaga, M.; Koini, T.; Colorado, R.; Lee, T. R. *Journal of the American Chemical Society* 1999, **121**, 3222-3223.

48. Williams, M. W. *AIP Advances* 2012, **2**, 010701.

49. Gibson, H. W.; Bailey, F. C. *Chemical Physics Letters* 1977, **51**, 352-355.

50. Baytekin, H. T.; Baytekin, B.; Soh, S.; Grzybowski, B. A. *Angewandte Chemie International Edition* 2011, **50**, 6766-6770.

51. Wiles, J. A.; Grzybowski, B. A.; Winkleman, A.; Whitesides, G. M. *Analytical Chemistry* 2003, **75**, 4859-4867.

52. McCarty, L. S.; Whitesides, G. M. *Angewandte Chemie International Edition* 2008, **47**, 2188-2207.

Chapter 5

Shear-Induced Fracture of a Silicone Release Coating Modified with a Thin Polyvinyl Alcohol Hydrogel

ABSTRACT

Marine biofouling is ubiquitous for a ship surface in contact with seawater. Silicone elastomers have been developed to be the easy-release coatings that facilitate biofoulant removal. Here, we introduced a new polyvinyl alcohol (PVA) / polydimethylsiloxane (PDMS) composite material to enhance the anti-fouling property of the easy-release coating PDMS. A silane coupling agent (11-(triethoxysilyl)udecanal) was used to covalently bond hydrophilic PVA to hydrophobic PDMS. The PVA coating was cross-linked by glutaraldehyde to form a polymer network. The stability of PVA layers was tested and examined by spectroscopic techniques, indicating the PVA coating was robust on a PDMS surface. The interfacial adhesion of this composite material was further investigated by a shear-induced test. The removal stress of a silanized glass prism from the PVA surface was reduced by ~60% in comparison with unmodified 40-micron-thick PDMS films under water. The shear tests performed in both systems in water and ethylene glycol suggested the PVA layer was able to swell and preserve the liquids at the interface as lubricants.

5.1. INTRODUCTION

Marine biofouling happens to all surfaces in contact with seawater due to the adsorption of marine organisms. The fouling organisms change the morphology of the ship surface, leading to a significant increase in the hydrodynamic drag and thus reducing the cruise efficiency. Removal of these biofoulants is a time- and money-consuming process.[1] Polymer films (e.g. silicone elastomers) with low elastic modulus and surface energy are found to promote easy release of marine organisms, such as barnacles. These properties ensure that marine organisms are bonded to it through weak interactions in an adhesive geometry which facilitates removal. Thus, the biofoulant will fall off via the hydrodynamic force created by the ship movement.[1-3] The easy-release coating has been studied for its physical and mechanical properties[4,5] and additives for antifouling enhancement[6]. As reviewed by Brady and Singer[3], the release mechanism of biofoulants on foulant-release coatings is related to the coating properties, such as surface energy, elastic modulus, and coating thickness. Chaudhury *et al.* have studied the release mechanism of a pseudo-barnacle by using pull-off[7] and shear-induced[8,9] experiments. The fracture stress ($\sigma*$) increases with the shear modulus (μ_s) of the polydimethylsiloxane (PDMS) and interfacial work of adhesion (W_a) but decreases with film thickness (h), i.e., $\sigma* \sim (\mu_s W_a/h)^{0.5}$. However, easy-release coatings are mainly used in fast moving boats and are more expensive than conventional paints.[2] Improvement in these coatings is necessary to increase their ease of application and prolong their in-service time (i.e., cost reduction).

In nature, a hydrogel with low friction can be found as natural cartilage tissue.[10, 11]

Hydrogels are good candidates for surface modification to reduce the interfacial friction. Gong *et al.*[12] have developed double-network hydrogel with strong mechanical properties and low surface friction. This double-network hydrogel (or interpenetrating polymer network hydrogel) is composed of a highly cross-linked poly(2-acrylamido-2-methyl-1-propanesulfonic acid) gel of which the mechanical properties are improved by adding loosely cross-linked poly(acryl amide) gel. Moreover, poly(ethylene glycol) and poly(vinyl alcohol) (PVA) hydrogels are widely studied to investigate their mechanical properties and friction coefficients.[13-15] Studies of gel friction have also been reviewed by Boumberger and Caroli[16] as well as Gong and Osada[17].

In this chapter, we present a novel technique to immobilize thin layers of PVA hydrogel onto polydimethylsiloxane (PDMS) films to alter the surface properties of PDMS. We aim to reduce the interfacial friction between the PDMS surface and fouling organisms, further enhancing the anti-biofouling abilities of the easy-release coating. This PVA/PDMS composite material is a combination of the high strength of PVA and the unique flexibility of silicone elastomer. Additionally, PVA is non-toxic and offers good thermal and chemical stability after it is cross-linked.[18] In order to apply the hydrophilic PVA coating to hydrophobic PDMS, a silane coupling agent (11-(triethoxysilyl)udecanal, terminated with aldehyde group) is used to bridge (chemically bond) these two different materials. The aldehyde moieties react with the hydroxyl groups in PVA to form covalent bonds[18,19] allowing the hydrogel layer to firmly attach to the PDMS underneath. The coated PVA layer is also cross-linked with

glutaraldehyde to ensure a robust thin PVA film is applied to the PDMS surface. The modified surfaces were further examined by underwater shear-induced tests to investigate the surface adhesion.

5.2. EXPERIMENTAL

5.2.1. Materials

n-hexadecyltrichlorosilane (HC-16, 95%; Gelsest), 11-(triethoxysilyl)udecanal (TESU, $(CH_3CH_2O)_3Si(CH_2)_{10}CHO$, 95%; Gelsest,), toluene (ACS grade, $\geq$99.5 %; Fisher Chemical), hydrochloric acid (HCl, 12 M, ACS grade; EMD Chemicals), acetone (general use HPLC/ACS grade; Pharmco-AAPER), ethanol (200 Proof; Decon Labs, Inc.) and ethylene glycol (EG, spectrophotometric grade, 99+%; Alfa Aesar) were used as received. 5 w/w% of polyvinyl alcohol (PVA) solution was prepared by dissolving PVA granules (MW 88000-97000, 98-99% hydrolyzed; Alfa Aesar) in de-ionized water (DI water; Barnstead) in a water bath at 90 ˚C. 2 w/v% glutaraldehyde (GA) was prepared by the dilution of 25% GA solution (Grade I; Sigma-Aldrich) with DI water. The pH of 2% GA solution was adjusted to 1 with the addition of 12-M HCl.

5.2.2. Preparation and Characterization of PDMS Films Coated with PVA

Polydimethylsiloxane (PDMS) was prepared by thoroughly mixing the Sylgard 184 (Dow Corning) silicone elastomer base and the curing agent with the weight ratio

of 10:1. After degassing in vacuum for 1 h, this homogeneous mixture was poured onto a glass slide that has been cleaned by piranha solution. Two spacers with the same and known thickness were placed on the two sides of the glass slide to control the PDMS film thickness. Subsequently, the mixture was carefully covered by another glass slide silanized[20] with HC-16, followed by curing in a preheated convection oven at 100 ˚C for 1 h. The silanized glass slide was gently peeled off after the PDMS film cooled at room temperature.[21]

A 0.5 vol% TESU toluene solution was prepared in a purge of ultra-high purity nitrogen followed by the addition of ~50 μL HCl into the solution. After 5 min, the PDMS bonded glass slide (Fig. 5.1a), which had been treated with the corona discharge from a Tesla coil for 1 min for surface oxidation, was immersed into this silane mixture for 3 h. The reacted samples were further rinsed with toluene, acetone, and ethanol in sequence. In every rinsing step, the samples were immersed in each solvent and sonicated for 10 min. These rinsing steps were utilized to remove the unreacted silane coupling agent from the PDMS network. The silanized PDMS samples were then dried with a nitrogen purge, and placed into a preheated oven at 70 ˚C for 3 h (Fig. 5.1b). The sample was preserved in a vacuum chamber at room temperature before further use.[22] The PDMS film bonded to a glass slide would be swollen in toluene during the reaction, and the film would restore to its original thickness after the toluene was fully removed in vacuum.

The cross-linking ratio of the PVA was calculated based on the molecular weight of the repeating unit of PVA and controlled by the mixing ratio of PVA and GA solutions
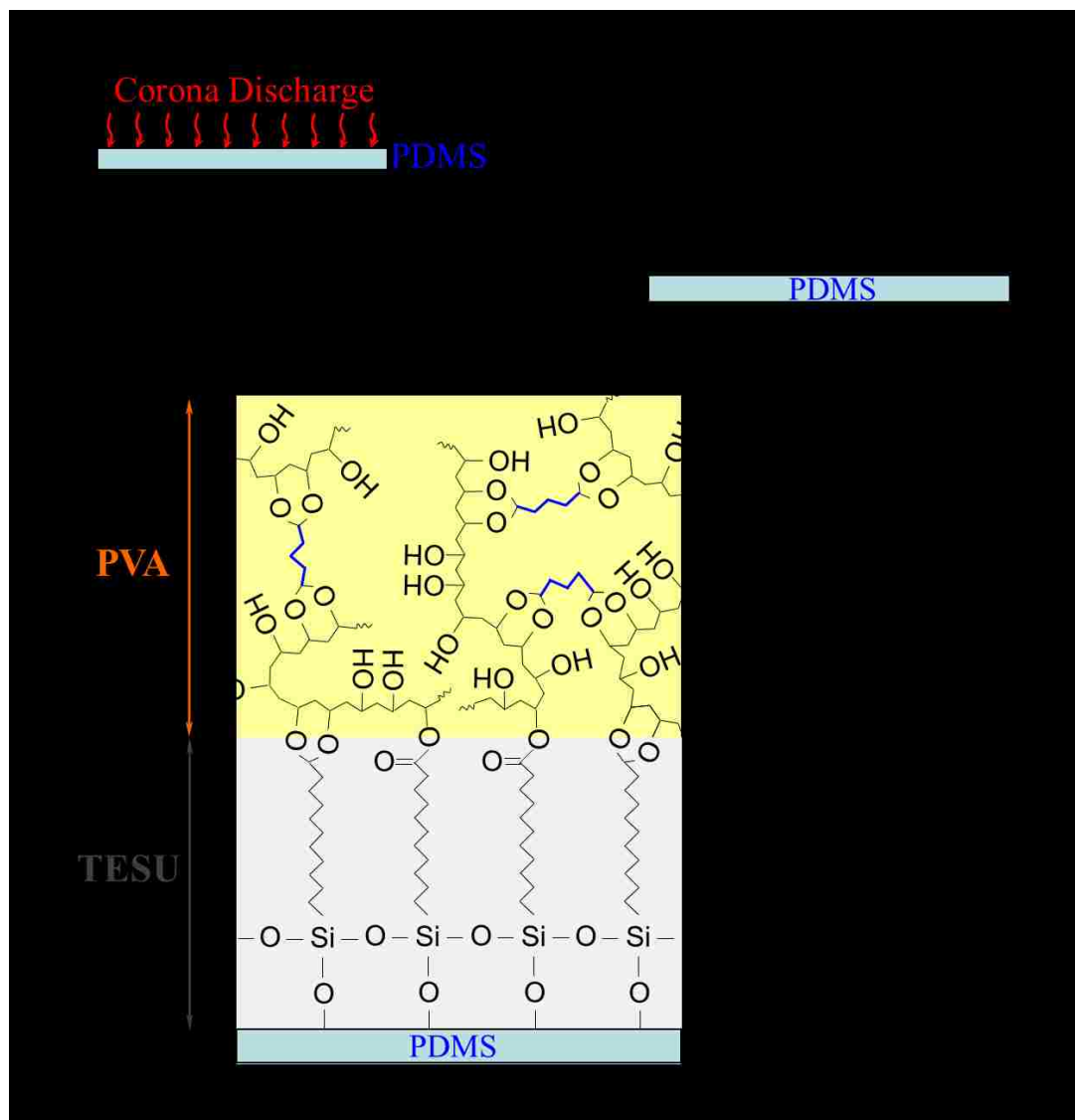
Figure 5.1. Schematic diagram of the polyvinyl alcohol (PVA) coating process. (a) The PDMS film was bonded onto a glass slide and exposed to a corona discharge. (b) The surface of the PDMS was modified by 11-(triethoxysilyl)udecanal (TESU). The aldehyde functionalities were partially oxidized to carboxyl groups as shown in XPS spectrum in Fig 5.3. (c) The TESU modified PDMS was further coated with the mixture of PVA and glutaraldehyde (GA). The blue lines indicate the cross-linking bridges of GA among the PVA chains after the reaction.

(Appendix B). After the PVA and GA solutions were mixed at the required ratio, the mixture was spread onto the TESU-modified PDMS surface for a spin coating treatment at 1200 rpm for 60 sec. The PVA-coated samples were kept in a Petri dish at room temperature overnight for further reaction of cross-linking between PVA and GA.[18,19] For the samples with multilayers of coatings, each additional layer was applied with the same PVA/GA mixture and spin coating conditions as the previous layer. In this work, the PDMS surfaces were modified with 2 layers of PVA coating. Finally, the samples (Fig. 5.1c) were rinsed with copious amounts of DI water and dried with a purge of ultra-high purity nitrogen.

High resolution x-ray photoelectron spectroscopy (XPS, Scienta ESCA-300) and attenuated total reflectance-Fourier transform infrared spectroscopy (ATR-FTIR, Nicolet iS10; Thermo Scientific) were used to characterize the PDMS surface before and after the modification of PVA. The thicknesses of the equivalent PVA coatings (on Si wafers) were measured by variable angle spectroscopic ellipsometry (model V-VASE® with WVASE32 software; J.A. Woollam Co., Inc.) in air and under water.

5.2.3. Underwater Shear Experiment

Utilizing double sided tape, the PVA coated PDMS sample was attached to the bottom of a square Falcon® Petri dish (10 × 10 × 1.5 cm; Becton Dickinson), which was affixed to the moving stage. (Fig. 5.2) The test sample was immersed in DI water overnight before the shear experiment. For the shear test of an unmodified PDMS

surface, fresh samples were used without the pre-immersion in water since water could slightly oxidize the surface to change its properties. The sharp edge of the aluminum protrusion was adjusted to 1 mm above the test surface. A glass prism (~10 × 10 × 6 mm) silanized with HC-16 was carefully brought into contact with the sharp edge of the protrusion under water. After the weight and the holder were placed on the glass prism for the test time interval, the motorized stage (Nanostep Motorized System, model #17NST103; Melles Griot) was set to start. The reading of the load cell (model LBB300; Futek Advanced Sensor Technology) was recorded via the data acquisition system (model NI USB-9215A; National Instruments) connected to a computer.[8]
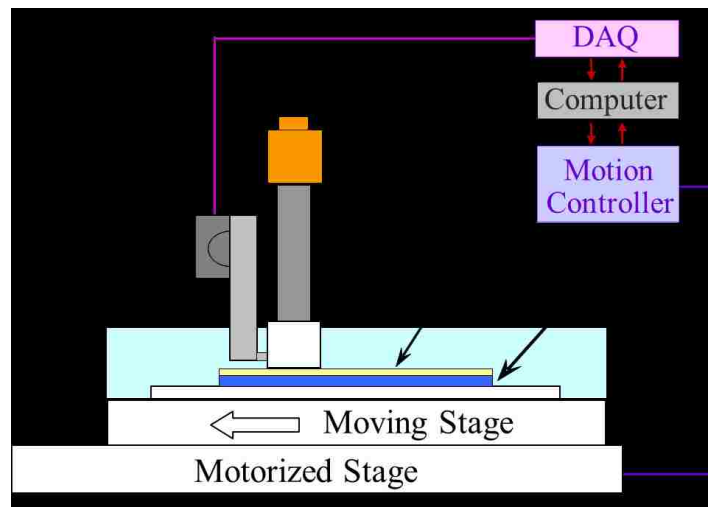
Figure 5.2. Schematic diagram of the underwater shear-test experiment. A square Petri dish is attached to the moving stage by using double sided tape. The test sample is affixed to the bottom of the Petri dish with double sided tape as well. A glass prism is brought into contact underwater with the test surface and the sharp edge of the protrusion, which is connected to a load cell. The water level in the Petri dish is higher than the interface of the glass prism and PVA coating. The weight holder along with the weight is subsequently placed on the glass prism carefully. The motion of the moving stage is controlled by the motorized stage connected to a computer. The reading of the load cell is also collected by the computer via a data acquisition system (DAQ). Illustration is not to scale.

5.3. RESULTS AND DISCUSSION

5.3.1. Surface Characterization of Modified PDMS Surfaces

The PVA coating was first prepared on a Si wafer to evaluate the feasibility of PVA coating on a silica substrate. The XPS spectrum (Fig. 5.3) showed that the surface of Si wafer is modified by aldehyde functionality in TESU, and that ~50% of the aldehyde groups were oxidized and turned into carboxyl groups. Additionally, in the spectrum of a PVA coated Si wafer, the O–C–O functionality, which was formed by the reaction between the aldehyde and the hydroxyl moieties (Fig. 5.1 and Appendix B), indicated that the PVA was partially cross-linked by glutaraldehyde (GA).[23,24] These results verified the methodology of PVA coating on a silica layer, so that the coating process was further applied to an oxidized PDMS surface. After the TESU-modified PDMS surface was coated with PVA, the Si atom was no longer observed on the surface. (Table 5.1) The atomic ratio (~ 2:1) between carbon and oxygen of the PVA coating surface was in accordance with the composition of PVA functionalities. This ratio, which remained the same after the immersion of water at 90 °C for 2 h, indicated the PVA coating was stable on PDMS. The ATR-FTIR spectra (Fig. 5.4) exhibiting the specific peaks (–OH at 3550-3200 cm^{-1} and –C=O at 1750-1735 cm^{-1}) of PVA also showed the modification of PDMS.[25,26] Since the thickness of the PVA film is smaller than the depth sensed by ATR-FTIR (~2 μm), the spectrum peaks (–C–H at 2950 cm^{-1}, –Si–O at 1000-1100 cm^{-1}, and –Si–CH$_3$ at 800 and 1250 cm^{-1})[26,27] due to the underneath PDMS substrate can still be observed. The same spectrum of PVA/PDMS material before and after the stability test confirmed the robust PVA coating on a PDMS surface.
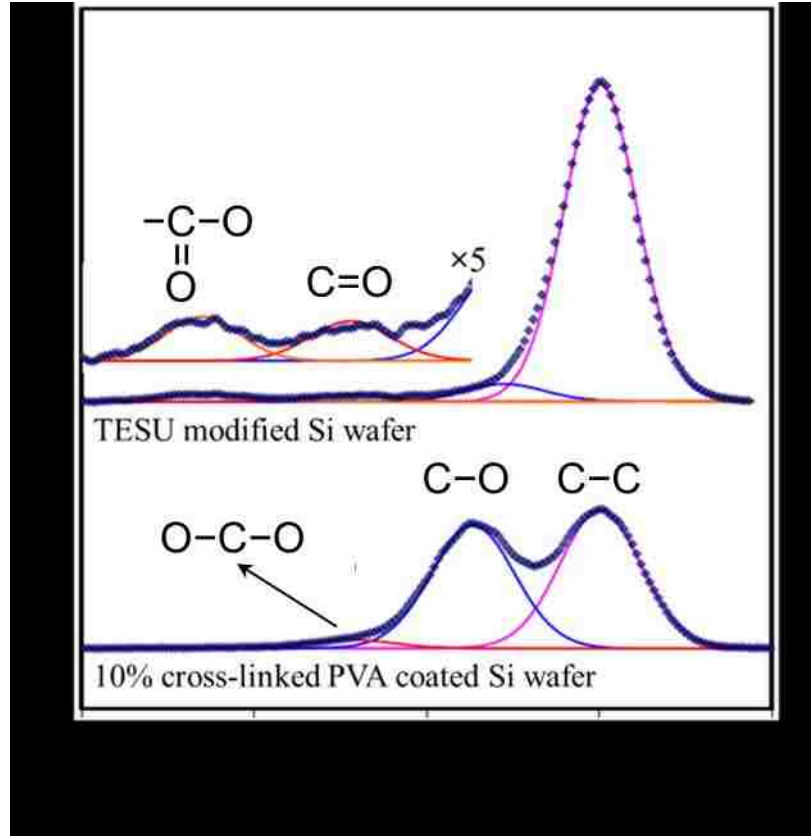
Figure 5.3. XPS C_{1s} spectra of Si wafer modified with TESU (top, tested with a take-off angle of 15°) and 10% cross-linked PVA (bottom).

Table 5.1. The atomic percentage of the PDMS coating before and after the modification of 10% cross-linked PVA.

Atomic percentage	Si	C	O
PDMS (Sylgard 184)	27.52	44.18	28.30
PVA/PDMS	0.02	66.10	33.88
PVA/PDMS (after the immersion of 90°C water)	0.00	66.68	33.32
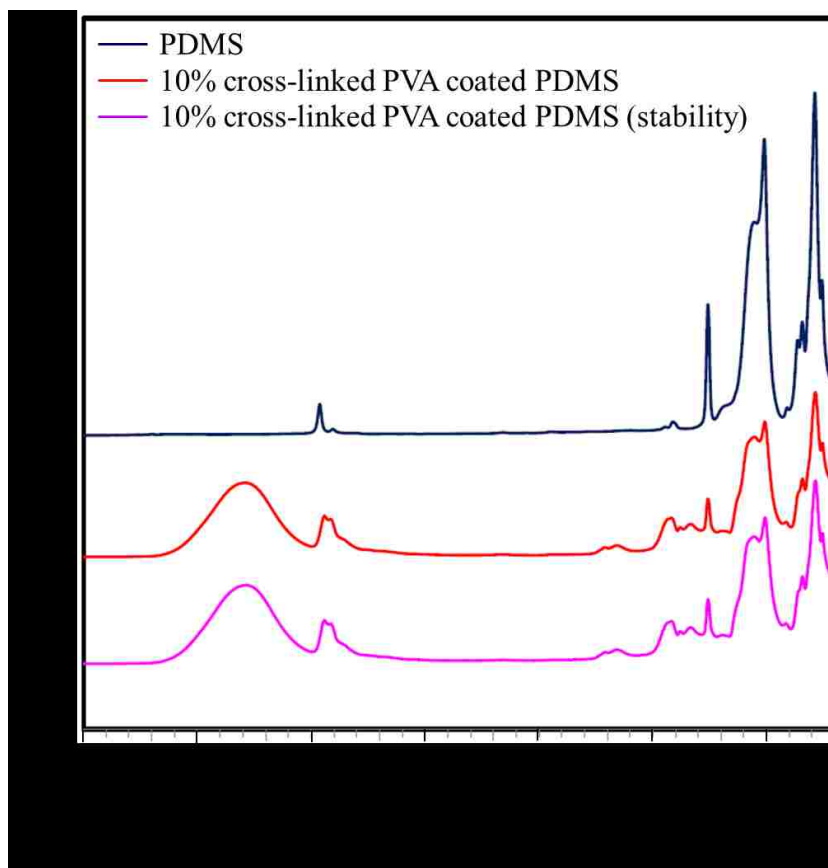
Figure 5.4. ATR-FTIR spectra of PDMS before (blue) and after (red and pink) the modification of 10% cross-linked PVA. The pink curve shows the spectrum tested with the PVA coating after the immersion of water at 90 °C for 2 h.

The thicknesses of PVA coatings on Si wafers were estimated using ellipsometry in air and under water (Fig. 5.5). Since the measurements of thicknesses of the PVA layers could not be performed on PDMS, because the refractive index of the substrate was closely matched to that of PVA, the thicknesses of equivalent layers (same coating process) on silicon wafers were characterized. The swelling ratio of the PVA coating

was calculated to be

$$\frac{\text{Wet film thickness - Dry film thickness}}{\text{Dry film thickness}} \times 100\% .$$

This swelling ratio was estimated based on the assumption that the PVA coating was confined on the Si wafer. Hence, while the PVA film swells, the volume change was exhibited on the manifested thickness. The swelling ratio of the PVA coating decreased with the cross-linking ratio as expected.
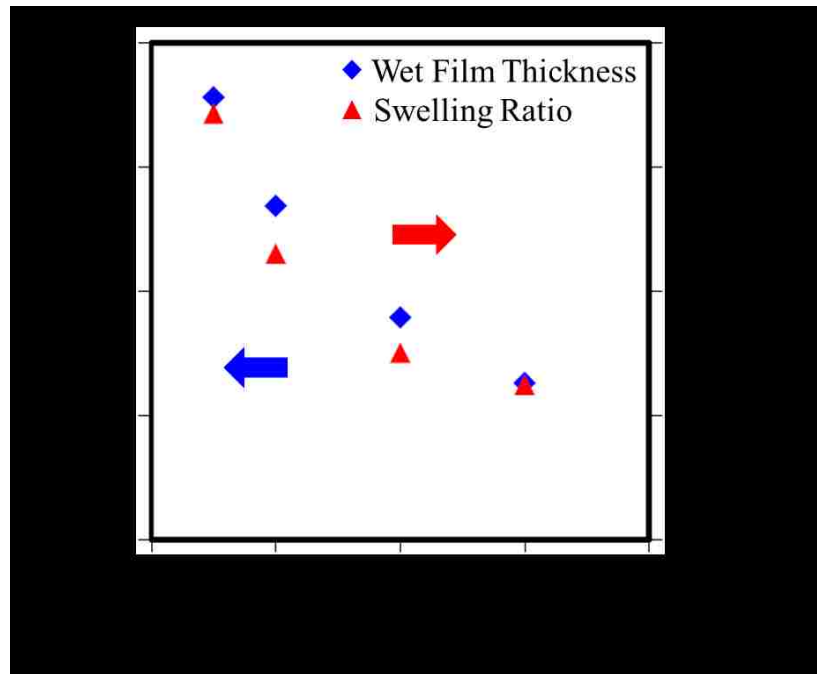
Figure 5.5. PVA film thickness and swelling ratio as a function of cross-linking ratio. The PVA was coated on a Si wafer in order to be examined by an ellipsometer in air and under water. 2 layers of PVA were coated onto the wafer as indicted in the text.

5.3.2. Underwater Shear Experiment of PVA/PDMS Composite Material

The underwater shear test is first utilized to investigate the systems of silanized glass prisms sliding against PDMS films bonded to glass slides as controls (Fig. 5.6a). While a silanized glass cube was brought into contact with a PDMS surface underwater, the dispersion force of these two surfaces expels most of the water at the interface and enables these two surfaces to make contact. As the glass cube is slid against the surface, a frictional force is developed at the interface. This frictional force and external force tilt the glass prism and generated a torque. If this torque is strong enough, it can cause a fracture at the interface of the glass prism and PDMS surface. The critical shear stress (σ_s^*) is defined to be the maximum shear stress before the glass cube comes off the surface (Fig. 5.6a).
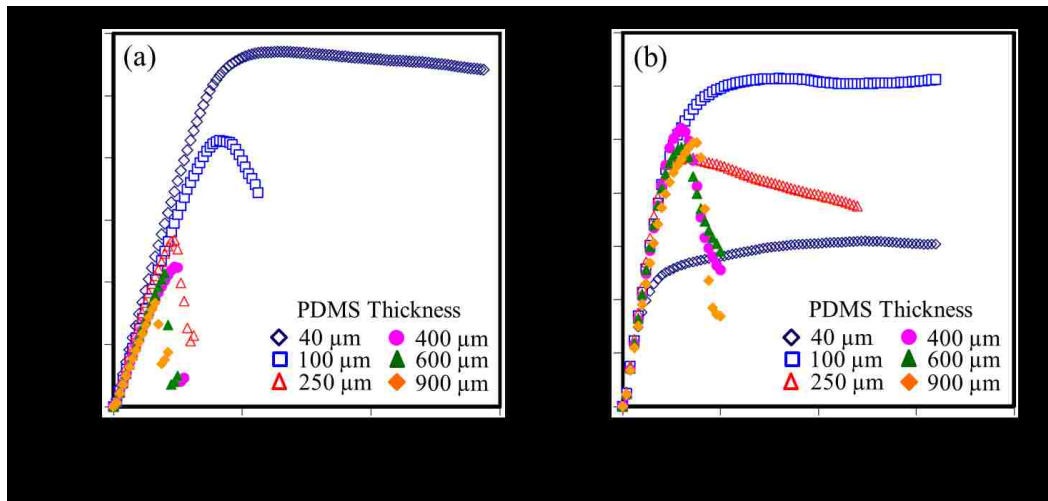
Figure 5.6. The profile of shear stress of a silanized glass prism sheared underwater on (a) PDMS films bonded to glass slides, and (b) PDMS films modified with 10% cross-linked PVA. The velocity of the moving stage was 20 μm/s. The total weight placed on the glass cube was 126 g.

When a prism of width a is sheared against an elastomer with a force applied at distance l above the interface, and if an elastic instability occurs at the interface, the critical shear stress (σ_s^*) was found to follow the relation[8,9]: $\sigma_s^* \sim (a/l)(W_a\mu_s/h)^{0.5}$, where W_a is the interfacial work of adhesion, μ_s is the is the shear modulus of the film, and h is the thickness of the film. Thus, a plot of σ_s^* vs. $\sqrt{\mu_s/h}$ will give a gradient of $(a/l)\sqrt{W_a}$. With the known dimension of a/l (~10), the value of W_a can be estimated. Here, similar to the result of a silanized glass cube sheared against a PDMS bonded glass slide in air, this underwater system shows that σ_s^* still varies with $1/\sqrt{h}$ under water. In order to have a rough idea of the underwater W_a, using $\sigma_s^* \sim (a/l)(W_a\mu_s/h)^{0.5}$, let us assume both regressive gradients in Figure 5.7 have the same pre-factor in two
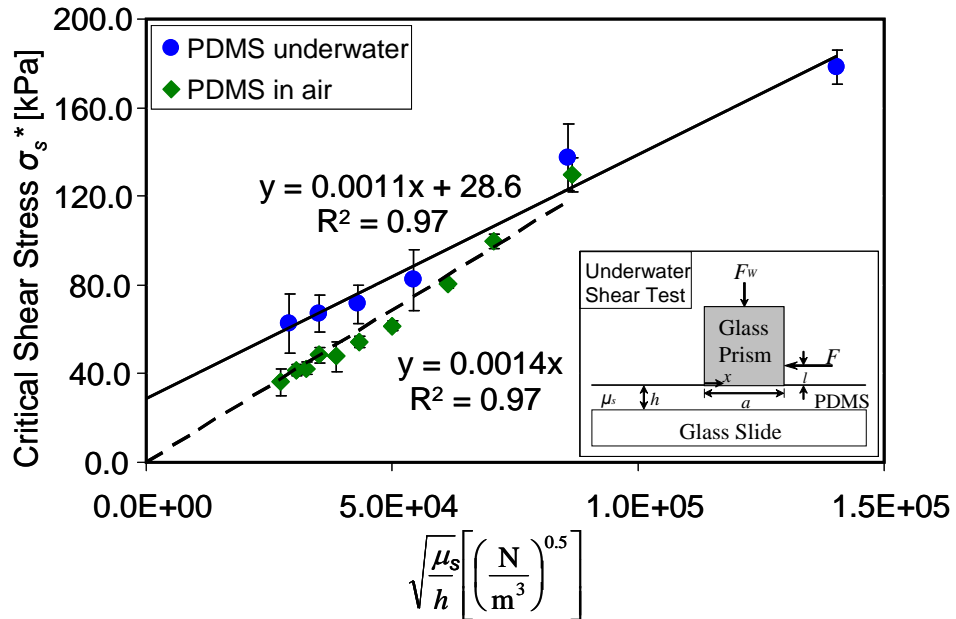
Figure 5.7. The relation between a silanized glass prism sheared against PDMS (Sylgard 184) under water (circles) or in air (diamonds; courtesy: Kyoung Hwan Kim[8]). The schematic shows the parameters for underwater shear test.

mediums. The value of W_a for the system in air is taken to be 40 mJ/m^2, which is a typical value for dispersion interactions. The underwater W_a can be estimated to be ~25 mJ/m^2 from the ratio of the two slopes. This estimation is based on the assumption that the pre-factor is mainly dependent on the geometric scales in the system. The reduction of W_a under water is due to water screening the van der Waals forces at the prism/PDMS.

We further applied this shear test to study the interfacial adhesion of a silanized glass cube sheared against a PVA/PDMS composite material (Fig. 5.6b). At a constant sliding velocity of 20 μm/s, the frictional force generated was not strong enough to remove the glass prism for the case of PDMS thickness smaller than 100 μm. For unmodified PDMS films, σ_s^* decreased with the PDMS thickness due to more restricted lateral contraction in the PDMS film. While a silanized cube was sheared against the PVA-coated PDMS film, both PVA and PDMS were deformed. As we could observe in the shearing profile of PVA modified PDMS (< 100 μm), the glass cube was sliding at some shear stress without coming off the surface. Since the lateral contraction of the PDMS was very limited, the cube was finally sheared and slipped on the PVA hydrogel layer. This shear stress was much lower than that of the cube sheared against PDMS. While the thickness of PDMS film increased, the degree of the lateral contraction of PDMS also increased. The shear stress was thus able to generate enough torque (PDMS thickness > 250 μm) to remove the cube from the surface at a constant σ_s^* (~ 50 kPa). The parameters of contact time and sliding velocity were also inspected to see if they were significant in our system. For the PVA/PDMS composite material, critical shear

stress is not a strong function of contact time (> 5 min) and moving velocity (< 100 μm/s) of the stage. (Fig. 5.8)
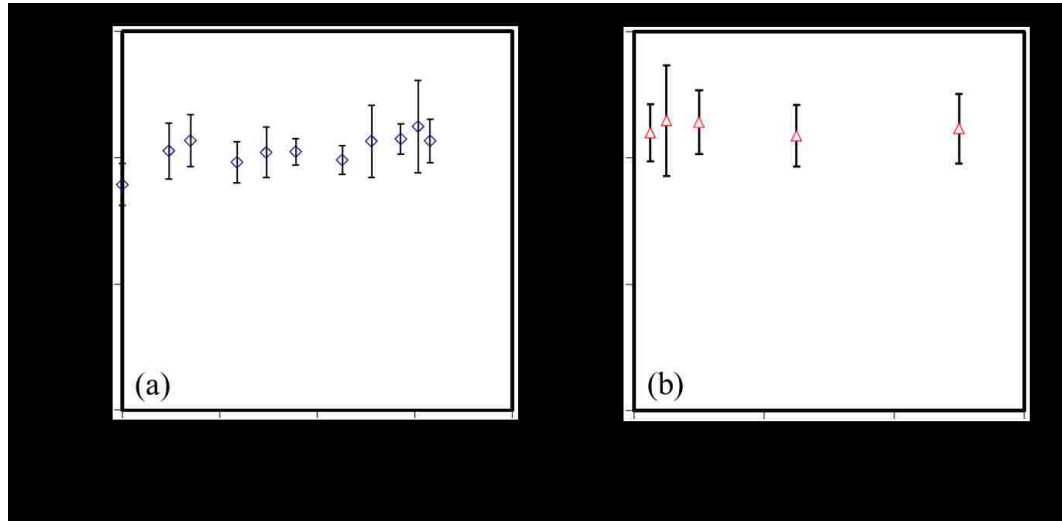
Figure 5.8. The critical shear stress (σ_s*) of a silanized glass cube shearing against 10% cross-linked PVA modified PDMS films, as a function of (a) contact time (at constant stage velocity of 20 μm/s) and (b) stage velocity (at constant contact time of 5 min). The PDMS thickness was 0.4 mm. The weight placed on the glass prism was 126g.

We further investigated the role of the cross-linking ratio of PVA to the friction of the interface between the silanized glass prism and PVA/PDMS material. After the treatment of PVA coating, with the same PVA cross-linking ratio, the difference among the values of σ_s* from various PDMS thicknesses was not significant (Fig. 5.9). This result showed that the PVA layer on PDMS plays an important role in the release mechanism. For the case of a silanized glass cube, when it was brought into contact with a PDMS surface under water, the water was gradually removed from the interface

as both surfaces are hydrophobic. In the case of PVA coated PDMS, the swollen hydrogel ensured that water must remain at the interface. It was possible that this layer of water at the interface acts as a thin lubrication layer. If this were the predominant release mechanism, then one would not expect the thickness of the PDMS to be important. This hypothesis complemented the experiment results shown in Fig. 5.9, where for a given cross-linking ratio, the critical shear stress remained independent of the PDMS thickness. In order for this hypothesis to be correct, one must assume that the deformation of the PDMS film is very small, such that the stress field generated at the surface is not felt by the PDMS/glass interface.
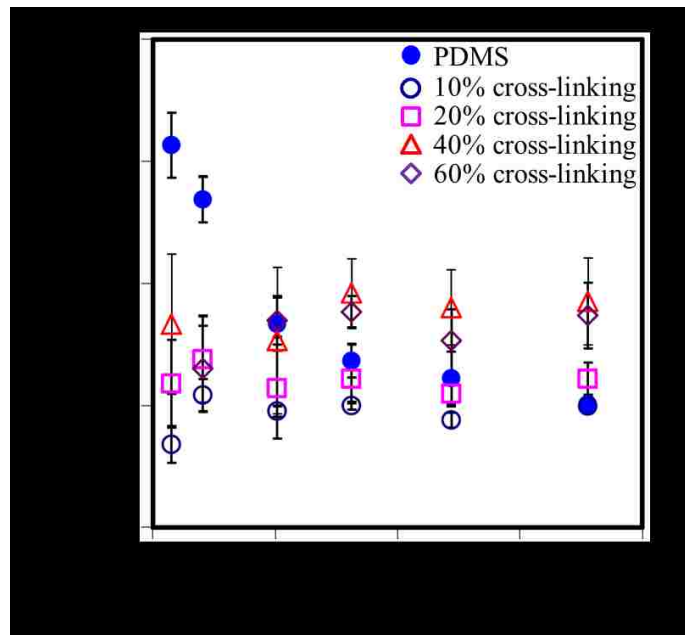
Figure 5.9. The relation between critical shear stress (σ_s*) and the thickness of PDMS films with/without coatings of PVA at different cross-linking ratios in an underwater shear test (Fig. 5.2). The weight placed on the silanized glass prism was 126 g. The contact time of the test is 15 min for PDMS and 5 min for PDMS coated with PVA.

5.3.3. Shear Experiment of PVA/PDMS Composite Material in Ethylene Glycol

While a silanized glass prism was sheared on the PVA/PDMS material in ethylene glycol (EG), the prism would slide across a distance before it reached σ_s^* (Fig. 5.10). In addition, the sliding distance decreased with the contact time. This sliding profile was different from the case of unmodified PDMS films, for which the prism stayed in contact with the surface before the interfacial fracture occurred.
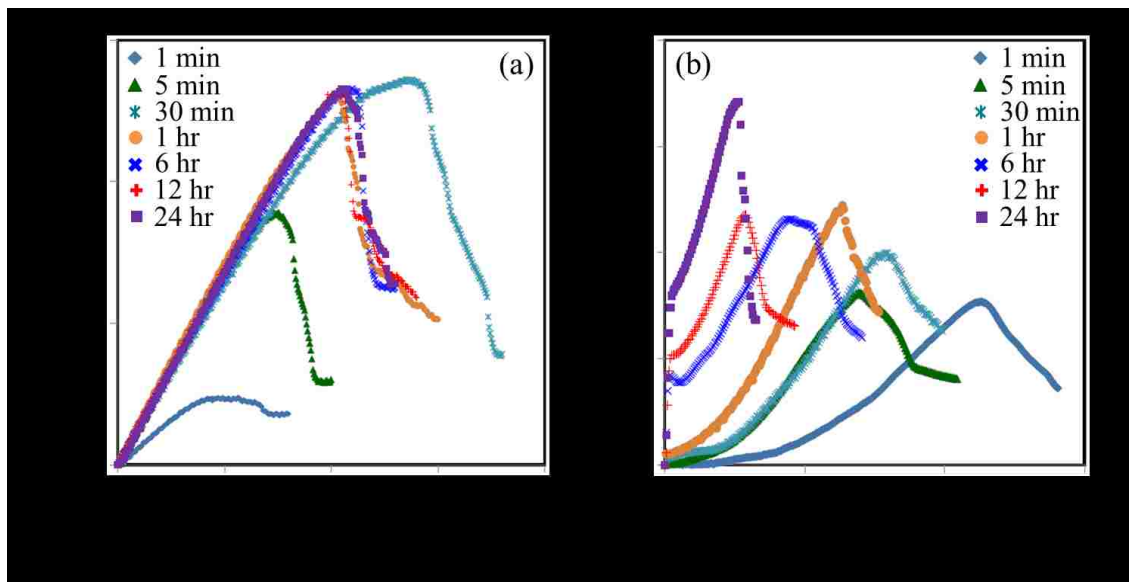
Figure 5.10. The shear stress profile of a silanized glass prism sheared on (a) PDMS films bonded to glass slides, and (b) PDMS films modified with 10% cross-linked PVA in ethylene glycol. These profiles were sampled at different contact time. The thickness of the PDMS film was 0.4 mm. The velocity of the moving stage was 20 μm/s. The total weight placed on the glass cube was 126 g.

As a silanized glass cube was brought into contact to the test surface in EG, the hydrophobic surface would slowly remove the EG at the interface due to the dispersion

force at the interface. Comparing the case tested in water, this solvent removal process would be slower in EG, ascribed to the viscosity of EG is higher than that of water. For the silanized prism/PDMS interface, most EG was expelled from the interface after 30 min so that the critical shear stress reached a constant value (~50 kPa) (Fig. 5.11). This critical shear stress, which was smaller than that measured in water (~75 kPa), indicated that the residual EG at that interface acted as a lubricant. Similar results were also observed in the system of silanized prism/PVA interface. The critical shear stress was significantly reduced in EG (~20 kPa) in comparison with the results tested in water (~60 kPa). The swollen PVA[28] was capable of retaining EG at the interface and thus reducing the critical shear stress.

Figure 5.11. Critical shear stress (σ_s*) as a function of contact time tested in water (open symbols) and in ethylene glycol (EG, closed symbols). A silanized glass prism was sheared against a 0.4-mm-thick PDMS film with (diamonds) or without (squares) the coating of 10% cross-linked PVA. The weight placed on the glass cube was 126 g. The stage velocity was controlled at 20 μm/s.

5.3.4. Shear Stress Relaxation of PVA/PDMS Composite Material

In order to further understand the release mechanism at the interface of the PVA coating and silanized glass prism, the relaxation o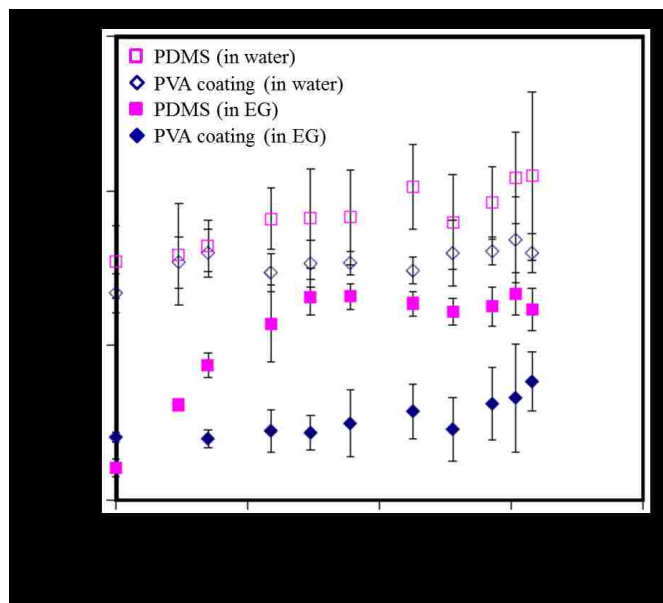f the PVA/PDMS material was studied by monitoring the shear stress profile after the moving stage stopped. The motor stage was controlled to stop when the shear stress reaches ~ 32 kPa (σ_{s0}). As shown in Fig. 5.12, the unmodified PDMS showed similar relaxation behavior for both thin (40 μm) and thick (900 μm) films. In the same time interval, the relaxation of a PVA/PDMS material became slower with the increasing thicknesses of PDMS films. The thicker (> 400 μm) PDMS films showed nearly equal relaxation, regardless of whether they were coated with PVA or not.

If there is no slippage at the prism/PVA interface, one can expect that, for a purely elastic material, there will be no shear stress relaxation on the stress profile after the motor stage is stopped due to the elasticity of the material generating a force that pushes the prism against the protrusion. Since PDMS bears more elasticity than PVA, for a PVA/PDMS composite material, the overall elastic property of the material will increase with the thickness of a PDMS film. This property gives a slower decay in shear stress for thicker PDMS films ascribed to the role of elasticity in the material pushing the glass prism against the protrusion. Moreover, the glass prism could slip due to the lubrication at the prism/PVA interface. This slippage can also contribute to the stress relaxation as well.
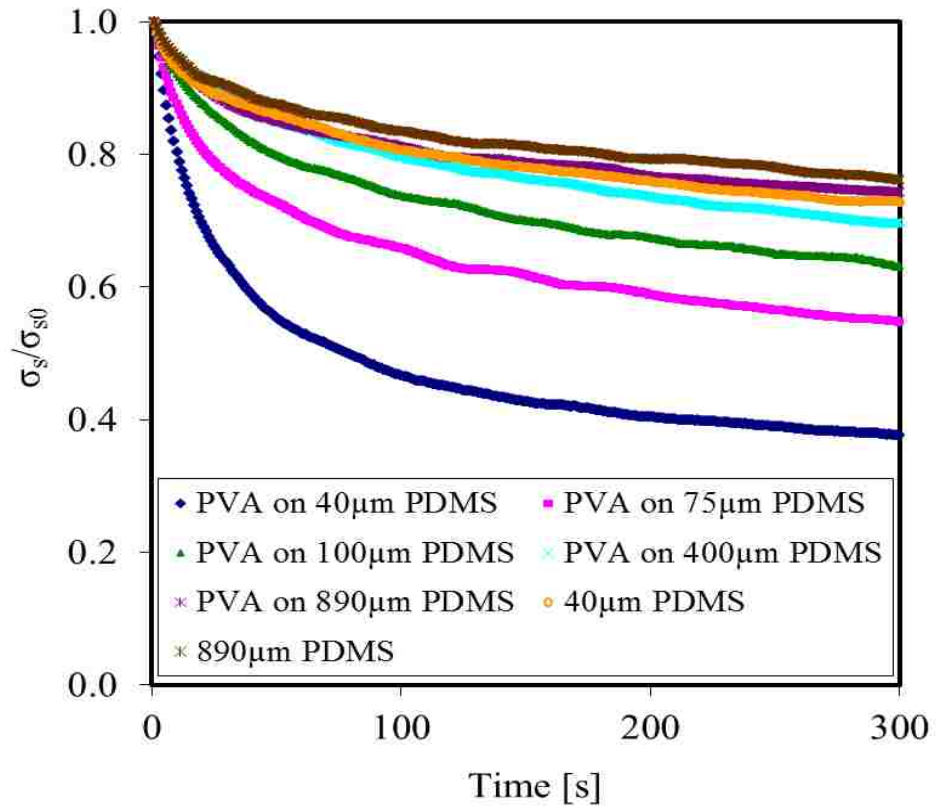
Figure 5.12. Shear stress (σ_s) relaxation of PDMS films with/without 10% cross-linked PVA coatings. σ_{s0} (~32 kPa) is the shear stress applied when the moving stage stops.

5.4. CONCLUSIONS

A silane coupling agent (TESU) was successfully utilized to covalently bond hydrophilic PVA and hydrophobic PDMS. The stability test and spectroscopic examinations (XPS and ATR-FTIR) showed that the PVA layer formed a robust coating on PDMS. The interfacial adhesion property of this PVA/PDMS composite material was further investigated by using an underwater shear test. The critical shear stress of a silanized glass cube removed from the surface of this material was reduced by ~60% compared to a 40-µm-thick unmodified PDMS film. Moreover, the critical shear stress of the PVA/PDMS composite material is not a strong function of the base PDMS thickness. Tested with both water and ethylene glycol systems, the results implied that the PVA layer was able to preserve the liquid as a lubrication layer to reduce the removal stress.

REFERENCES

1. Yebra, D. M., Kiil, S., and Dam-Johansen, K. *Progress in Organic Coatings* 2004, **50**, 75-104.

2. Clarkson, N. The Antifouling Potential of Silicone Elastomer Polymers. In *Recent Advances in Marine Biotechnology, Volume 3: Biofilms, Bioadhesion, Corrosion, and Biofouling*. Fingerman, M., Nagabhushanam, R., and Thompson, M.-F., Eds.; Science Publishers, Inc.: Enfield, NH, 1999, p87-180.

3. Brady, R. F. and Singer, I. L. *Biofouling* 2000, **15**, 73-81.

4. Griffith, J. R. Nontoxic Antifouling System. US Patent No. 7847401, 6 March 1992.

5. Burnell, T.; Carpenter, J.; Truby, K.; Serth-Guzzo, J.; Stein, J.; Wiebe, D. Advances in Non-Toxic Silicone Biofouling Release Coatings. In *ACS Symposium Series 729: Silicones and Silicone-Modified Materials*. Clarson, S. J.; Fitzgerald, J. J.; Owen, M. J.; Smith, S. D. Eds.; American Chemical Society: Washington, DC, 2000, p 180-193.

6. Edwards, D. P.; Nevell, T. G.; Plunkett, B. A.; Ochiltree, B. C. *International Biodeterioration & Biodegradation* 1994, **34**, 349-359.

7. Chung, J. Y. and Chaudhury, M. K. *The Journal of Adhesion* 2005, **81**, 1119-1145.

8. Chaudhury, M. K. and Kim, K. H. *The European Physical Journal E* 2007, **23**, 175-183.

9. Kim, K. H. and Chaudhury, M. K. *The Journal of Adhesion* 2009, **85**, 792-811.

10. McCutchen, C. W. *Wear* 1962, **5**, 1-17.

11. Hodge, A.; Fijan, R. S.; Carlson, K. L.; Burgess, R. G.; Harris, W. H.; Mann, R. W. *Proceedings of the National Academy of Sciences USA* 1986, **83**, 2879-2883.

12. Gong, J. P., Katsuyama, Y., Kurokawa, T., and Osada, Y. *Advanced Material* 2003, **15**, 1155-1158.

13. Peak, C. W.; Wilker, J. J.; Schmidt, G. *Colloid and Polymer Science* 2013, **291**, 2031-2047.

14. Cha, W.-I.; Hyon, S.-H.; Oka, M.; Ikada Y. *Macromolecular Symposia* 1996, **109**, 115-126.

15. Pan, Y.-S.; Xiong, D.-S. Ma R.-Y. *Wear* 2007, **262**, 1021-1025.

16. Baumberger, T.; Caroli, C. *Advances in Physics* 2006, **55**, 279-348.

17. Gong, J. P.; Osada, Y. *Progress in Polymer Science* 2002, **27**, 3-38.

18. Bolto, B., Tran, T., Hoang, M., and Xie, Z. L. *Progress in Polymer Science* 2009, **34**, 969-981

19. Yu, L., Li, C. M., Zhou, Q., Luong, J. H. T. *Bioconjugate Chemistry* 2007, **18**, 281-284.

20. Lin, C.-H.; Chaudhury, M. K. *Langmuir* 2008, **24**, 14276-14281.

21. Chung, J. Y.; Chaudhury, M. K. *The Journal of Adhesion* 2005, **81**, 1119-1145.

22. Janssen, D.; De Palma, R.; Verlaak, S.; Heremans, P.; Dehaen, W. Thin Solid Films 2006, **515**, 1433-1438.

23. Belder, D.; Deege, A.; Husmann, H.; Kohler, F.; Ludwig, M. *Electrophoresis* 2001, **22**, 3813-3818

24. Beamson, G.; Briggs, D. *High Resolution XPS of Organic Polymers: The Scienta ESCA300 Database.* John Wiley & Sons, Inc.: Chichester, England, 1992.

25. Blout, E. R.; Karplus, R. *Journal of the American Chemical Society* 1948, **70**, 862-864.

26. Silverstein, R. M.; Webster, F. X. *Spectrometric Identification of Organic Compounds, 6th ed.* John Wiley & Sons, Inc.: Hoboken, NJ, 1998.

27. Hanoosh, W. S.; Abdelrazaq, E. M. *Malaysian Polymer Journal* 2009, **4**, 52-61.

28. Du, H. Y.; Zhang, J. H. *Soft Matter* 2010, **6**, 3370-3376.

Chapter 6

Dissertation Summary

6.1. SUMMARY

This dissertation aims at studying the charge at hydrophobe/liquid interface and hydrogel adhesion. The conclusions are as follows.

6.1.1. Charge at Hydrophobe/Liquid Interface

In order to study the charge on a hydrophobic surface in contact with a liquid, we developed a new technique to measure the zeta potential of planar hydrophobic surfaces by combining electroosmosis and capillarity. In this new technique, an electric field is applied across the channel filled with aqueous solution seeded with fluorescent tracer particles. Some excess liquid is applied on both ends of the channel to modulate the capillary force across the channel by adjusting its curvature. While the velocity profile in the channel reaches steady state, a balance of the electroosmotic stress and Laplace pressure difference is achieved across the channel. However, as soon as the electric field is turned off, a Poiseuille flow develops in the channel due to the difference in the curvatures of the liquid bulges. We show that the measurement of the centerline velocity of the liquid inside the channel is enough to deduce the zeta potential of the surface.

This new method was further used to measure the zeta potentials of hydrocarbon

and fluorocarbon surfaces in contact with pure water with and without a nonionic surfactant, polyoxyethylene (23) lauryl ether (Brij 35). This surfactant was composed of hydrocarbon and oligo(ethylene oxide) (OEO) functionalities. It was adsorbed onto the silanized surfaces via its hydrocarbon chain with the OEO groups pointing toward to water. The addition of Brij 35 changes the strength of the zeta potential of both hydrocarbon and fluorocarbon surfaces. It was observed that, below the critical micelle concentration (CMC) of Brij 35, the zeta potentials of these two substrates remain constant, however, they decrease systematically with the surfactant concentration above the CMC. The reasons for the reduction of zeta potential strength are presumably due to hydroxide ion adsorption or the decrease of water/water and water/OEO H-bonds near the solid/liquid interface. These results inspired us to further investigate the origin of the charge at the hydrophobe/liquid interface.

We further modified our setup to measure the zeta potentials of alkyl siloxanes, fluoroalkyl siloxanes, and polydimethylsiloxane (PDMS) grafted glass surfaces in contact with polar protic (water, ethylene glycol, and formamide) and aprotic (dimethyl sulfoxide (DMSO)) liquids. These solvents contain limited ions and allow us to inspect the effect of hydroxide ions on the zeta potential. All of these surfaces exhibited negative zeta potentials in contact with these liquids. It was observed that the fluorocarbon surface shows the strongest electrokinetic effect, while the PDMS-grafted substrate is the weakest. Although these hygroscopic liquids contain a trace of water, the analyses show that the current model of charging via the adsorption of hydroxide ions or dissociation of pre-existing functional groups (e.g. silanol groups) is not sufficient to

interpret the observations. We feel that the recent suggestions of charging of hydrophobic surfaces in contact with water based on the charge transfer in hydrogen bonding deserve careful consideration. In this model, the imbalance between the H-bond donors and acceptors of water dimers near a hydrophobic surface causes a net negative charge. This explanation implies that other types of H-bonding liquids such as ethylene glycol and formamide could induce similar effects. For the case of aprotic DMSO on a fluorocarbon surface, the zeta potential (comparable to water and ethylene glycol) could be due to the substantial donor-acceptor interaction between basic DMSO with the silica underneath the fluoroalkyl siloxanes and/or the acidic α-methylene of the fluorocarbon.

6.1.2. Adhesion of a New PVA/PDMS Composite Material

A new composite polyvinyl alcohol (PVA)/polydimethylsiloxane (PDMS) material was developed and characterized by using spectroscopic methods (XPS and ATR-FTIR). A silane coupling agent (11-(triethoxysilyl)udecanal) was utilized in order to covalently bond hydrophilic PVA and hydrophobic PDMS. The PVA layer was cross-linked with glutaraldehyde, and the material passed a stability test of hot water immersion. This composite material adhesion was further tested by contact with a silanized glass cube. The critical shear stress ($\sigma_s{}^*$) required to remove the glass prism from the surface was ~60% less than an unmodified 40-μm-thick PDMS film. Tested with the same PVA cross-linking ratio, this $\sigma_s{}^*$ was independent of the PDMS thickness. The reduction of

σ_s^* could be due to capability of the PVA layer to retain water as a lubrication layer. This hypothesis was further verified with the adhesion test in ethylene glycol.

6.2. RECOMENDATIONS FOR FUTURE STUDY

<u>6.2.1. Charge at the Solid/Liquid Interface</u>

The observations of negative zeta potentials of hydrophobic surfaces in contact with polar liquids suggest the need to extend the experimental and theoretical studies of electrokinetic phenomena beyond water and oil. In order to achieve this goal, one can utilize different liquid-substrate combinations. The tests can be carried out not only with more polar liquids (e.g. diethylene glycol), but also with non-polar liquids, such as hydrocarbon and fluorocarbon solvents, as a comparison to the polar ones. The substrates with different functionalities can be modified with self-assembled monolayers of headgroup moieties[1] or polymeric coatings, for example, polystyrene and polyvinyl alcohol. The origin of this interfacial charge can be studied by exploring different substrate-liquid systems via molecular dynamic simulations as well.

Moreover, the effect of the nonionic surfactant (Brij 35, polyoxyethylene (23) lauryl ether) to the zeta potential of hydrocarbon and fluorocarbon surfaces still remains unresolved. In order to further study this phenomenon, it is important to investigate the adsorption patterns of the surfactant on the hydrophobic surfaces. These patterns may affect the distribution of ions and water molecules near the surfaces. There are two possible techniques can be applied to study the adsorption behaviors of Brig 35:

ellipsometry and underwater atomic force microscopy (AFM).[2] Ellipsometry can be utilized to study the thickness of the adsorption layer, and underwater AFM is able to provide the morphology information of the adsorption layer. Combining the results of these two techniques, one can deduce the possible adsorption patterns of Brij 35 on hydrophobic surfaces. In addition, it is also important to understand the role of micelles to the zeta potential. Experiments can also be performed by using similar nonionic surfactants with shorter hydrophobic or hydrophilic chains. This application will assist us to examine whether the zeta potential of a hydrophobic surface is related to the micelle size, and will further our understanding the effect of the micelles in this system.

6.2.2. PVA Coating on PDMS

In marine biofouling, the adsorption of non-specific proteins leads to further adsorption of bacteria and diatoms to form a microbial biofilm.[3-6] The biofilm is capable of trapping more organic biofoulants such as barnacles. As a result, reducing the adsorption of non-specific proteins is able to diminish the formation of biofilms. It has been reported that PVA can be used to reduce protein adsorption.[7,8] The adsorption of proteins onto a PVA modified silicon wafer can be studied by using variable angle spectroscopic ellipsometry (VASE). Ellipsometry has been utilized to investigate protein adsorption on solid surfaces with/without modification of polymer brushes.[9-11] Utilizing a dynamic scan mode of VASE, the thickness variance of the PVA hydrogel coating with the presence of proteins can be examined.

Moreover, for a PVA hydrogel, the increase of cross-linking ratio lowers the hydrogel toughness, which was tested qualitatively by pressing down a free-standing PVA hydrogel. This simple test was consistent with the result in the literature.[12] The mechanical property of the PVA hydrogel needs to be enhanced for further practical use. Different species of clay have been reported[13-16] to form unique organic/inorganic networks with polymers. Addition of proper clay into the PVA coating can potentially toughen the gel. Furthermore, the idea of double-network hydrogel can also be applied to enhance the mechanical property of the gel. A double network hydrogel (or interpenetrating polymer network hydrogel) is a highly cross-linked hydrogel filled by a second loosely cross-linked gel. The second gel network is capable of adsorbing local crack energy. The mechanical strength of the hydrogel is thus enhanced. For example, the literature has shown that the mechanical property of poly(2-acrylamido-2-methyl-1-propanesulfonic acid) gel can be improved by adding polyacrylamide (PAAm) gel[17], while that of poly(ethylene glycol) gel can be enhanced with the addition poly(acrylic acid) (PAA) gel[18]. To improve the mechanical property of the PVA hydrogel coating, PAAm and PAA networks can be tested and introduced into PVA hydrogel separately.

REFERENCES

1. Graupe, M.; Takenaga, M.; Koini, T.; Colorado, R.; Lee, T. R. *Journal of the American Chemical Society* 1999, **121**, 3222-3223.

2. Tiberg, F.; Brinck, J.; Grant, L. *Current Opinion in Colloid and Interface Science* 2000, **4**, 411-419.

3. Yebra, D. M., Kiil, S., and Dam-Johansen, K. *Progress in Organic Coatings* 2004, **50**, 75-104.

4. Vladkova, T. *Journal of the University of Chemical Technology and Metallurgy* 2007, **42**, 239-256.

5. Aldred, N. and Clare, A. S. *Biofouling* 2008, **24**, 351-363.

6. Banerjee, I., Pangule, R. C., and Kane, R. S. *Advanced Materials* 2011, **23**, 690-718.

7. Liu, S. X., Kim, J. T., and Kim, S. *Journal of Food Science* 2008, **73**, E143-E150.

8. Carneiro, L. B., Ferreira, J., Santos, M. J. L., Monteiro, J. P., Girotto, E. M. *Applied Surface Science* 2011, **257**, 10514-10519.

9. Malmsten, M. and Lassen, B. Ellipsometry Studies of Protein Adsorption at Hydrophobic Surfaces. In *Proteins at Interfaces II - Fundamentals and Applications*, Horbett, T. A. and Brash, J. L. Eds.; Oxford University Press: 1995, p 228-238.

10. Werner, C., Eichhorn, K.-J., Grundke, K., Simon, F., Grahlert, W., and Jacobasch, H.-J. *Colloids and Surfaces A: Physicochemical and Engineering Aspects* 1999, **156**, 3-17.

11. Bittrich, E., Rodenhausen, K. B., Eichhorn, K. J., Hofmann, T., Schubert, M., Stamm, M., and Uhlmann, P. *Biointerphases* 2010, **5**, 159-167.

12. Anseth, K. S., Bowman, C. N., and Brannon-Peppas, L. *Biomaterials* 1996, **17**, 1647-1657.

13. Liu, J. and Hoffmann, H. *Colloid and Polymer Science* 2004, **283**, 24-32.

14. Okada, .A and Usuki, A. *Macromolecular Materials and Engineering* 2006, **291**, 1449-1476.

15. Haraguchi, K. *Polymer Journal* 2011, **43**, 223-241.

16. Liu, Y., Zhu, M. F., Liu, X. L., Zhang, W., Sun, B., Chen, Y. M., and Adler, H. J. P. *Polymer* 2006, **47**, 1-5.

17. Gong, J. P., Katsuyama, Y., Kurokawa, T., and Osada, Y. *Advanced Material* 2003, **15**, 1155-1158.

18. Myung, D., Koh, W. U., Ko, J. M., Hu, Y., Carrasco, M., Noolandi, J., Ta, C. N., and Frank, C. W. *Polymer* 2007, **48**, 5376-5387.

Appendix A

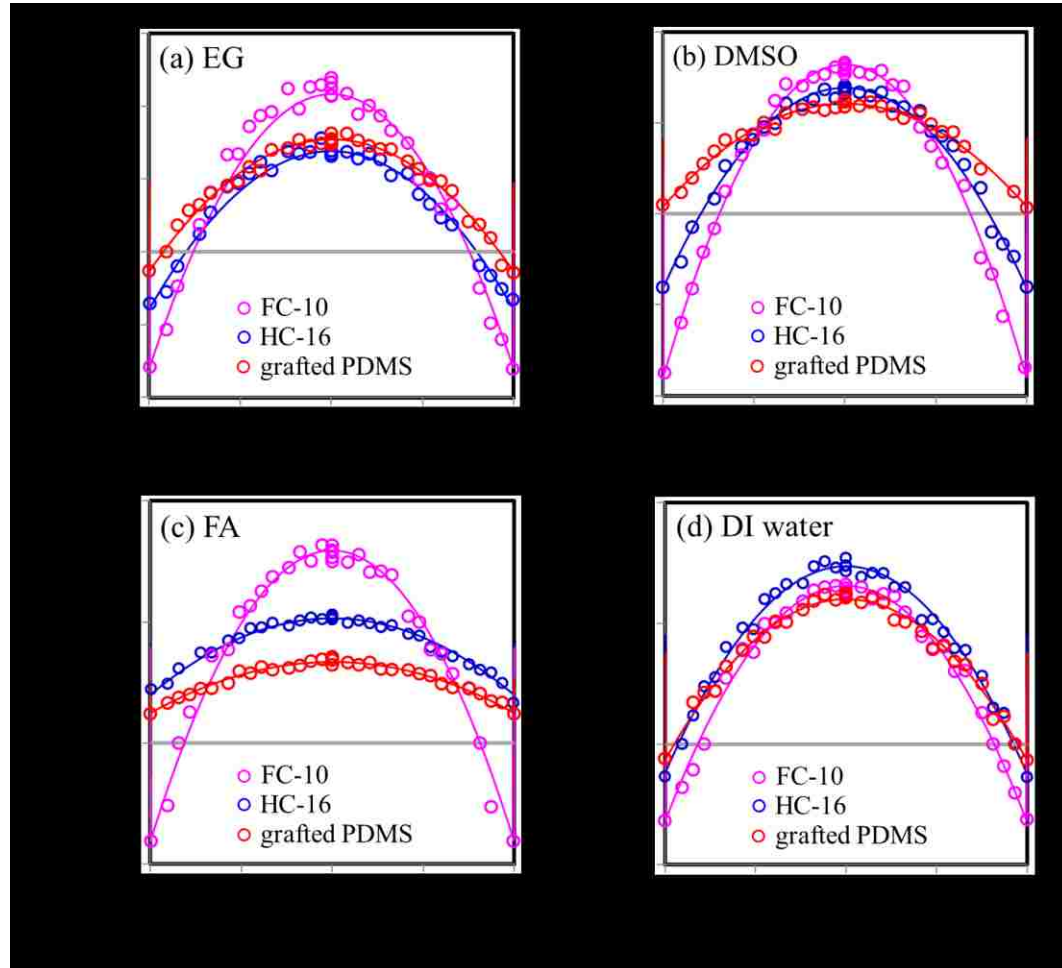## Mobility of Particles in Hydrophobic Channels

Figure A.1. The mobility ($\tilde{v}_{exp}$) of the particles across the height (H) of a channel hydrophobized with fluorocarbon silane (pink), hydrocarbon silane (blue) and grafted PDMS (red). The experiment was carried out with (a) ethylene glycol (EG), (b) dimethyl sulfoxide (DMSO), (c) formamide (FA) and (d) DI water as test liquids. The curves are obtained from eq. 4.12 as described in the text of Chapter 4.

Appendix B

Calculation of Cross-linking Ratio of PVA
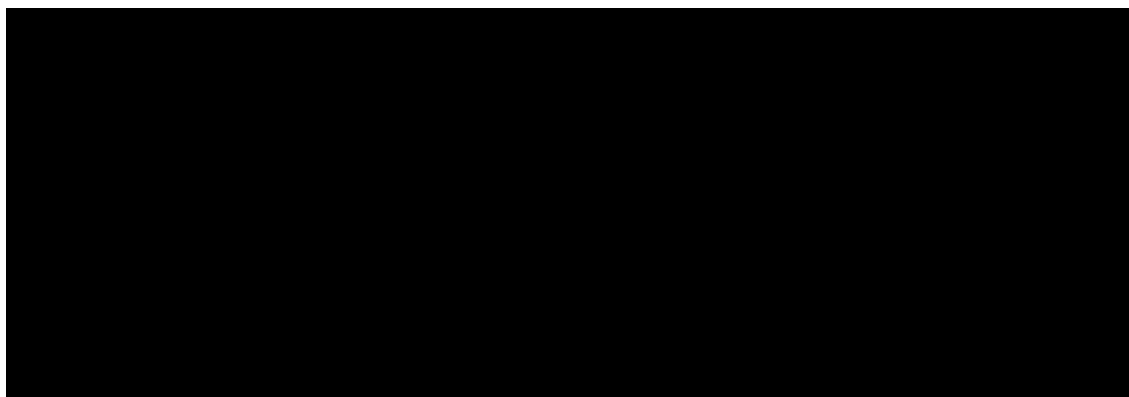
The above diagram shows the cross-linking reaction between the polyvinyl alcohol (PVA) and glutaraldehyde (GA). The molecular weight of the PVA repeating unit is 44, and that of GA is 100. For each aldehyde group (–CHO), it can react with two hydroxyl groups (–OH). Hence, in order to prepare a fully (100%) cross-linked PVA sample, the weight ratio between PVA and GA is 176:100 (i.e., 1.76:1). Similarly, for a 10% cross-linked PVA sample, the ratio of PVA/ GA is 17.6:1. Moreover, the cross-linking ratio calculated here does not include the functionalities of the silane coupling agent grafted on the polydimethylsiloxane (PDMS) surface due to that the number of these surface functionalities is negligible comparing with the added –CHO in GA.

Vita

    Chih-Hsiu Lin was born to Tso-Chung Lin and Shu-Ying Wu on February 10, 1982 in Kaohsiung, Taiwan. He attended National Cheng Kung University and obtained Bachelor of Science degree in Chemical Engineering in 2004. In college, he worked for Prof. Jui-Che Lin to develop a new biliary stent with biocompatibility by successfully coating chitosan onto the inner surface of a polyethylene (PE) tube. After serving the compulsory military service for 15 months, he began his graduate studies in Department of Chemical Engineering, Lehigh University on fall 2006. Under the guidance of Prof. Manoj K. Chaudhury, he obtained the Master of Science degree on May 2008 and continued pursuing his doctoral degree. His research focused on investigating the origin of the charge at the hydrophobe/liquid interface and studying the adhesion of thin soft hydrogels. After graduation, Chih-Hsiu will start his career as a process engineer in Intel at Portland, Oregon.